UNIVERSITÀ DEGLI STUDI DI PADOVA

Dipartimento di Fisica e Astronomia "Galileo Galilei"

Master Degree in Physics

Final Dissertation

Probing lepton flavor violation on all energy frontiers

Thesis supervisor

Prof. Paride Paradisi

Candidate

Riccardo Bartocci

Academic Year 2021/2022

Abstract

The Standard Model (SM) of particle physics has proven to be highly successful in describing elementary particles and their interactions. However, it is widely believed that the SM is the low-energy version of a more fundamental theory. In particular, there are hints for New Physics (NP) in the flavor sector. In this Master's thesis work, we aim to investigate the phenomenology of Lepton Flavor Violation (LFV). Such phenomena are strongly suppressed in the SM and therefore any evidence for them would unambiguously signal the presence of NP. We investigate the reaches of all current and expected facilities at any energy frontiers. In particular, we exploit the reaches of low-energy experiments such as MEG-II or Belle-II as well as high-energy experiments such as LHC and future lepton colliders. Our study of LFV effects is based on tools and techniques of effective field theory. In particular, we evaluate the decay rates for the processes $\ell_i \to \ell_j \gamma$, $\ell_i \to \ell_j \ell_k \ell_l$, $Z \to \ell_i \ell_j$, $h \to \ell_i \ell_j$, $B \to (K/\pi) \ell_i \ell_j$ and $\tau \to \ell \pi$ as well as the cross sections for the LFV scatterings $\ell_i \ell_i \to \ell_k \ell_l$, $\ell + N \to \tau + X$ and $pp \to \ell_k \ell_l$. Our primary goal is to analyze the potentialities of discovering LFV phenomena and/or to put relevant bounds on the fundamental parameters of the considered NP frameworks.

Contents

1 Lepton Flavor Violation probes of New Physics **5**

1.1 The Standard Model and Beyond . . . 5

1.1.1 The Standard Model of particle physics . . . 5

1.1.2 The success of the SM . . . 7

1.1.3 Shortcomings of the SM . . . 8

1.2 Charged Lepton Flavor Violation . . . 12

1.2.1 The Standard Model flavor structure . . . 12

1.2.2 CLFV in the SM with massive neutrinos . . . 14

1.3 Experimental searches for CLFV . . . 16

1.3.1 CLFV processes . . . 16

1.3.2 Present bounds and future experimental directions . . . 18

2 An effective approach to Lepton Flavor Violation **21**

2.1 Effective Field Theory . . . 21

2.1.1 Fermi theory of Weak Interactions . . . 21

2.1.2 Removing degrees of freedom . . . 22

2.1.3 Top-Down and Bottom-Up approach . . . 23

2.1.4 SMEFT and LEFT . . . 25

2.1.5 Spontaneous symmetry breaking in the SMEFT . . . 27

3 Low-energy probes of Lepton Flavor Violation **31**

3.1 Tree-level LFV decays . . . 31

3.1.1 SMEFT-LEFT tree-level matching . . . 31

3.1.2 $\ell_i \to \ell_j \gamma$ . . . 33

3.1.3 $\ell_i^\pm \to \ell_j^\pm \ell_l^\pm \ell_k^\mp$ . . . 36

3.1.4 $Z \to \ell_i^\pm \ell_f^\mp$ . . . 43

3.1.5 $h \to \ell_i^\pm \ell_j^\mp$ . . . 43

3.1.6 CLFV decays through semileptonic operators . . . 45

3.2 One-loop contributions to LFV decays . . . 47

3.2.1 $\ell_i \to \ell_j \gamma$ at 1-loop induced by 4-fermion operators . . . 47

3.2.2 $\ell_i \to \ell_j \gamma$ induced by Higgs modified couplings . . . 54

3.2.3 $\ell_i \to \ell_j \gamma$ at 1-loop induced by Z and W modified couplings . . . 55

3.2.4 One loop matching of SMEFT into LEFT for dipole operators . . . 59

4 High-energy probes of Lepton Flavor Violation **63**

4.1 LFV scatterings . . . 63

4.1.1 $\ell_i \ell_i \to \ell_j \ell_k$ . . . 63

4.1.2 $\ell + N \to \tau + X$ . . . 65

4.1.3 $pp \to \ell_k \ell_l$ 67

5 Numerical analysis **71**

5.1 Low energy analysis 71

5.2 High-energy analysis 74

Conclusion **79**

A Useful formulas **81**

B Mathematica codes **83**

Chapter 1

Lepton Flavor Violation probes of New Physics

1.1 The Standard Model and Beyond

In this section, the main features of the Standard Model (SM) of particle physics are presented to define the notation that will be used in the entire dissertation. Even if the SM has proven to be highly successful in describing fundamental interactions, there are some hints for New Physics which are listed in the following. Therefore, the search for a high-energy completion is becoming more and more necessary.

1.1.1 The Standard Model of particle physics

The Standard Model of particle physics (SM) is a theory that describes electromagnetic, weak, and strong interactions, at the fundamental level, between particles. It was built through an interplay between experimental discoveries and theoretical predictions in the last century and today represents one of the most successful theories in physics. The SM is based on the formalism of Quantum Field Theory (QFT) that is able to combine Classical Field Theory, Special Relativity and Quantum Mechanics, treating particles as quanta of their underlying quantum fields. Being a relativistic theory the first requirement on the SM is to be Lorentz invariant, therefore, in the Lagrangian both vector and spinor Lorentz indices must be contracted in order not to break the space-time symmetry. Moreover, the SM is built as a Gauge theory, which means that the total Lagrangian is left invariant by local transformations of the fields under the so-called SM Gauge group [1]

$$G_{SM} = SU(3)_c \times SU(2)_L \times U(1)_Y, \tag{1.1}$$

where the subscript c denotes color, L denotes left and Y denots hypercharge. To completely fix the Lagrangian, there is only one more ingredient, called renormalizability. Renormaliability means that all the operators in the Lagrangian have a dimension equal or smaller than four, guaranteeing the possibility to reabsorb all loop divergencies in a finite number of parameters called counterterms. This is achieved introducing scale dependent coupling constants and allowing, at least in principle, to make computation at any order in perturbation theory[1]. Before introducing the total Lagrangian, let us see which is the field content of the Standard Model:

- **Fermions**:

[1] Actually, the modern point of view is that every QFT is an effective theory and therefore its predictions must be believed only until some energy scale, where extra degrees of freedom appear.

They can be divided into left-handed $SU(2)_L$ doublets

$$Q_L^i(3,2,+\frac{1}{6}) = \begin{pmatrix} u_L^i \\ d_L^i \end{pmatrix}, \qquad L_L^i(1,2,-\frac{1}{2}) = \begin{pmatrix} e_L^i \\ \nu_L^i \end{pmatrix}, \tag{1.2}$$

and three right-handed singlets

$$u_R^i(3,1,+\frac{2}{3}), \quad d_R^i(3,1,-\frac{1}{3}), \qquad e_R^i(1,1,-1). \tag{1.3}$$

The numbers in the parenthesis are the quantum numbers under the SM group G_{SM} and the index $i = 1,2,3$ represents the flavor index. Indeed, fermions can be divided in three families called flavors, as far as leptons L are concerned, each one of the three families contains an electrically charged particle: electron (e) the first, muon (μ) the second, tau (τ) the third and for each of them there is a neutral particle called neutrino, they are ν_e, ν_μ and ν_τ, respectively. Regarding the quarks Q, the upper components carry electric charge $\frac{2}{3}$ and are called up (u), charm (c) and top (t), while the lower components have charge $-\frac{1}{3}$ and are referred to us as down (d), strange (s) and bottom (b). The only thing that distinguishes the members of each family with the same charge is the mass. The fermion mass range is extremely wide, considering that the least massive fermion[2] is the electron with $m_e = 0.511\,MeV$, while the heaviest is the top quark with $m_t = 170\,GeV$.

- **Higgs scalar**:
  It is an $SU(2)_L$ doublet

$$\Phi(1,2,+\frac{1}{2}). \tag{1.4}$$

  It couples to fermions and Gauge bosons and its potential breaks spontaneously G_{SM} as

$$SU(3)_c \times SU(2)_L \times U(1)_Y \to SU(3)_c \times U(1)_{EM}, \tag{1.5}$$

  where EM means electromagnetic. This Spontaneous Symmetry Breaking is called electroweak symmetry breaking, and it allows to provide a mass to fermions and gauge bosons in a gauge-invariant way.

- **Gauge fields**:
  They are

$$G_\mu = G_\mu^\mu \lambda^a, \qquad W_\mu = W_\mu^i \tau^i, \qquad B_\mu, \tag{1.6}$$

  where λ^a are the Gell-Mann matrices and τ^i the Pauli matrices. The first one is associated with eight gluon fields, and since it is associated with a non-Abelian group, its field strength is defined as $G_{\mu\nu} = \partial_\mu G_\nu - \partial_\nu G_\mu + i g_s [G_\mu, G_\nu]$. The second one is associated to three $SU(2)_L$ fields and the field strength is given by $W_{\mu\nu} = \partial_\mu W_\nu - \partial_\nu W_\mu + ig[W_\mu, W_\nu]$. The last one is the hypercharge field and it is the only Abelian Gauge boson, its field strength reads $B_{\mu\nu} = \partial_\mu B_\nu - \partial_\nu B_\mu$. After electroweak symmetry breaking, the two fields W and B mix through the Weinberg angle θ_W. They give rise to the physically interacting vector bosons of the weak and electromagnetic force, which are:

  - The W bosons $W_\pm^\mu = \frac{1}{\sqrt{2}}(W_1^\mu \mp i W_2^\mu)$, mediators of the charged current weak interactions;

[2] Neutrinos are not massive in the original SM.

- The Z boson $Z^\mu = W_3^\mu cos\theta_W - B^\mu sin\theta_W$, mediator of the neutral current weak interactions;
- The photon $A^\mu = B^\mu cos\theta_W + W_3^\mu sin\theta_W$, mediator of the electromagnetic interactions.

Once the field content and symmetry are understood, the most general renormalizable Lagrangian is the following

$$\mathscr{L}_{SM} = \mathscr{L}_k + \mathscr{L}_H + \mathscr{L}_Y, \tag{1.7}$$

where the first piece contains the kinetic terms for both fermions and gauge bosons

$$\mathscr{L}_k = -\frac{1}{4}G^a_{\mu\nu}G^{a,\mu\nu} - \frac{1}{4}W^a_{\mu\nu}W^{a,\mu\nu} - \frac{1}{4}B_{\mu\nu}B^{\mu\nu} + \sum_f \bar{\psi}_f i\not{D}\psi_f, \tag{1.8}$$

where ψ_f is a generic fermion and $D_\mu = \partial_\mu - i\frac{g_s}{2}\lambda_a G^a_\mu - i\frac{g}{2}\tau_j W^j_\mu - i\frac{g'}{2}YB_\mu$ the covariant derivative built through the gauge fields, where Y is the hypercharge coupling.
The second piece is the Higgs Lagrangian

$$\mathscr{L}_H = (D_\mu\Phi)^\dagger(D^\mu\Phi) - \mu^2\Phi^\dagger\Phi - \lambda(\Phi^\dagger\Phi)^2, \tag{1.9}$$

where μ^2 and λ are real parameters. It is responsible for Higgs-Gauge interactions, Higgs self-interactions and Gauge boson masses when Φ assumes its vacuum expectation value $\Phi = \begin{pmatrix} 0 \\ \frac{v}{\sqrt{2}} \end{pmatrix}$ with $v = \sqrt{\frac{-\mu^2}{\lambda}}$.

The last term is the Yukawa Lagrangian

$$\mathscr{L}_Y = -Y_u^{ij}\bar{Q}_{Li}u_{Rj}\tilde{\Phi} - Y_d^{ij}\bar{Q}_{Li}d_{Rj}\Phi - Y_e^{ij}\bar{L}_{Li}e_{Rj}\Phi + h.c. \tag{1.10}$$

where Y matrices are called Yukawa matrices and $\tilde{\Phi} = i\tau_2\Phi^*$ is the conjugate Higgs field. It is responsible for gauge-fermion interactions and fermion masses. This last piece contains the whole flavor structure of the SM that is going to be analyzed in the following.

1.1.2 The success of the SM

With the discovery at the LHC [2] of a particle that, in all its properties, appears just as the Higgs boson of the Standard Model (SM), the main missing block for the experimental validation of the theory is now in place. The Higgs discovery is the last milestone in the long history, almost 130 years, of the development of a field theory of fundamental interactions. An additional LHC result of great importance is that a large new territory has been explored, and no new physics was found. If one considers that there has been a big step in going from the Tevatron at 2 TeV up to the LHC at 8 TeV (a factor of 4) and that only another factor of 1.75 remains to go up to 14 TeV, the negative result of all searches for new physics is particularly astonishing. In particular, while NP can still appear at any moment, clearly it is now less unconceivable that no new physics will show up at the LHC. As is well known, in addition to the negative searches for new particles, the constraints on new physics from flavor phenomenology are extremely demanding: When adding higher-dimensional effective operators to the SM, flavor constraints generically lead to very large suppression scales Λ in the denominators of the corresponding coefficients. In fact in the SM there are powerful protections against flavor-changing neutral currents and CP violation effects, in particular through the smallness of quark mixing angles. Powerful constraints also arise from the leptonic sector. In particular, we refer to the recently improved MEG result on the $\mu \to e\gamma$ branching ratio, $Br(\mu \to e\gamma) \leq 4.2 \times 10^{-13}$ at

90% C.L. and other similar processes such as $\tau \to (e \text{ or } \mu)\gamma$ and to the bound on the electron dipole moment $|d_e| \leq 8.7\ 10^{-29}$ e cm by the ACME Collaboration. In this respect the SM is very special and, as a consequence, if there is new physics, it must be highly non-generic in order to satisfy the present constraints.

1.1.3 Shortcomings of the SM

The Standard Model is a very successful theory: its predictions, tested in the last three decades with increasingly high precision, are in excellent agreement with experimental data for a wide range of phenomena, but new-physics signals are anyway present both in cosmological observations and naturalness problems. Let us first of all point out that the SM does not include gravity and nowadays there are not fully consistent theories able to embed gravity within a QFT context compatible with the SM. Therefore, an extension of the SM or a drastic modification of our way of conceiving fundamental interactions is needed to unify the four fundamental forces. This fixes an upper bound with respect to the validity of the SM at the Planck scale $M_{Pl} = 1.2209 \times 10^{19} GeV$, where quantum gravity effects become important[3]. However, nothing forbids that the SM fails before this energy scale, for instance, for the appearance of new degrees of freedom, which at the energy of present colliders cannot go on-shell.
The first evidence for Beyond Standard Model (BSM) physics is neutrino oscillations: In the last decades several experiments have shown that solar and atmospheric neutrinos change their flavor along the path between their production and their detection point[4]. In the original Standard Model these transitions are not allowed because neutrinos are massless, therefore the SM must be extended including a neutrino mass term. This important observation modifies the structure of the SM Lagrangian, in particular the flavor structure of the lepton sector. The first extension of the SM we can build is obtained just by adding a Dirac mass term for neutrinos; however, this would lead to the question: "Why are neutrino Yukawa couplings so much smaller than for other fermions?" Therefore, research efforts are focused on finding some alternatives and their implications, for example, a Majorana mass term for neutrinos.
From the cosmological point of view, the SM is unable to explain different observations. Here, we list some of them:

- Dark Matter (DM) evidence: Galaxies in our universe are rotating with such speed that the gravity generated by their observable matter could not possibly hold them together; they should have torn themselves apart long ago. The same is true for galaxies in clusters, therefore there is something we cannot see at work. Extra gravity needed to hold galaxies together is called "dark matter" since it is not visible. A well-established measurement of Dark Matter abundance states that it constitutes around 26% of the energy budget of the universe. However, the only particle in the SM that can act as DM is the neutrino, but due to its small mass, it can only constitute hot dark matter and can account only for a small amount of the entire energy density of DM[5]. Therefore, an extension of the SM is needed to take this matter into account. These new particles must be stable, very weakly interacting, and non-relativistic. Several candidates have been proposed, such as the axion [6], which through the misalignment mechanism can provide the observed amount of cold DM. Other candidates are present in supersymmetric extensions of the Standard Model, such as gravitinos and neutralinos.

- Baryon asymmetry: In our universe, the number of baryons is much larger than the number of antibaryons. It can be shown that to have such a big difference a dynamical mechanism called baryogenesis is necessary. But in order to have baryogenesis, three conditions must be

satisfied, called the Sakharov conditions. In particular, Sakharov conditions require baryon number violating interactions. However, in the SM, due to an accidental symmetry, B violation is absent.[3] In addition CP violating interactions are also necessary and they are present in the SM, at least in the quark sector, but in a so small amount that it is not enough to explain the asymmetry[7]. Finally, the third condition is interaction out of thermal equilibrium.

- Inflation: It is a dynamical process set right after the Big Bang which can solve some early universe problems such as the flatness problem or the horizon problem[8]. However, there is no field that can be identified with the inflaton field, the particle that drives the inflation mechanism.

The inflation mechanism, DM particle production, and baryon asymmetry show that the SM is not able to explain completely our present observable universe and need to be revisited to account for these missing pieces.
These problems are all consequences of some experimental observations, on the other hand, some other problems are present within the SM and are related to the naturalness problem. The naturalness problem arises from the fact that in our theory the observables are usually the sum of more than one contribution and if one of these contributions is predicted to be far from the observed one, then the other contributions must be fine tuned to reproduce the experimental result. However, this fine-tuning is unpleasant in the sense that the choice of peculiar values for some parameters can be justified only through symmetry arguments. If these arguments are not present, the fine-tuning problem suggests that there can be something beyond the physics that we know. To better understand this point, let us start with a classical example: the physical mass of the electron in classical field theory. Electron mass according to electromagnetism can be written as the sum of the bare mass and the total energy stored in the EM field

$$m_e c^2 = m_{e,b} c^2 + \frac{e^2}{4\pi\epsilon_0 a}, \tag{1.11}$$

with $a \approx 10^{-17}\, cm$ the classical radius of the electron and ϵ_0 the vacuum dielectric constant. Substituting the numbers, one finds that the Coulomb energy is about $10\, GeV$ and therefore, to obtain the electron mass, the bare mass must be set to a very peculiar value $m_{e,b} = -9.9995\, GeV$. A so strong fine-tuning signals physics beyond the classical field theory of electromagnetism. In particular, at scale length as the classical electron radius, quantum effects are important and today we know that to describe EM interactions at so small distances QED must be adopted. This example shows that fine tuning problems are a very good hint to look for new physics and this can be applied also to the Standard Model. Very well-known examples of naturalness problems in the SM are[9]:

- The Higgs hierarchy problem: It consists of the huge hierarchy between the Planck mass $M_{Pl} \sim 10^{18}\,\text{GeV}$ and the Higgs mass parameter $|m_h| \sim 100\,\text{GeV}$. This problem becomes manifest in the one-loop correction to the dimension-2 Higgs mass parameter due to the top loops, as follows,

$$\Delta m_h^2 = -\frac{N_c y_t^2}{8\pi^2}\,\Lambda^2 + \cdots, \tag{1.12}$$

with Λ being the UV cut-off for the loop momentum and is typically of order M_{Pl}. Moreover, if a heavy particle couples to the Higgs doublet, it greatly corrects the Higgs mass parameter. For example, suppose that a heavy scalar X with mass M_X has a quartic coupling to the Higgs doublet given by $\mathcal{L}_{\text{int}} = -\frac{1}{2}\lambda_{hX} X^2 |h|^2$. Then, the one-loop correction to the Higgs mass

[3] To be precise, one can have baryon number violation through non-perturbative effects.

parameter in dimensional regularization is

$$\Delta m_h^2 = \frac{\lambda_{hX}}{16\pi^2} M_X^2 \log \frac{M_X^2}{\mu^2}. \tag{1.13}$$

When a right-handed neutrino ν_R with mass M_R couples to the Higgs doublet by $\mathcal{L}_{\rm int} = -y_N \bar{l}_L \tilde{\Phi} \nu_R + \text{h.c.}$, it also contributes to the Higgs mass parameter as

$$\Delta m_h^2 = \frac{y_N^2}{4\pi^2} M_R^2 \log \frac{M_R^2}{\mu^2}. \tag{1.14}$$

Therefore, unless λ_{hX} or y_N is small, M_X or M_R much larger than the weak scale leads to a tuning in choosing a correct Higgs mass parameter. Simple solutions to the hierarchy problem include low-energy supersymmetry, composite Higgs models (including twin Higgs models), and extra dimensions. The hierarchy problem represents the best hint that new physics is not far from the TeV scale.

- The strong CP problem: The QCD Lagrangian has an additional gauge-invariant term, the so-called θ term,

$$\mathcal{L}_\theta = \theta \frac{g^2}{32\pi^2} G^a_{\mu\nu} \tilde{G}^{\mu\nu}_a, \tag{1.15}$$

with $\tilde{G}^{\mu\nu}_a = \frac{1}{2}\epsilon^{\mu\mu\rho\sigma} G^a_{\rho\sigma}$. It turns out that the θ-term is a total derivative,

$$\frac{g^2}{32\pi^2} G^a_{\mu\nu} \tilde{G}^{\mu\nu}_a = \partial_\mu K^\mu, \tag{1.16}$$

with

$$K^\mu = \frac{g^2}{32\pi^2} \epsilon^{\mu\nu\rho\sigma} G^a_\nu \Big[G^a_{\rho\sigma} - \frac{g}{3} f^{abc} G^b_\rho G^c_\sigma \Big]. \tag{1.17}$$

Therefore, the θ-term does not affect local QFT properties, but there is a vacuum gauge configuration with a non-trivial topological (winding) number, $n \neq 0$, due to

$$\frac{g^2}{32\pi^2} \int d^4x G^a_{\mu\nu} \tilde{G}^{\mu\nu}_a = \int dS^\mu K_\mu = n, \tag{1.18}$$

with n being integer. The non-perturbative effects are proportional to e^{-c/g^2} so only the QCD θ-term is important. In fact, the QCD θ-term contributes to the neutron electric dipole moment (EDM) as

$$d_n = \frac{e}{\Lambda^2_{\rm QCD}} \frac{m_u m_d}{m_u + m_d} \theta < 3.0 \times 10^{-26}\, e\,\text{cm}, \tag{1.19}$$

which sets the limit to $|\theta| < 10^{-10}$. This is the strong CP problem. Nothing forbids such a small value, but it is more natural to explain it through a symmetry argument like in the Peccei-Quinn solution, where a new $U(1)_{PQ}$ symmetry is added and the parameter θ is dynamically driven to zero[10].

- The SM flavor puzzle: It is about the hierarchical patterns of fermion masses and the mixing

patterns of quarks and leptons. In particular, neutrino masses are much lighter than any of the quarks and leptons: $m_{\nu_j}/m_{l,q} \lesssim 10^{-6}$. But also in the original formulation of the SM we find that the mass spectrum ranges from around $0.5\,MeV$ for the electron and $170\,GeV$ for the top quark, and again this huge difference between the masses of different fermions is not natural[11]. The flavor problem originates from the dimension-4 Yukawa couplings for quarks and leptons, and partly from the dimension-5 operators for neutrino masses.

In addition, there are some observables that present a tension between theory and experiments.

- Lepton flavor universality violation[12]: The Standard Model predicts the electroweak interactions to have the same amplitudes for all the three different lepton generations, except for phase-space differences or helicity suppression effects. This property is called lepton flavor universality (LFU) and has been experimentally verified in meson decays, τ decays, and Z boson decays. However, evidence of LFU violation has recently been observed by the LHCb collaboration in $B^+ \to K^+\ell^+\ell^-$ ($\ell = e, \mu$) decays: yet another piece in the larger set of anomalies observed in the last decade in decays of B meson, which show a consistent tension with SM predictions. Beyond Standard Model (BSM) theories that could explain the anomalies are leptoquarks or new heavy gauge boson such as Z', generally also imply a sizeable lepton flavor violation.

- The magnetic moment of the muon[13]: For an elementary particle with intrinsic angular momentum (spin, $\vec{S}$) and charge q, its magnetic moment $\vec{\mu}$ is given (in natural units) by

$$\vec{\mu} = g\frac{q}{2m}\vec{S}\,, \tag{1.20}$$

  where g is the gyromagnetic ratio and m is the mass of the particle. From his original formulation of quantum mechanics, Dirac predicted $g = 2$ for the electron (and, consequently, any spin-$\frac{1}{2}$ elementary particle) in 1928. However, this quantity receives contributions from radiative corrections, where the interaction of the elementary particle with a photon is modified by additional interactions with virtual particles. These quantum fluctuations modify g, where interactions with virtual particles increase its value from the tree-level prediction of $g = 2$. For charged leptons ($l = e, \mu, \tau$), the magnetic anomaly a_l is defined as the fractional deviation from Dirac's prediction of $g_l = 2$, namely

$$a_l = (g_l - 2)/2\,. \tag{1.21}$$

  Comparisons with experimental measurements a_l^{EXP} result in studies of the magnetic moments of leptons being a powerful indirect search of new physics, and recent results present a deviation of 4.2σ between the experimental measurement and the theoretical prediction.

Therefore, even if the predictions of the SM in the last decades are astonishingly precise, the theory clearly needs some ultraviolet completion that is able to explain the mentioned observations and the internal consistency problems. A particularly promising sector is the flavor sector, especially Charged Lepton Flavor Violation (CLFV) searches are very suitable to test several ideas that were proposed to address the aforementioned issues. In more general terms, the capability of CLFV searches to explore scales far beyond the energies of our current colliders could prove crucial in establishing the next fundamental scale of new physics[14].

1.2 Charged Lepton Flavor Violation

In this second section, the Yukawa Lagrangian is analyzed in more detail, to understand better which are the extensions of the Standard Model which leads to Charged Lepton Flavor Violation. In particular, the SM prediction for CLFV processes is evaluated in the case of massive neutrinos, showing the strong suppression of these channels.

1.2.1 The Standard Model flavor structure

The flavor sector of the Standard Model (SM)[14], *i.e.* the fermion masses and mixing among different generations, arises from the Yukawa couplings of the fermion fields with the Higgs field Φ:

$$-\mathscr{L}_Y = (Y_u)_{ij}\ \overline{Q}_{L\,i}\, u_{R\,j}\, \widetilde{\Phi} + (Y_d)_{ij}\ \overline{Q}_{L\,i}\, d_{R\,j}\, \Phi + (Y_e)_{ij}\ \overline{L}_{L\,i}\, e_{R\,j}\, \Phi + h.c. \tag{1.22}$$

where $SU(2)_L$ indices were omitted and i and j run over the three families, such that Y_f ($f = u, d, e$) are, in general, complex 3×3 matrices. The conjugate Higgs field is defined as $\widetilde{\Phi} \equiv i\tau_2\Phi^*$, where τ_2 is the second Pauli matrix. Fermion mass terms of the kind $m_f \overline{f}_L f_R$ arise upon the breaking of the electro-weak (EW) symmetry $SU(2)_L \times U(1)_Y$ by the vacuum expectation value (vev) of the Higgs field, $\langle\Phi\rangle^T = (0\ v)/\sqrt{2}$ ($v \simeq 246$ GeV), such that:

$$(m_f)_{ij} = \frac{v}{\sqrt{2}}(Y_f)_{ij} \qquad \text{with} \qquad f = u, d, e. \tag{1.23}$$

In the original formulation of Standard Model, the Lagrangian in Eq. (1.22) does not give rise to mass terms for the neutrinos, which are thus exactly massless. The Yukawa matrices and thus the fermion mass matrices can be diagonalised by unitary rotations of the fields, as follows:

$$Y_f = V_f \hat{Y}_f W_f^\dagger \qquad \text{with} \qquad f = u, d, e. \tag{1.24}$$

where $\hat{Y}_f$ denotes diagonal Yukawa matrices. Given the unitarity of the matrices V_f and W_f, applying these transformations does not modify the kinetic terms and the neutral-current interactions, such as the fermion couplings to the photon and the Z boson, which then result flavor conserving. Similarly the fermion couplings to the physical Higgs h are proportional to the mass matrix, thus they can be diagonalised in the same basis and no flavor violation is induced in the interactions with the Higgs either:

$$-\mathscr{L}_{h\bar{f}f} = \frac{m_f}{v}\, \bar{f}_L f_R\, h + h.c. \tag{1.25}$$

On the other hand, the two rotations in Eq. (1.24) do induce flavor violation in the charged-current interactions with the W bosons:

$$\mathscr{L}_{cc} = \frac{g}{\sqrt{2}} \left(\overline{u}_L \gamma^\mu (V_u^\dagger V_d) d_L + \overline{\nu}_L \gamma^\mu (V_\nu^\dagger V_e) e_L \right) W_\mu^+ + h.c. \tag{1.26}$$

As we can see, flavor violation in quark sector arises from the fact that, in general, diagonalising Y_u and Y_d requires $V_u \neq V_d$. Such a misalignment gives rise to flavor-changing transitions controlled by the matrix $V_{\rm CKM} \equiv V_u^\dagger V_d$, which is nothing but the Cabibbo-Kobayashi-Maskawa (CKM) matrix. On the other hand, in the lepton sector of the original Standard Model with massless neutrinos, one can choose $V_\nu = V_e$, because no other term in the Lagrangian involves the lepton doublets, and the leptonic flavor is exactly conserved. Clearly, this feature does not hold any longer in extensions of the Standard Model addressing the generation of mass terms for the neutrinos, as we will discuss in the

next section. In other words, the Lagrangian in Eq. (1.22) is invariant under three independent global $U(1)$ rotations associated to each lepton family, which implies three conserved charges: the lepton family numbers L_e, L_μ, and L_τ.

To summarize, in the Standard Model the lepton family numbers are individually conserved because of the minimality of the construction, which also implies that neutrinos are massless. In fact, the matrix of the lepton Yukawa couplings Y_e defines a single direction in the space of leptonic flavor. Hence, as we have seen, one can use the freedom of rotating LH and RH lepton fields to make the matrix diagonal without inducing flavor-changing effects in other sectors of the theory. This is in contrast to the quark sector where there are two different Yukawa matrices, Y_u and Y_d, both involving Q_L, such that they can not be simultaneously diagonalised in the same basis.

From the above discussion, we can immediately see under which condition an extension of the Standard Model features flavor violation in the leptonic sector: the presence in the Lagrangian of at least another term involving the lepton fields, *i.e.* of another non-trivial direction in the flavor space. This is for instance the case of a neutrino mass term (Dirac or Majorana), as we will see in the next section. Here we mention another minimal extension of the Standard Model leading to lepton flavor violation, namely the introduction of a second Higgs doublet. In fact, in presence of two scalar doublets Φ_1 and Φ_2, the gauge symmetries allow couplings of the fermion fields to both:

$$-\mathscr{L}_{\text{2HDM}} = \sum_{a=1,2} \Big[(Y_u^{(a)})_{ij}\ \overline{Q}_{L\,i}\, u_{R\,j}\, \widetilde{\Phi_a} + (Y_d^{(a)})_{ij}\ \overline{Q}_{L\,i}\, d_{R\,j}\, \Phi_a + (Y_e^{(a)})_{ij}\ \overline{L}_{L\,i}\, e_{R\,j}\, \Phi_a + h.c. \Big]. \tag{1.27}$$

In particular, we see that in the lepton sector there are two Yukawa matrices $Y_e^{(1)}$ and $Y_e^{(2)}$, hence from the above discussion we expect that lepton family numbers are violated in this framework. Indeed, while the fermion masses are now generated by the vevs of both Higgs fields, v_1 and v_2,

$$m_f = \frac{1}{\sqrt{2}} \left(Y_f^{(1)} v_1 + Y_f^{(2)} v_2 \right) \qquad \text{with} \qquad f = u, d, e, \tag{1.28}$$

the couplings of the physical Higgs particles – which are now five: two neutral CP-even states, one neutral CP-odd state, two charged states – are no longer aligned to the fermion masses as in Eq. (1.25). Let us consider as an example the case of the two CP-even states, h and H, which are mixtures of the real parts of the neutral components of the two doublets:

$$h = \sqrt{2}(\text{Re}(\Phi_1^0)\sin\alpha + \text{Re}(\Phi_2^0)\cos\alpha), \tag{1.29}$$

$$H = \sqrt{2}(\text{Re}(\Phi_1^0)\cos\alpha - \text{Re}(\Phi_2^0)\sin\alpha), \tag{1.30}$$

where the mixing angle α depends on the couplings of the scalar potential that we have assumed to be CP conserving. In order to highlight the above-mentioned misalignment, it is convenient to rotate the scalar doublets such that only Φ_1 has a vev, i.e. $v_1 = v$, $v_2 = 0$. The couplings of these two physical CP-even Higgses to the fermions are then:

$$-\mathscr{L}_{h\bar{f}f} = \left(\frac{m_f}{v} \sin\alpha + Y_f^{(2)} \cos\alpha \right)\ \bar{f}_L f_R\, h + h.c. \tag{1.31}$$

$$-\mathscr{L}_{H\bar{f}f} = \left(\frac{m_f}{v} \cos\alpha - Y_f^{(2)} \sin\alpha \right)\ \bar{f}_L f_R\, H + h.c. \tag{1.32}$$

While only the matrices $Y_f^{(1)}$ contribute to the fermion mass terms, the above couplings depend on the $Y_f^{(2)}$ too. Hence, as we can see, these couplings are in general not diagonal in the mass basis where

m_f are. As a consequence, flavor-changing neutral currents (FCNC) are generated already at the tree level by diagrams exchanging h and H.

1.2.2 CLFV in the SM with massive neutrinos

As pointed out in the previous subsection, also in the lepton sector charged flavor violation is possible, but within the Standard Model it can only occur at the loop level. Let us consider as an example the case of $\mu \to e\gamma$, its Feynman diagram is:

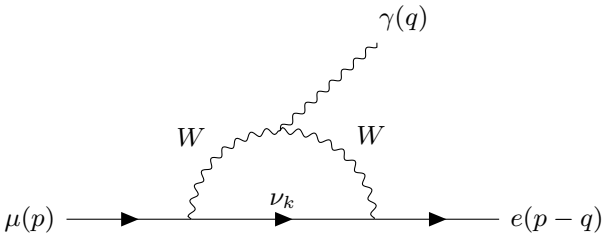

Figure 1.1: Feynman diagram contributing to $\mu \to e\gamma$ in the SM with massive neutrinos.

The transition can be described by an effective operator as[14]

$$\mathcal{M}(\mu \to e\gamma) = i\bar{u}_e(p-q)V_\alpha u_\mu(p)\epsilon^{*\alpha}(q), \tag{1.33}$$

where $V_\alpha = \sigma_{\alpha\beta}q^\beta(F_1 + F_2\gamma_5) + \gamma_\alpha(F_3 + F_4\gamma_5) + q_\alpha(F_5 + F_6\gamma_5)$, with $\sigma_{\alpha\beta} = \frac{i}{2}[\gamma_\alpha, \gamma_\beta]$. The $F_1, ..., F_6$ are invariant amplitudes and are not all independent, indeed imposing charge conservation $\frac{\partial}{\partial q_\alpha}V_\alpha = 0$ one gets rid of four of them and the resulting amplitude is:

$$\mathcal{M}(\mu \to e\gamma) = i\bar{u}_e(p-q)\sigma_{\alpha\beta}q^\beta(A_R P_R + A_L P_L)u_\mu(p)\epsilon^{*\alpha}(q), \tag{1.34}$$

where $A_{R,L} = F_1 \pm F_2$ and $P_{R,L}$ are the chirality projectors. Finally, the unpolarized amplitude is given by:

$$|\mathcal{M}|^2 = m_\mu^4(|A_R|^2 + |A_L|^2), \tag{1.35}$$

and the decay rate, neglecting the electron mass, is[14]

$$\Gamma(\mu \to e\gamma) = \frac{m_\mu^3}{16\pi}(|A_R|^2 + |A_L|^2). \tag{1.36}$$

Let us observe that since $\sigma_{\alpha\beta}$ and $P_{R,L}$ commute, electron and muon spinors must have opposite chiralities, but the weak interactions involved are only left-handed and the chirality flip can only be due to the mass terms of external leptons. Therefore, since $A_R \propto m_\mu$ and $A_L \propto m_e$ we have

$$|A_L|^2 \ll |A_R|^2. \tag{1.37}$$

Thus, we neglect the contribution of A_L.
Let us see what the contribution is to A_R in the SM[14] writing the amplitude corresponding to the

diagram reported above:

$$\mathcal{M} = i\sum_{k=1}^{3}\int \frac{d^4k}{(2\pi)^4}\bar{u}_e(p-q)\left(-i\frac{gU_{ek}^*}{\sqrt{2}}\gamma_\alpha P_L\right)\frac{\not{p}+\not{k}}{(p+k)^2-m_{\nu_k}^2}\left(i\frac{gU_{\mu k}}{\sqrt{2}}\gamma_\beta P_L\right)u_\mu(p) \\ \times (i\Delta^{\alpha\mu}(k+q))(-ie\Gamma_{\lambda\mu\nu}(-q,k+q,-k))(i\Delta^{\nu\beta}(k)\epsilon^{*\lambda}(q)), \tag{1.38}$$

where

$$\Delta^{\alpha\beta}(k) = -\frac{g_{\alpha\beta}-(1-\xi)\frac{k_\alpha k_\beta}{k^2-\xi M_W^2}}{k^2-M_W^2}, \tag{1.39}$$

is the W propagator in the R_ξ gauge, and

$$\Gamma_{\lambda\mu\nu}(-q,k+q,-k) = ((q-k)_\mu g_{\lambda\nu}+(2k+q)_\lambda g_{\mu\nu})-(2q+k)_\nu g_{\lambda\mu}, \tag{1.40}$$

is the photon-W vertex. Let us now focus on the sum over neutrino eigenstates:

$$\sum_{k=1}^{3}\frac{U_{\mu k}U_{ek}^*}{(p+k)^2-m_{\nu_k}^2} \approx \sum_{k=1}^{3}\left[\frac{U_{\mu k}U_{ek}^*}{(p+k)^2}+\frac{U_{\mu k}U_{ek}^*m_{\nu_k}^2}{(p+k)^4}+\mathcal{O}\left(m_{\nu_k}^2\right)\right]. \tag{1.41}$$

The first term in the expansion vanishes because of the unitarity of the PMNS matrix, thus the leading term is the second one, but it is proportional to the difference of the square of neutrino masses and therefore gives very little contribution. This observation shows that a GIM-like mechanism also applies to the case of flavor violation in the lepton sector owing to the small neutrinos mass differences. Finally, integrating in k and taking the Unitary Gauge limit $\xi \to \infty$ one gets[15]:

$$A_R = \frac{g^2 e}{128\pi^2}\frac{m_\mu}{M_W^4}\sum_{k=1}^{3}U_{\mu k}U_{ek}^*m_{\nu_k}^2. \tag{1.42}$$

This amplitude gives a branching ratio for $\mu \to e\gamma$ of

$$BR(\mu\to e\gamma) \approx \frac{\Gamma(\mu\to e\gamma)}{\Gamma(\mu\to e\nu\bar{\nu})} \approx 10^{-55}. \tag{1.43}$$

That is forty orders of magnitude smaller than the sensitivity of the present-day experiments. The presented scenario is what we call a Golden Channel, indeed, since the SM prediction for the decay rate is so small, an experimental observation of CLFV would be an unambiguous sign of new dynamics in the lepton sector: highly suppressed processes like this reduce the background noise arising from SM-mediated processes when looking for new physics effects.
Summarizing, although the lepton family numbers are an $\mathcal{O}(1)$ breaking, as suggested by mixing angles among neutrino generations, CLFV processes represent a Golden Channel for the following reasons:

- They only occur at loop level;
- they only occur through weak interactions;
- the GIM cancellation due to the unitarity of U_{PMNS} strongly suppresses the amplitude;
- the dumping due to the smallness of neutrino masses compared to the M_W.

It is also interesting to see what happens when instead of a Dirac mass term, a Majorana mass term is considered[14]. In this case, we have the mixing between LH and RH neutrinos and the unitary

matrix that diagonalizes m_ν, the PMNS matrix U, no longer coincides with the matrix that appears in the charged current, Eq. (1.26), being this latter one, which we call $\mathcal{U}$, a submatrix of a matrix of higher dimension for both LH and RH neutrinos. Most importantly, $\mathcal{U}$ is not unitary and can be written in terms of the matrices Y_ν and M_R as

$$\mathcal{U} = \left(1 - \frac{v^2}{2} Y_\nu^\dagger M_R^{-2} Y_\nu\right) U \,. \tag{1.44}$$

We can now understand why this setup possibly has a large impact on CLFV: entries of $\mathcal{U}$, instead of U, now appear at the vertices of the Feynman diagram, and the GIM cancellation of Eq. (1.41) does not occur anymore. Taking this into account, it becomes

$$\mathrm{BR}(\mu \to e\gamma) = \frac{3\alpha}{32\pi} \frac{\left|\sum_k \mathcal{U}_{\mu k} \mathcal{U}_{ek}^* F(x_k)\right|^2}{(\mathcal{U}\mathcal{U}^\dagger)_{\mu\mu} (\mathcal{U}\mathcal{U}^\dagger)_{ee}}, \tag{1.45}$$

where $x_k = m_{\nu_k}^2 / M_W^2$ and the loop function is $F(x_k) = \frac{10}{3} - x_k + \mathcal{O}\left(x_k^2\right)$. As we can see, in the limit $\mathcal{U} \to U$, the previous expression is recovered, but for a significant deviation of $\mathcal{U}$ from unitarity, the first term of $F(x_k)$,which is not suppressed by the small neutrino masses, dominate. As a consequence, CLFV rates can be raised at observable levels for low-scale RH neutrinos. However, from Eq. (1.44), we can see that sizeable CLFV requires both M_R not too far above the EW scale and large neutrino Yukawa couplings. These two conditions are not compatible with the smallness of the neutrino masses in generic realizations of the seesaw mechanism.

1.3 Experimental searches for CLFV

Let us see in this section which are the main processes of Charged Lepton Flavor Violation that the experiments are trying to detect. In particular, we explore their signatures, their background, and future improvements of the experimental techniques. In addition, the present bounds on the various CLFV channels are reported.

1.3.1 CLFV processes

Let us start, first of all, with the muon channel: the muon has a quite long lifetime $\tau_\mu \approx 2.2 \times 10^{-6}\, s$ and muon beams can be produced starting from pion decay, so that they are suitable particles for these kinds of experiments. In addition, cosmic rays are a source of muons in a very large energy range, allowing also the study of very high energy processes. The main muon channels are the following[14]:

- $\mu \to e\gamma$: The signature of the $\mu^+ \to e^+\gamma$ decay is a time coincident, back-to-back pair of a monoenergetic photon and a monoenergetic positron, both with an energy equal to half of the muon mass ($E_e = E_\gamma \approx 52.8$ MeV). If one were able to measure the energies, relative time and relative angle with infinite precision this would be a bakground-free search. Finite experimental resolutions on the other hand imply that non $\mu^+ \to e^+\gamma$ events can mimic its topology. There are two major backgrounds in this search: one is a prompt background from radiative muon decay, $\mu^+ \to e^+\nu_e\overline{\nu}_\mu\gamma$, when the e^+ and the photon are emitted back-to-back with the two neutrinos carrying away little energy. In this decay the two particles are emitted at the same time. The other background is an accidental coincidence of an e^+ in a normal muon decay, $\mu^+ \to e^+\nu_e\overline{\nu}_\mu$, accompanied by a high energy photon. The sources of the latter might be either $\mu^+ \to e^+\nu_e\overline{\nu}_\mu\gamma$ decay, annihilation-in-flight or external bremsstrahlung of e^+s from normal muon decay.

- $\mu \to eee$: In the $\mu^+ \to e^+e^-e^+$ decay one searches for two positrons and one electron coming from a common vertex and with a total energy equal to the muon mass $E_{\text{tot}} \approx 105.6$ MeV. Being a three-body decay the daughter particles are emitted in a common plane. Simple relativistic kinematics teaches us that each particle has a maximum momentum of about $m_\mu/2$ and that the decay can be described by two independent variables. The energy distribution of each daughter particle depends on the exact dynamics of the underlying unknown physics. In general the highest energy particle has a momentum larger than 35 MeV, while the distribution of the lowest energy particle peaks near zero and decreases quickly as its energy tends to its upper limit so that only about one half have an energy larger than 15 MeV. A $\mu^+ \to e^+e^-e^+$ search experiment must have an excellent tracker as thin as possible since in order to achieve the high acceptance the detector must be able to reconstruct tracks with momenta ranging from a few MeVs up to half of the muon mass. As a consequence, unlike $\mu^+ \to e^+\gamma$ and $\mu \to e$ conversion, to get a limit on the $\mu \to eee$ decay one has to make some assumption on the unknown operator: since the detector is sensitive to particles above a defined momentum, it is necessary to know which is the probability of having all three particles above that momentum threshold, and this depends on the matrix element. Furthermore unlike the case of the $\mu^+ \to e^+\gamma$ search there is no mono-energetic particle in the final state, but the backgrounds are very similar. There is a prompt background due to the allowed muon decay $\mu^+ \to e^+e^-e^+\bar{\nu}_\mu\nu_e$ – whose branching ratio is $(3.4 \pm 0.4) \times 10^{-5}$– which becomes serious when the two neutrinos have very little energy.

- $\mu^- N \to e^- N$: Muon to electron conversion is the spontaneous decay of a muon to an electron without the emission of neutrinos, within the Coulomb potential of an atomic nucleus: it is therefore only possible for negative muons. For conversions leaving the nucleus in its ground state the nucleons act coherently enhancing its probability relative to the rate of muon capture. The constraint of unchanged nucleus means that all the energy of the muon goes into the kinetic energy of the electron and the recoil of the parent nucleus, hence the signature of such a process is the presence of a monochromatic electron at an energy which is essentially the muon mass, corrected for the binding energy and nuclear recoil. Experimentally, coherent μ to e conversion offers many advantages over $\mu \to e\gamma$ search: the electron is emitted at the kinematic endpoint of the muon decay in orbit, which constitutes the only intrinsic background.

- $h \to \mu e$: Higgs flavor violating decay is the spontaneous decay of the Higgs boson into a flavor violating couple such as $e\mu$[16]. The signature is an electron and a muon back to back with energy half of the Higgs mass ($E_e = E_\mu = 62.5\,\text{GeV}$). The decay $h \to \mu e$ is quite similar to the standard model $h \to \mu\mu$, this implies that existing SM Higgs searches, with only small or no modifications at all, can already be used to place bounds on the flavor violating decay. The LHC searches for this decay suffers large QCD backgrounds, for example one can have combinations between jets and Z decay mimicking the final state.

- $Z \to \mu e$: The Z flavor violating decay signature is given by an opposite-charge lepton-pair events, while events with same-charge lepton pairs are used for estimates of background processes[17].The main backgrounds include events from the production and decay of top quarks, pairs of gauge bosons and the Higgs. boson.

Another promising channel is the tau channel[18] that thanks to its large mass $m_\tau = 1777 MeV$ allows many flavor violating channels such as $\tau \to \mu\gamma$, $\tau \to e\gamma$, $\tau \to 3e$, $\tau \to 3\mu$, but also decays with hadrons in the final state like $\tau \to e\pi_0$ or $\tau \to e\pi^+\pi^-$. On the other hand, it has a very short lifetime with respect to the muon $\tau_\tau = 2.9 \times 10^{-13}\,s$ and it is impossible to produce tau beams. Therefore, the enhanced sensitivity due to the large mass is reduced by the low number of taus that can be observed.

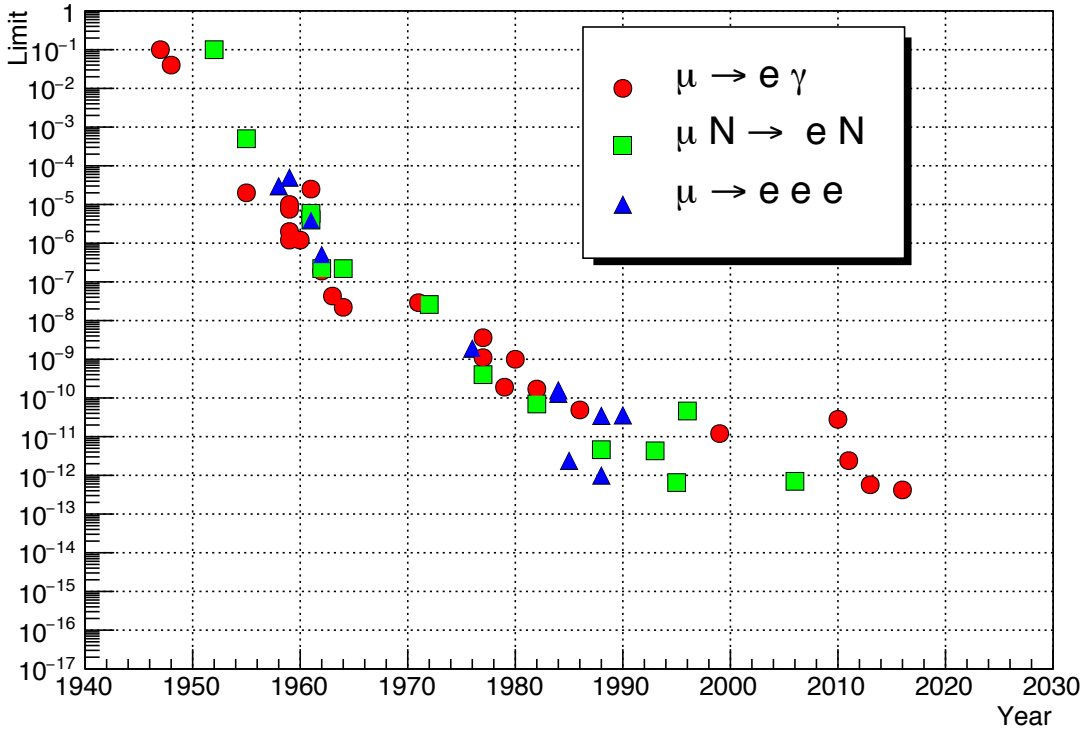

Figure 1.2: Branching ratios limit as function of the time for $\mu \to e\gamma$, $\mu N \to eN$ and $\mu \to eee$.[14]

1.3.2 Present bounds and future experimental directions

The interest in this CLFV has increased during the years because golden channels seem to be one of the best ways to go beyond the SM and this pushes the improvement of the experimental apparatus of the main experiments that are looking for these processes. The graph in Figure 1.2 shows how the limits on the branching ratios of muon channels have decreased over the years.

It is appropriate to examine what the next steps might be toward a sensitivity improvement and to examine whether there are objective limitations to these explorations[14]. If on the one hand the sensitivity scales with the number of muons, on the other hand, the capability to reject the background is related to the experimental acceptances and resolutions on the measurement of daughter particles. Furthermore, these two lines should proceed in parallel. $\mu^+ \to e^+\gamma$ and $\mu^+ \to e^+e^-e^+$ searches require intense muon beams. While the search of $\mu^+ \to e^+\gamma$ is not presently limited by the intensity of the beam, the staged approach of Mu3e requires the development of a high intensity beam line which is still in progress. Its estimated flux (10^{10} surface μ^+/s) is two order of magnitude larger than presently available. This does not necessarily translate into a two-order-of-magnitude increase in sensitivity, since with this flux the $\mu^+ \to e^+\gamma$ search will be completely overwhelmed by random coincidences at present-day resolutions. To reach the desired resolutions one could think of converting the photon and measuring the resulting e^+e^- pair to improve the energy measurement on the photon leg at the percent level. The usage of conversion pairs would allow tracking the photon back to the target, permitting a vertex constraint that is absent in present and planned experiments. A pointing calorimeter with a degree resolution could play the same role since the advantage of better resolutions of the pair spectrometer is partly spoiled by the additional multiple scattering on the converting material. An active target pinpointing the parent muon decay position could also help reduce the number of accidentals, both in $\mu^+ \to e^+\gamma$ and in $\mu \to eee$ searches, while spreading the muon beam decay points to several targets, and identifying the starting target of both positron and photon, would cut the random $e\gamma$ coincidences linearly with the number of targets. However, it must be taken into

account that the radiative background is at the level of 10^{-16} and 10^{-18} for $\mu^+ \to e^+\gamma$ and $\mu \to eee$ respectively even at excellent resolutions hence it seems reasonable to assume that $10^{-16} - 10^{-15}$ represent an ultimate limit for the $\mu^+ \to e^+\gamma$ decay search, maybe done with an "extended" Mu3e experiment, while the sensitivity to the $\mu \to eee$ decay itself could be pushed by a further order of magnitude with respect to the projected sensitivity by the usage of an active target but not much below. For $\mu \to e$ conversion experiments, there is no contribution from random coincidences and the DIO background could be kept below 10^{-19} provided the energy resolution is good enough. Reaching the level of 10^{-18} or above $R_{\mu e}$ would require an increase in signal and a reduction in background induced by beam pions and out-of-time particles. In this respect, the PRISM project (Phase Rotated Intense Slow Muon-source) is studying the production of a more intense negative muon pulsed beam (10^{11} μ^-/s) with an energy spread so small (below 0.5 MeV) to be able to stop the beam in a single thin target, to reduce the target contribution to the electron energy measurement. Instead of selecting monochromatic muons, reducing their number, their phase space is rotated so as to pass from a bunch of particles with a large energy spread but a sharp timing to particles spread in time ($\sim$ 100 ns) but with a narrow energy distribution, by means of a few turns in a fixed field, alternating gradient (FFAG) storage ring. Coupled to a COMET-like detector, this should allow one to reach a SES of $\approx 3 \times 10^{-18}$. A similar study is being conducted at the FNAL complex to increase by a factor of 10 of the muon beam line intensity using a 1 or 3 GeV proton beam on a production target while delivering the neutrino beam to LBNF. In this environment, a Mu2e-II experiment that reuses a large fraction of the Mu2e apparatus could provide a factor of 10 improved sensitivity. In any case, the limitation of low-energy photon and electron detection pinpoints the difficulty to go much beyond the present experimental resolutions. As a consequence, one might ask if innovative detection techniques should be explored. One promising technique is being applied in the field of direct measurement of neutrino mass and/or relic neutrino background detection by means of detecting the cyclotron radiation from electrons (of $\sim$ 20 keV energy) spiraling in a homogeneous magnetic field. They in fact follow helical orbits with an angular frequency that is independent of the emission angle, during which they lose energy, in the form of microwave radiation, due to cyclotron emission.
Let us eventually see what the current sensitivities and the expected future limit are for the main CLFV processes. The values reported in Table 1.1 are also those used in the rest of the dissertation.

Reaction	Present limit	Expected Limit	Experiment
$\mu^+ \to e^+\gamma$	$< 4.2 \times 10^{-13}$	5×10^{-14}	MEG II
$\mu^+ \to e^+e^-e^+$	$< 1.0 \times 10^{-12}$	10^{-16}	Mu3e
$\tau \to e\gamma$	$< 3.3 \times 10^{-8}$	5×10^{-9}	Belle II
$\tau \to \mu\gamma$	$< 4.4 \times 10^{-8}$	10^{-9}	”
$\tau \to eee$	$< 2.7 \times 10^{-8}$	5×10^{-10}	”
$\tau \to \mu\mu\mu$	$< 2.1 \times 10^{-8}$	5×10^{-10}	”
$\tau \to e$ had	$< 1.8 \times 10^{-8}$	3×10^{-10}	”
$\tau \to \mu$ had	$< 1.2 \times 10^{-8}$	3×10^{-10}	”
$h \to e\mu$	$< 3.5 \times 10^{-4}$	3×10^{-5}	HL-LHC
$h \to e^\pm\tau^\mp$	$< 2.2 \times 10^{-3}$	–	CMS
$h \to \mu^\pm\tau^\mp$	$< 1.5 \times 10^{-3}$	–	CMS
$Z \to e\mu$	$< 1.7 \times 10^{-6}$	–	DELPHI
$Z \to e^\pm\tau^\mp$	$< 5.0 \times 10^{-6}$	–	ATLAS
$Z \to \mu^\pm\tau^\mp$	$< 6.5 \times 10^{-6}$	–	ATLAS
$B^0 \to e^\pm\tau^\mp$	$< 2.8 \times 10^{-5}$	–	BaBar
$B^0 \to \mu^\pm\tau^\mp$	$< 1.2 \times 10^{-5}$	–	LHCb
$B^+ \to \pi^+e^\pm\tau^\mp$	$< 7.5 \times 10^{-5}$	–	BaBar
$B^+ \to \pi^+\mu^\pm\tau^\mp$	$< 7.2 \times 10^{-5}$	–	BaBar
$B^+ \to K^+e^\pm\tau^\mp$	$< 3.0 \times 10^{-5}$	–	BaBar
$B^+ \to K^+\mu^\pm\tau^\mp$	$< 4.8 \times 10^{-5}$	–	BaBar
$B^+ \to K^+\mu^-\tau^+$	$< 3.9 \times 10^{-5}$	–	LHCb
$B_s^0 \to \mu^\pm\tau^\mp$	$< 3.4 \times 10^{-5}$	–	LHCb

Table 1.1: Present and future limits for selected CLFV processes from [14] and [19].

Chapter 2

An effective approach to Lepton Flavor Violation

2.1 Effective Field Theory

In this section, generalities about Effective Field Theory are introduced to present a model-independent approach to study new physics effects. In particular, the so-called Standard Model Effective Field Theory (SMEFT) and the Low Energy Effective Field Theory (LEFT) are presented. At the end of this section, we report the considered effective operators contributing to CLFV and how they modify the Spontaneous Symmetry Breaking (SSB) of the SM.

2.1.1 Fermi theory of Weak Interactions

Starting from the experimental success of Quantum Electrodynamics and the second quantization formalism, in '30, Enrico Fermi proposed a theory for the proton $\beta-$decay, namely:

$$p \to n e^+ \nu_e.$$

This theory was based on a point-like interaction between two vector currents described by the Lagrangian[20]:

$$\mathscr{L}_F = -\frac{G_F}{\sqrt{2}} \left(\bar{p}\gamma_\mu n\right) \left(\bar{e}\gamma^\mu \nu_e\right), \tag{2.1}$$

where $G_F = 1.1663787(6) \cdot 10^{-5}\, GeV^{-2}$ is the Fermi constant. From this, we can evaluate the total decay rate which matches the experimental result quite well. This Lagrangian can be generalized introducing both a left-handed and a right-handed current as:

$$\mathscr{L}_F = -4\frac{G_F}{\sqrt{2}} \left(\bar{\psi}\gamma_\mu \left(c_L P_L + c_R P_R\right)\psi\right) \left(\bar{\psi}\gamma^\mu \left(c_L P_L + c_R P_R n\right)\psi\right), \tag{2.2}$$

where $P_{R,L} = \frac{1\pm\gamma_5}{2}$ are the chirality projectors and $c_{R,L}$ the associated weight. Finally, the Wu experiment showed that in weak interactions parity is maximally violated, therefore we obtain the so-called $V - A$ structure:

$$\mathscr{L}_F = -\frac{G_F}{\sqrt{2}} \left(\bar{\psi}\gamma_\mu \left(1 - \gamma_5\right)\psi\right) \left(\bar{\psi}\gamma^\mu \left(1 - \gamma_5\right)\psi\right). \tag{2.3}$$

This Lagrangian can be used to evaluate the decay width and cross section of weak interaction processes, for instance, for the muon decay ($\mu^- \to e^- \bar{\nu}_e \nu_\mu$) we obtain:

$$\Gamma(\mu^- \to e^- \bar{\nu}_e \nu_\mu) = \frac{G_F^2 m_\mu^5}{192\pi^3}, \tag{2.4}$$

which corresponds to a lifetime of $\tau_\mu = 2.2 \times 10^{-6}\, s$, in very good agreement with the experimental result $\tau_\mu^{exp} = (2.19703 \pm 0.00004) \times 10^{-6}\, s$. This calculation shows that the Fermi theory is a predictive theory as far as interactions at energies around the muon mass are concerned.
Let us move to the case of the scattering $\nu_\mu e^- \to \nu_e \mu^-$. Starting from the Fermi Lagrangian and neglecting electron and muon masses is straightforward to obtain:

$$\sigma(\nu_\mu e^- \to \nu_e \mu^-) \approx \frac{G_F^2 s}{\pi}, \tag{2.5}$$

this result has a good experimental comparison for low energies, but it fails when the centre of mass energy $\sqrt{s}$ increases. But this is not the only shortcoming, indeed since the cross section is proportional to s at some point unitarity will be broken, showing a bad ultraviolet behaviour. The violation of unitarity is linked to another feature of the theory: the non-renormalizability of the Fermi Lagrangian, indeed the mass dimension of the Fermi constant is $[G_F] = -2$, this implies that our theory cannot be predictive at any energy scale. The breaking of the Fermi theory is in fact associated to the appearance of other degrees of freedom. Today, these degrees of freedom are well know and they are the $W^\pm$ and the Z bosons. Once they are allowed to go on-shell, the predictions of the UV theory will be different from the predictions of the effective theory.
This brief discussion of the Fermi theory encodes the main aspects of Effective Field Theories which are going to be presented in the following.

2.1.2 Removing degrees of freedom

As discussed in the previous section, the building of an effective field theory is associated with neglecting degrees of freedom that at some energy scale, usually identified with the mass of the neglected particles, cannot go on-shell. Formally, we start from an ultraviolet action $S_{UV}[\phi_l, \phi_h]$, which is a functional of both light and heavy fields. However, working at energies $E \ll m_h$ we can get rid of the heavy degree of freedom and find an action $S_{IR}[\phi_l]$ which depends only on ϕ_l. The requirement is that the predictions of the two theories are the same in the energy range in which both are valid, this condition is referred to us as matching condition. In order to achieve this, one can define the infrared action through the Wilsonian effective action obtained integrating out ϕ_h[21]:

$$e^{iS_{IR}[\phi_l]} = \int D\phi_h e^{iS_{UV}[\phi_l, \phi_h]}. \tag{2.6}$$

After the integration, the original interactions of the light field change: not only the couplings get modified but also new interactions can appear. The object $S_{IR}[\phi_l]$ is usually a non-local functional, but it can be expanded in a series of local operators giving an effective Lagrangian of the form:

$$\mathscr{L}_{IR} = \frac{1}{2}\partial_\mu \phi_l \partial^\mu \phi_l - \frac{1}{2} m^2 \phi_l^2 - \sum_n \frac{c_n}{\Lambda_{UV}^{d_n - 4}} O^n[\phi_l, \partial\phi_l], \tag{2.7}$$

where c_n are dimensionless couplings, O^n is a generic operator respecting the symmetry imposed by the details of the UV theory on ϕ_l, d_n is its dimension and Λ_{UV} is an energy scale that signals the cut-off of the validity of the low energy theory. Therefore, the main aspects of an effective theory are

the following:

- The theory is valid only until a given energy scale at which the d.o.f. which have been integrated out are relevant again;
- The theory is not renormalizable: after the integration all higher dimension operators compatible with the symmetry appear, but the more the dimension the more the suppression due to the high energy scale Λ_{UV};
- The theory is predictive: one can match any experimental precision just taking as many terms in the expansion as needed.

2.1.3 Top-Down and Bottom-Up approach

In the Top-Down approach the UV theory is usually known, but maybe it is too complicated for the problem we are facing. For instance at the energies in which we are interested in, some degrees of freedom are not present and therefore one can build an effective theory integrating out those fields. Thinking about the example of the Fermi theory, if we want to evaluate the muon decay rate, since $m_\mu \ll M_W$ we can get rid of the Gauge W boson obtaining the Fermi Theory. To achieve the result, we can adopt a perturbative approach and perform the matching order by order in perturbation theory. The tree-level Feynman diagram of the UV theory is:

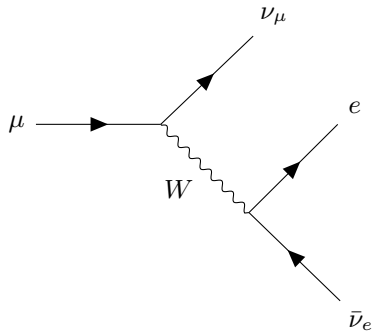

Figure 2.1: Feynman diagram contributing to the muon decay.

that gives an amplitude:

$$i\mathcal{M}_{UV} = -\frac{g^2}{2}(\bar{u}_{\nu_\mu}\gamma^\alpha P_L u_\mu)(\bar{u}_e\gamma^\beta P_L v_{\bar{\nu_e}})\Delta_{\alpha\beta}, \tag{2.8}$$

where

$$\Delta_{\alpha\beta}(k) = \frac{-i}{k^2 - M_W^2}(g_{\alpha\beta} - \frac{k_\alpha k_\beta}{M_W^2}), \tag{2.9}$$

is the W propagator. Since to perform the matching we are interested only in the low energy amplitude, where both the electro-weak theory and the Fermi theory are valid, we can approximate it as

$$\Delta_{\alpha\beta} = \frac{-i}{M_W^2}g_{\alpha\beta}. \tag{2.10}$$

Now, just comparing with the Lagrangian in Eq. (2.3), which is related to the amplitude of the muon decay predicted by the Fermi theory, we obtain the tree-level matching condition:

$$\frac{G_F}{\sqrt{2}} = \frac{g^2}{8M_W^2}. \tag{2.11}$$

An alternative way to perform the matching at tree level is the so-called equation of motion method, which consists of the substitution of the heavy mode with its classical equation of motion solution. Indeed, the condition in Eq. (2.6) becomes very easy neglecting higher loop corrections:

$$S_{IR}[\phi_l] = S_{UV}[\phi_l, \phi_h^c(\phi_l)], \tag{2.12}$$

where $\phi_h^c(\phi_l)$ is the solution of the Euler-Lagrange equation of motion, namely

$$\frac{\delta S_{UV}}{\delta \phi_h} = 0. \tag{2.13}$$

It is possible to reproduce the result in Eq. (2.11) applying this procedure to the Lagrangian of the standard model electroweak sector:

$$\mathscr{L} = M_W^2 W_+^\mu W_\mu^- - \frac{g}{\sqrt{2}}(W_\mu^- J_+^\mu + W_\mu^+ J_-^\mu), \tag{2.14}$$

where $J_+^\mu = \bar{e}\gamma^\mu P_L \nu_e$ and J_-^μ is the Hermitian conjugate. In the Lagrangian 2.14 higher orders in g and derivative terms have been neglected. Within this approximation the solution of the equation of motion is straightforward, and it is

$$W_\pm^\mu = \frac{g}{\sqrt{2}M_W^2} J_\pm^\mu. \tag{2.15}$$

Finally, substituting in 2.14 we get:

$$\mathscr{L} = -\frac{g^2}{2M_W^2} J_-^\mu J_\mu^+, \tag{2.16}$$

comparing with 2.3, it again leads to $\frac{G_F}{\sqrt{2}} = \frac{g^2}{8M_W^2}$. If needed, we could systematically improve the Fermi theory so that, in its validity regime, it approximates even better the SM predictions: we could maintain the kinetic term in the Lagrangian 2.14, in order to obtain a series of higher-order operators that are going to be increasingly suppressed by the W mass. For example, an operator with two derivatives and four fermions, such as $aG_F^2 \bar{\psi}\psi\Box\bar{\psi}\psi$. Less trivially, we could calculate loop corrections to the muon decay process in the SM, and those could also be reproduced in the EFT at any order in perturbation theory[22].
The previous procedures are possible to follow only in the case where we know the UV theory and its details. Nevertheless, even if we do not have an UV completion, the EFT approach is, anyway, very powerful to investigate the properties of an unknown theory. The point is that once we know the degrees of freedom and symmetries of our theory, we can build the most general Lagrangian in terms of dimensionless coefficients and some energy scale Λ that marks the UV cut-off point of our effective theory.

Let us take again the case of the Fermi theory, but in this case we suppose that we do not know anything about the Standard Model. At this stage, we can write down the most general Lorentz invariant Lagrangian involving only fermions:

$$\begin{aligned}\mathscr{L} =& \bar{\psi}(i\partial\!\!\!/ - m)\psi - \frac{c_1}{\Lambda^2}(\bar{\psi}\psi)(\bar{\psi}\psi) - \frac{c_2}{\Lambda^2}(\bar{\psi}\gamma_5\psi)(\bar{\psi}\gamma_5\psi) - \frac{c_3}{\Lambda^2}(\bar{\psi}\gamma_\mu\psi)(\bar{\psi}\gamma^\mu\psi) \\ &- \frac{c_4}{\Lambda^2}(\bar{\psi}\gamma_\mu\gamma_5\psi)(\bar{\psi}\gamma^\mu\gamma_5\psi) - ...\end{aligned} \tag{2.17}$$

From this theory and comparing its predictions with the experimental results, one can fix the ratios

$\frac{c_i}{\Lambda^2}$, which makes this Lagrangian suitable for other predictions. But this is not the end of the story; indeed, one can understand the structure of the interactions involved in the analyzed experiment. For example, for muon decay the operators associated with c_3 and c_4 are going to contribute, allowing understanding of the $V-A$ structure of Fermi theory and the violation of parity of the weak interactions. Furthermore, once we measure the ratios $\frac{c_i}{\Lambda^2}$ with an assumption on the coefficients, such as the naturalness assumption $c_i \sim \mathcal{O}(1)$, it is possible to infer an estimation for the scale Λ and therefore the energy at which unknown physics becomes relevant.
Therefore, the Bottom-Up approach is useful to push our knowledge to a more fundamental level, and can be applied to the Standard Model, building the so-called Standard Model Effective Field Theory (SMEFT).

2.1.4 SMEFT and LEFT

The Standard Model Effective Field Theory corresponds to the most general Lagrangian involving the standard model fields, that is, Lorentz invariant and Gauge $SU(3)_c \times SU(2)_L \times U(1)_Y$ invariant. Therefore, it can be written as:

$$\mathscr{L}_{SMEFT} = \mathscr{L}_{SM} + \sum_{d>4} \sum_i \frac{C_i^{(d)}}{\Lambda^{d-4}} Q_i^{(d)}. \tag{2.18}$$

The $C_i^{(d)}$ are referred to us as Wilson coefficients and $Q_i^{(d)}$ are generic operators respecting the symmetry conditions of dimension d. This Lagrangian allows for a model-independent study of the new-physics effects: The unknown degrees of freedom of the UV completion have been integrated out, and their effect can be encoded only into the Wilson coefficients. Since the Standard Model Lagrangian already contains all renormalizable operators, the first operator of the effective theory can arise only at dimension five. Actually, it turns out that there is only one five-dimensional operator, called the Weinberg operator[23]:

$$Q_1^{(5)} = \epsilon_{ij}\epsilon_{kl}(L_{ir}^T C L_{ks})\Phi_j \Phi_l + h.c. \tag{2.19}$$

Here, r, s are flavor indices, i, j, k, l are $SU(2)$ Gauge indices, L represents a lepton field, and Φ is the Higgs field. This interaction violates the lepton number by two units and gives a Majorana mass term to neutrinos when Φ gets a vacuum expectation value. At dimension six there are eight different operator classes: three field strengths X^3, six Higgs fields Φ^6, four Higgs and two derivatives $\Phi^4 D^2$, two field strengths and two Higgs $\Phi^2 X^2$, two fermions and three Higgs $\psi^2\Phi^3$, two fermions, one Higgs and one field strength $\psi^2\Phi X$, two fermions, two Higgs and one derivative $\psi^2\Phi^2 X$ and four fermions ψ^4[23]. The main task is then to find a basis on which all operators are truly independent; the list of independent operators is reported in [24]. The higher the dimension of the operators, the more the coefficients are suppressed by the UV scale Λ, therefore, in the following we stop the expansion at dimension six, neglecting higher dimension operators.
The procedure to investigate new-physics effects is the following:

- To build up the effective Lagrangian identifying the operators at a given dimension, which contributes to the processes we are interested in;
- to compute physical quantities that are going to be a function of the Wilson coefficients;
- to compare the results with the present experimental bounds, in order to derive constraints about the Wilson coefficients, assuming a reference value for the cut-off Λ or infer bounds on the scale Λ, with some assumptions on the Wilson coefficients.

The above procedure encounters some technical problems that can only be solved by improving the usual perturbation approach adopted within the SM calculations. The main point is that the new physics arises at the energy scale Λ, but usually we have to evaluate the observable at the energies of the process of interest to be compared with the experiment; let us call it E. In ordinary perturbation theory, the tree-level plus 1-loop matching gives terms like[23]:

$$C_i(\mu) = C_i^0(\Lambda) + k\frac{\alpha}{4\pi} log\frac{\Lambda}{\mu}, \tag{2.20}$$

and if we try to set $\mu = E$ we get the so-called Large Logarithm: If the two scales E and Λ are widely separated this can spoil the perturbative hypothesis even if $\alpha < 4\pi$. To solve this problem, the adopted procedure is the renormalization group improved perturbation theory: the idea is to perform the matching at the high scale to avoid the Large Logs and then to follow the flow of the renormalization group through the renormalization group equation until the low-energy scale. To understand the correct procedure, let us first of all observe that since we are dealing with a non-renormalizable theory, the wave function and coupling renormalization are not enough to fix all the divergencies; therefore an additional renormalization, referred to as operator renormalization, is necessary. Defining the bare operator Q_i^0, the renormalized one Q_i and the renormalization matrix Z_{ij}, we can then write

$$Q_i^0 = Z_{ij} Q_i. \tag{2.21}$$

The first important observation is that we can have the so-called operator mixing: after the renormalization procedure, we could possibly find nonvanishing coefficients even for operators that are not present at the beginning as long as they respect the symmetry. This operator renormalization is completely equivalent to the renormalization of the Wilson coefficients because the bare term of the Lagrangian is related to the renormalized one by:

$$C_i^{(0)} Q_i^0 = Z_{ij} C_i Q_j, \tag{2.22}$$

and therefore the result of the renormalization procedure on the couplings reads:

$$C_i^{(0)} = Z_{ji} C_j. \tag{2.23}$$

Then, since the bare coefficients are independent on the scale, we can differentiate this relation obtaining:

$$\frac{d}{d\, log\mu} C_i(\mu) = \gamma_{ji} C_j(\mu), \tag{2.24}$$

where γ is called anomalous dimension matrix defined as:

$$\gamma = Z^{-1} \frac{d}{d\, log\mu} Z, \tag{2.25}$$

and it can be computed using ordinary perturbation theory. At this stage we are ready to obtain the running of the Wilson coefficients through[25]:

$$C_i(\mu) = Pexp\left[\int_{g(\Lambda)}^{g(\mu)} \frac{\gamma^T(g)}{\beta(g)} dg\right]_{ij} C_j(\Lambda), \tag{2.26}$$

where P denotes the coupling constant ordering and β is the β-function. As pointed out before, the

initial condition is set to the coupling at the high scale, as written in the lower integration bound. The advantage of the renormalization group improved perturbation theory is that now the logarithmic corrections $(\frac{\alpha}{4\pi} log \frac{\Lambda}{\mu})^n$[23] are resummed to all orders; this is what is called Leading Log Approximation and allows us to avoid the spoiling of perturbation theory.
An analogous discussion can be repeated for the effective theory below the electroweak scale. In this case, one can write a Low-Energy Effective Theory (LEFT) with quark and lepton fields, and only QCD and QED gauge fields. Operators have been classified in [26]. Since $SU(2)$ gauge invariance is no longer required, there are several new types of operator beyond those in SMEFT.

- There are dimension-three $\nu\nu$ operators which give a Majorana neutrino mass for left-handed neutrinos.
- There are dimension-five dipole operators. These are the analogs of the $(\bar{L}R)X\Phi$ operators of SMEFT, which turn into dimension-five operators when Φ is replaced by its vacuum expectation value v. There are 70 Hermitian $\Delta B = \Delta L = 0$ dipole operators for three generations.
- There are X^3 and ψ^4 operators as in SMEFT, but operators containing Φ are no longer present.
- There are $\Delta L = 4$ ν^4 operators, and $\Delta L = 2$ $(\bar{\psi}\psi)\nu\nu$ four-fermion operators, as well as four-fermion $\Delta B = -\Delta L$ operators.
- There are 3631 Hermitian $\Delta B = \Delta L = 0$ dimension-six operators for three generations.

The complete renormalization group equations up to dimension six have been worked out in [26]. As far as LEFT is concerned, since the theory has dimension-five operators, there are nonlinear terms from two insertions of dimension-five operators for the dimension-six running.
Let us see how the Standard Model Effective Field theory provides a model-independent approach to describe the possible deviations from the SM in CLFV processes. As seen before, the only five-dimensional operator is the Weinberg operator in Eq. (2.19) but it induces CLFV only at the loop level and with negligible small rates. Therefore, the first relevant CLFV effects arise at dimension six from the operators shown in Table 2.1. where τ_I are the Pauli matrices, a and b flavor indices, $B_{\mu\nu}$ and $W^I_{\mu\nu}$ are the $U(1)_Y$ and $SU(2)_L$ field strengths, respectively, as explained in Chapter 1.
Since the first part of the dissertation consists in studying low-energy CLFV processes, the first step is to understand how the SMEFT operators influence physics below the electroweak scale. The starting point is the SMEFT Lagrangian:

$$\mathscr{L}_{SMEFT} = \mathscr{L}_{SM} + \sum_i \frac{C_i}{\Lambda^2} Q_i, \tag{2.27}$$

where Q_i are the operators reported in Table 2.1. On the other hand, the operators that survive at low energies are classified in the LEFT, whose Lagrangian reads:

$$\mathscr{L}_{LEFT} = \mathscr{L}_{QED} + \mathscr{L}_{QCD} + \mathscr{L}_F + \sum_i \frac{c_i}{\Lambda^2} O_i, \tag{2.28}$$

where the operators O_i, relevant for our purpose, are presented in Table 2.2. The goal of the next chapter is to obtain an effective Lagrangian below the electroweak scale able to describe the main CLFV processes in terms of the SMEFT Wilson coefficients.

2.1.5 Spontaneous symmetry breaking in the SMEFT

Since we are interested in the low-energy regime, it is useful to work in the spontaneously broken SMEFT. In particular, there are some differences with respect to the Standard Model, which can

4-leptons operators		Dipole operators	
$Q_{\ell\ell}$	$(\bar{L}_L\gamma_\mu L_L)(\bar{L}_L\gamma^\mu L_L)$	Q_{eW}	$(\bar{L}_L\sigma^{\mu\nu}e_R)\tau_I\Phi W^I_{\mu\nu}$
Q_{ee}	$(\bar{e}_R\gamma_\mu e_R)(\bar{e}_R\gamma^\mu e_R)$	Q_{eB}	$(\bar{L}_L\sigma^{\mu\nu}e_R)\Phi B_{\mu\nu}$
$Q_{\ell e}$	$(\bar{L}_L\gamma_\mu L_L)(\bar{e}_R\gamma^\mu e_R)$		
2-lepton 2-quark operators			
$Q^{(1)}_{\ell q}$	$(\bar{L}_L\gamma_\mu L_L)(\bar{Q}_L\gamma^\mu Q_L)$	$Q_{\ell u}$	$(\bar{L}_L\gamma_\mu L_L)(\bar{u}_R\gamma^\mu u_R)$
$Q^{(3)}_{\ell q}$	$(\bar{L}_L\gamma_\mu\tau_I L_L)(\bar{Q}_L\gamma^\mu\tau_I Q_L)$	Q_{eu}	$(\bar{e}_R\gamma_\mu e_R)(\bar{u}_R\gamma^\mu u_R)$
Q_{eq}	$(\bar{e}_R\gamma^\mu e_R)(\bar{Q}_L\gamma_\mu Q_L)$	$Q_{\ell edq}$	$(\bar{L}^a_L e_R)(\bar{d}_R Q^a_L)$
$Q_{\ell d}$	$(\bar{L}_L\gamma_\mu L_L)(\bar{d}_R\gamma^\mu d_R)$	$Q^{(1)}_{\ell equ}$	$(\bar{L}^a_L e_R)\epsilon_{ab}(\bar{Q}^b_L u_R)$
Q_{ed}	$(\bar{e}_R\gamma_\mu e_R)(\bar{d}_R\gamma^\mu d_R)$	$Q^{(3)}_{\ell equ}$	$(\bar{L}^a_i\sigma_{\mu\nu}e_R)\epsilon_{ab}(\bar{Q}^b_L\sigma^{\mu\nu}u_R)$
Lepton-Higgs operators			
$Q^{(1)}_{\Phi\ell}$	$(\Phi^\dagger i\overleftrightarrow{D}_\mu\Phi)(\bar{L}_L\gamma^\mu L_L)$	$Q^{(3)}_{\Phi\ell}$	$(\Phi^\dagger i\overleftrightarrow{D}^I_\mu\Phi)(\bar{L}_L\tau_I\gamma^\mu L_L)$
$Q_{\Phi e}$	$(\Phi^\dagger i\overleftrightarrow{D}_\mu\Phi)(\bar{e}_R\gamma^\mu e_R)$	$Q_{e\Phi 3}$	$(\bar{L}_L e_R\Phi)(\Phi^\dagger\Phi)$

Table 2.1: Complete list of CLFV dimension-6 operators in SMEFT from [27]. Flavor indices of the fermions are not indicated.

Vector 4-leptons operators	
$O^V_{\ell\ell}$	$(\bar{L}_L\gamma_\mu L_L)(\bar{L}_L\gamma^\mu L_L)$
O^V_{ee}	$(\bar{e}_R\gamma_\mu e_R)(\bar{e}_R\gamma^\mu e_R)$
$O^V_{\ell e}$	$(\bar{L}_L\gamma_\mu L_L)(\bar{e}_R\gamma^\mu e_R)$
Dipole operator	
$O_{e\gamma}+h.c.$	$(\bar{L}_L\sigma^{\mu\nu}e_R)F_{\mu\nu}$
Scalar 4-leptons operators	
$O^S_{ee}+h.c.$	$(\bar{e}_L e_R)(\bar{e}_L e_R)$

Table 2.2: Complete list of CLFV dimension-6 operators in LEFT from [26]. Flavor indices of the fermions are not indicated.

introduce flavor violation.
Let us first notice that spontaneous symmetry breaking of the Standard Model is modified in SMEFT due to the operator $Q_{e\Phi 3}$. Therefore, fermion mass matrices and Higgs-fermion couplings change. In particular, we obtain:

$$\begin{aligned}\mathscr{L}_{SMEFT} \supset & -\bar{e}^i_R [Y_e]_{ij} \Phi^\dagger L^j_L + \frac{[C^*_{e\Phi 3}]_{ji}}{\Lambda^2} (\Phi^\dagger \Phi)(\bar{e}^i_R L^j_L \Phi^\dagger) + h.c \\ = & - [M_e]_{ij} \bar{e}^i_R e^j_L - h [\mathcal{Y}_e]_{ij} \bar{e}^i_R e^j_L + h.c.\end{aligned} \tag{2.29}$$

where the modified mass and fermion-Higgs coupling are given by:

$$\begin{aligned}[M_e]_{ij} =& \frac{v}{\sqrt{2}} \left([Y_e]_{ij} - \frac{v^2}{2} \frac{[C^*_{e\Phi 3}]_{ji}}{\Lambda^2} \right), \\ [\mathcal{Y}_e]_{ij} =& \frac{1}{\sqrt{2}} \left([Y_e]_{ij} - \frac{3v^2}{2} \frac{[C^*_{e\Phi 3}]_{ji}}{\Lambda^2} \right) = \frac{[M_e]_{ij}}{v} - \frac{v^2}{\sqrt{2}} \frac{[C^*_{e\Phi 3}]_{ji}}{\Lambda^2}.\end{aligned} \tag{2.30}$$

Finally, we have to move from the interaction basis to the mass-eigenstate basis through the following unitary transformations:

$$L_L \to L_e L_L, \quad e_R \to R_e e_R. \tag{2.31}$$

Clearly, as in the unextended Standard Model, these transformations bring the mass matrix in diagonal form:

$$M_e \to \hat{M}_e = L^\dagger_e M_e R_e = diag(m_e, m_\mu, m_\tau). \tag{2.32}$$

Conversely, the couplings of the Higgs boson to leptons are not proportional to the mass matrix anymore, and flavor violating couplings are generated:

$$\mathcal{Y}_e \to \hat{\mathcal{Y}}_e = L^\dagger_e \mathcal{Y}_e R_e = \frac{\hat{M}_e}{v} - \frac{v^2}{\sqrt{2}\Lambda^2} L^\dagger_e C^\dagger_{e\Phi 3} R_e. \tag{2.33}$$

The rest of the Lagrangian is left unchanged by these unitary transformations. Clearly, analogous rotations need to be performed in the quark sector, but they are irrelevant for our purpose.
The next step is to consider the dipole operators Q_{eW} and Q_{eB}. Below the electroweak scale, Higgs field acquires its vacuum expectation value $\Phi = \begin{pmatrix} 0 \\ \frac{v}{\sqrt{2}} \end{pmatrix}$, in addition W and B mix giving rise to photon and Z dipole operators:

$$\begin{aligned}\mathscr{L}_{eff} =& \frac{C^{ij}_{e\gamma}}{\Lambda^2} \frac{v}{\sqrt{2}} \bar{e}_i \sigma_{\mu\nu} P_R e_j F^{\mu\nu} + \frac{C^{ji}_{e\gamma}}{\Lambda^2} \frac{v}{\sqrt{2}} \bar{e}_j \sigma_{\mu\nu} P_R e_i F^{\mu\nu} + \\ & - \frac{C^{ij}_{eZ}}{\Lambda^2} \frac{v}{\sqrt{2}} \bar{e}_i \sigma_{\mu\nu} P_R e_j Z^{\mu\nu} - \frac{C^{ji}_{eZ}}{\Lambda^2} \frac{v}{\sqrt{2}} \bar{e}_j \sigma_{\mu\nu} P_R e_i Z^{\mu\nu} + h.c.\end{aligned} \tag{2.34}$$

where the coefficients are defined as:

$$C^{ij}_{e\gamma} = cos\theta_W C^{ij}_{eB} - sin\theta_W C^{ij}_{eW}, \qquad C^{ij}_{eZ} = cos\theta_W C^{ij}_{eW} + sin\theta_W C^{ij}_{eB}. \tag{2.35}$$

Therefore, lepton flavor violating γ and Z vertices arise naturally at tree level in SMEFT. However, since we are also interested in evaluating the Higgs radiative decay, above the electroweak scale, we

have the following additional interactions:

$$\begin{aligned}\mathscr{L}_{eff} =&\frac{C_{e\gamma}^{ij}}{\Lambda^2}\frac{h}{\sqrt{2}}\bar{e}_i\sigma_{\mu\nu}P_R e_j F^{\mu\nu} + \frac{C_{e\gamma}^{ji}}{\Lambda^2}\frac{h}{\sqrt{2}}\bar{e}_j\sigma_{\mu\nu}P_R e_i F^{\mu\nu} + \\ &-\frac{C_{eZ}^{ij}}{\Lambda^2}\frac{h}{\sqrt{2}}\bar{e}_i\sigma_{\mu\nu}P_R e_j Z^{\mu\nu} - \frac{C_{eZ}^{ji}}{\Lambda^2}\frac{h}{\sqrt{2}}\bar{e}_j\sigma_{\mu\nu}P_R e_i Z^{\mu\nu} + h.c.\end{aligned} \tag{2.36}$$

In addition, considering Table 2.1, one realizes that the Lepton-Higgs operators can modify the usual couplings of the standard model Lagrangian for the weak interactions. Indeed, considering $Q_{\Phi\ell}^{(1)}$, $Q_{\Phi\ell}^{(3)}$ and $Q_{\Phi e}$, setting the Higgs field to its vacuum expectation value and moving to the mass basis a lepton flavor violating vertex is obtained. We parameterize this interaction as follows:

$$i\Gamma_{Z,ij}^{\mu} = i\left(\gamma^{\mu}\left[a_{ij}^{Z}P_L + b_{ij}^{Z}P_R\right]\right). \tag{2.37}$$

The contributions arising from the Lepton-Higgs operators are:

$$\begin{aligned}a_{ij}^{Z} &= \frac{g_2}{2cos\theta_W}\left(\frac{v^2}{\Lambda^2}\left(C_{\Phi\ell}^{(1)ij} + C_{\Phi\ell}^{(3)ij}\right) + \left(1 - 2sin^2\theta_W\right)\delta_{ij}\right), \\ b_{ij}^{Z} &= \frac{g_2}{2cos\theta_W}\left(\frac{v^2}{\Lambda^2}C_{\Phi e}^{ij} - 2sin^2\theta_W\delta_{ij}\right),\end{aligned} \tag{2.38}$$

where the diagonal part is the SM coupling.
Not only the Z-boson interactions, but also the W-boson interactions get modification from the Lepton-Higgs operators, parametrizing the vertex between the W boson, lepton and neutrino as:

$$i\Gamma_{W,ij}^{\mu} = i\gamma^{\mu}a_{ij}^{W}P_L, \tag{2.39}$$

the contribution arising from the Lepton-Higgs operators is:

$$a_{ij}^{W} = -\frac{g_2}{\sqrt{2}}\left(\frac{v^2}{\Lambda^2}C_{\phi\ell}^{(3)ik} + \delta_{ik}\right)U_{kj}. \tag{2.40}$$

In the following sections we are going to see how the aforementioned new or modified couplings affect the low-energy observables both at tree level and 1-loop level.

Chapter 3

Low-energy probes of Lepton Flavor Violation

3.1 Tree-level LFV decays

In this section, we present the results, with detailed calculations, of the considered decay processes at tree-level. In addition, several constraints on the SMEFT operators are obtained comparing the branching fractions to the experimental bounds.

3.1.1 SMEFT-LEFT tree-level matching

In the previous section we have evaluated the modification of the SM couplings due to the SMEFT operators, now we want to understand their contributions to the Low Energy Effective Field Theory coefficients.
The first set of operators that we consider are the dipole operators Q_{eW} and Q_{eB}. Starting from Eq. (2.34), the matching with the LEFT Lagrangian gives

$$c_{e\gamma}^{ij} = C_{e\gamma}^{ij}\frac{v}{\sqrt{2}}, \qquad c_{e\gamma}^{ji} = C_{e\gamma}^{ji}\frac{v}{\sqrt{2}}, \tag{3.1}$$

with

$$C_{e\gamma}^{ij} = cos\theta_W C_{eB}^{ij} - sin\theta_W C_{eW}^{ij}. \tag{3.2}$$

In addition, we have modification to the 4-fermion operators through Z-boson exchange due to the Z-dipoles in Eq. (2.34). However, in the low energy limit, we can safely neglect this contribution. Indeed, because of the fact that the momentum appears in the numerator of the amplitude, the decay rate would be suppressed by the ratio between external lepton masses and the Z mass. The situation will be different in the case of the high energy scattering where the Z-dipole operator will give an important contribution.
The next contributions arise trivially from the 4-lepton operators which directly give non vanishing coefficients for the vector 4-lepton operators of the LEFT. The matching conditions are simply given by:

$$c_{\ell\ell}^{V,ijlk} = C_{\ell\ell}^{ijlk}, \qquad c_{\ell e}^{V,ijlk} = C_{\ell e}^{ijlk}, \qquad c_{ee}^{V,ijlk} = C_{ee}^{ijlk}. \tag{3.3}$$

The other contributions come from diagrams where either a Z-boson or a Higgs boson is exchanged. Let us start from the first one, the Feynman diagram in the spontaneously broken SMEFT is the

following:

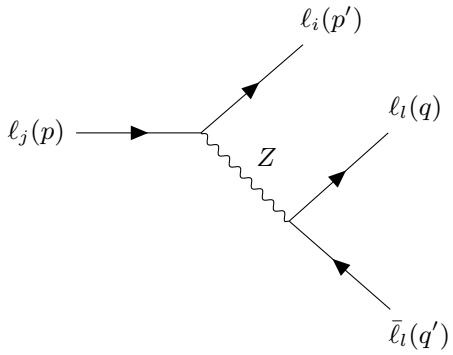

Figure 3.1: Feynman diagram contributing to LFV four-lepton interactions through Z exchange.

The Feynman rules are the same as the ones reported in Eq. (2.38) and therefore the amplitude in the unitary Gauge is given by:

$$i\mathcal{M} = \bar{u}_i(p')\gamma_\mu(a^Z_{ij}P_L + b^Z_{ij}P_R)u_j(p)\frac{i}{(p-p')^2 - M_Z^2}\bar{u}_l(q)\gamma^\mu(a^Z_{ll}P_L + b^Z_{ll}P_R)u_l(q'). \tag{3.4}$$

In the low-energy approximation we can integrate out the Z-boson at tree level obtaining

$$i\mathcal{M} = -\frac{i}{M_Z^2}\bar{u}_i(p')\gamma_\mu(a^Z_{ij}P_L + b^Z_{ij}P_R)u_j(p)\bar{u}_l(q)\gamma^\mu(a^Z_{ll}P_L + b^Z_{ll}P_R)u_l(q'). \tag{3.5}$$

The last equation provides us the matching conditions regarding the vector LEFT coefficients:

$$\begin{aligned}
\frac{c^{V,ijll}_{\ell\ell}}{\Lambda^2} &= \frac{a^Z_{ij}a^Z_{ll}}{M_Z^2} = \frac{\left(C^{(1)ij}_{\Phi\ell} + C^{(3)ij}_{\Phi\ell}\right)}{\Lambda^2}(2sin^2\theta_W - 1),\\
\frac{c^{V,ijll}_{ee}}{\Lambda^2} &= \frac{b^Z_{ij}b^Z_{ll}}{M_Z^2} = 2sin^2\theta_W\frac{C^{ij}_{\Phi e}}{\Lambda^2},\\
\frac{c^{V,ijll}_{\ell e}}{\Lambda^2} &= \frac{a^Z_{ij}b^Z_{ll}}{M_Z^2} = 2sin^2\theta_W\frac{\left(C^{(1)ij}_{\Phi\ell} + C^{(3)ij}_{\Phi\ell}\right)}{\Lambda^2},\\
\frac{c^{V,llij}_{\ell e}}{\Lambda^2} &= \frac{b^Z_{ij}a^Z_{ll}}{M_Z^2} = (2sin^2\theta_W - 1)\frac{C^{ij}_{\Phi e}}{\Lambda^2}.
\end{aligned} \tag{3.6}$$

Moreover, from Eq. (2.30) we obtain an additional diagram involving the exchange of the Higgs boson:

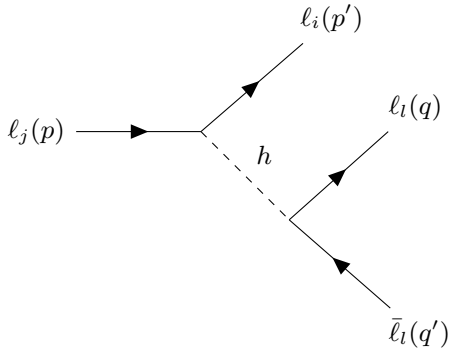

Figure 3.2: Feynman diagram contributing to LFV four-lepton interactions through Higgs exchange.

Therefore, the amplitude is:

$$\mathcal{M} = -\frac{m_l v}{\sqrt{2}\Lambda^2}\bar{u}_i(p')\left[([L_e^\dagger C^\dagger_{e\Phi 3}R_e]_{ji}P_L + [L_e^\dagger C^\dagger_{e\Phi 3}R_e]_{ij}P_R)\right]u_j(p)\frac{1}{(p-p')^2 - m_h^2}\bar{u}_l(q)u_l(q'), \quad (3.7)$$

and below the electroweak scale, integrating out the h-boson we get

$$\mathcal{M} = \frac{m_l v}{\sqrt{2}m_h^2\Lambda^2}\bar{u}_i(p')\left[([L_e^\dagger C^\dagger_{e\Phi 3}R_e]_{ji}P_L + [L_e^\dagger C^\dagger_{e\Phi 3}R_e]_{ij}P_R)\right]u_j(p)\bar{u}_l(q)u_l(q'), \quad (3.8)$$

and finally we find the matching results

$$\begin{aligned}
\frac{c^{S,ijll}_{\ell\ell}}{\Lambda^2} &= \frac{m_l v}{\sqrt{2}m_h^2\Lambda^2}[L_e^\dagger C^\dagger_{e\Phi 3}R_e]_{ji},\\
\frac{c^{S,ijll}_{\ell e}}{\Lambda^2} &= \frac{m_l v}{\sqrt{2}m_h^2\Lambda^2}[L_e^\dagger C^\dagger_{e\Phi 3}R_e]_{ji},\\
\frac{c^{S,llij}_{\ell e}}{\Lambda^2} &= \frac{m_l v}{\sqrt{2}m_i m_h^2\Lambda^2}[L_e^\dagger C^\dagger_{e\Phi 3}R_e]_{ij},\\
\frac{c^{S,ijll}_{ee}}{\Lambda^2} &= \frac{m_l v}{\sqrt{2}m_h^2\Lambda^2}[L_e^\dagger C^\dagger_{e\Phi 3}R_e]_{ij}.
\end{aligned} \quad (3.9)$$

It is worth noting that coefficients with flavor indices like $(ijlk)$, but also $(iklk)$ receive contribution only from the 4-lepton operators. Indeed, in the case of boson exchange two effective operators are required and thus they would be suppressed by $\frac{1}{\Lambda^4}$.
The calculations carried out until now, allow us to obtain the final results for the matching between SMEFT and LEFT at tree level, for the operators of Table 2.1. The vector four-leptons operators coefficients are given in Table 3.1. From these vector operators using Fierz identities (reported in Appendix A) one can find also a contribution to the scalar coefficients, indeed the following relation holds:

$$(\bar{a}P_L b)(\bar{c}P_R d) = -\frac{1}{2}(\bar{a}\gamma_\mu P_R d)(\bar{c}\gamma^\mu P_L b). \quad (3.10)$$

In Table 3.2 the final results for the scalar 4-lepton operators are presented and eventually we report also the matching for the photon dipole operators at tree-level in Table 3.3. In the next section the modification of the matching conditions at the one loop level are evaluated.

3.1.2 $\ell_i \to \ell_j\gamma$

Let us start analyzing the case of $\mu \to e\gamma$, but the same calculations are valid also in the case of $\tau \to e\gamma$ and $\tau \to \mu\gamma$. This decay is induced already at tree level through the dipole operators Q_{eW} and Q_{eB} shown in Table 2.1. Indeed, in the previous subsection we have seen that

$$c^{ij}_{e\gamma} = C^{ij}_{e\gamma}\frac{v}{\sqrt{2}}, \qquad c^{ji}_{e\gamma} = C^{ji}_{e\gamma}\frac{v}{\sqrt{2}}. \quad (3.11)$$

The initial 4−momentum of the muon and the final 4−momentum of the electron are referred to us as p_1 and p_2 respectively, while the photon momentum is called k. The Feynman diagram associated with the tree-level muon decay is:

O_i	c_i
$(\bar{e}_L\gamma_\mu\mu_L)(\bar{e}_L\gamma^\mu e_L)$	$C_{\ell\ell}^{e\mu ee} + \left(C_{\Phi\ell}^{(1)e\mu} + C_{\Phi\ell}^{(3)e\mu}\right)(2sin^2\theta_W - 1)$
$(\bar{\mu}_L\gamma_\mu\tau_L)(\bar{\mu}_L\gamma^\mu\mu_L)$	$C_{\ell\ell}^{\mu\tau\mu\mu} + \left(C_{\Phi\ell}^{(1)\mu\tau} + C_{\Phi\ell}^{(3)\mu\tau}\right)(2sin^2\theta_W - 1)$
$(\bar{e}_L\gamma_\mu\tau_L)(\bar{e}_L\gamma^\mu e_L)$	$C_{\ell\ell}^{e\tau ee} + \left(C_{\Phi\ell}^{(1)e\tau} + C_{\Phi\ell}^{(3)e\tau}\right)(2sin^2\theta_W - 1)$
$(\bar{\mu}_L\gamma_\mu\tau_L)(\bar{e}_L\gamma^\mu e_L)$	$C_{\ell\ell}^{\mu\tau ee} + \left(C_{\Phi\ell}^{(1)\mu\tau} + C_{\Phi\ell}^{(3)\mu\tau}\right)(2sin^2\theta_W - 1)$
$(\bar{e}_L\gamma_\mu\tau_L)(\bar{\mu}_L\gamma^\mu\mu_L)$	$C_{\ell\ell}^{e\tau\mu\mu} + \left(C_{\Phi\ell}^{(1)e\tau} + C_{\Phi\ell}^{(3)e\tau}\right)(2sin^2\theta_W - 1)$
$(\bar{e}_L\gamma_\mu\tau_L)(\bar{\mu}_L\gamma^\mu\mu_L)$	$C_{\ell\ell}^{e\tau e\mu}$
$(\bar{\mu}_L\gamma_\mu\tau_L)(\bar{\mu}_L\gamma^\mu e_L)$	$C_{\ell\ell}^{\mu\tau\mu e}$
$(\bar{e}_R\gamma_\mu\mu_R)(\bar{e}_R\gamma^\mu e_R)$	$C_{ee}^{e\mu ee} + 2sin^2\theta_W C_{\Phi e}^{e\mu}$
$(\bar{\mu}_R\gamma_\mu\tau_R)(\bar{\mu}_R\gamma^\mu\mu_R)$	$C_{ee}^{\mu\tau\mu\mu} + 2sin^2\theta_W C_{\Phi e}^{\mu\tau}$
$(\bar{e}_R\gamma_\mu\tau_R)(\bar{e}_R\gamma^\mu e_R)$	$C_{ee}^{e\tau ee} + 2sin^2\theta_W C_{\Phi e}^{e\tau}$
$(\bar{\mu}_R\gamma_\mu\tau_R)(\bar{e}_R\gamma^\mu e_R)$	$C_{ee}^{\mu\tau ee} + 2sin^2\theta_W C_{\Phi e}^{\mu\tau}$
$(\bar{e}_R\gamma_\mu\tau_R)(\bar{\mu}_R\gamma^\mu\mu_R)$	$C_{ee}^{e\tau\mu\mu} + 2sin^2\theta_W C_{\Phi e}^{e\tau}$
$(\bar{e}_R\gamma_\mu\tau_R)(\bar{e}_R\gamma^\mu\mu_R)$	$C_{ee}^{e\tau e\mu}$
$(\bar{\mu}_R\gamma_\mu\tau_R)(\bar{\mu}_R\gamma^\mu e_R)$	$C_{ee}^{\mu\tau\mu e}$
$(\bar{e}_L\gamma_\mu\mu_L)(\bar{e}_R\gamma^\mu e_R)$	$C_{\ell e}^{e\mu ee} + 2sin^2\theta_W\left(C_{\Phi\ell}^{(1)e\mu} + C_{\Phi\ell}^{(3)e\mu}\right)$
$(\bar{\mu}_L\gamma_\mu\tau_L)(\bar{\mu}_R\gamma^\mu\mu_R)$	$C_{\ell e}^{\mu\tau\mu\mu} + 2sin^2\theta_W\left(C_{\Phi\ell}^{(1)\mu\tau} + C_{\Phi\ell}^{(3)\mu\tau}\right)$
$(\bar{e}_L\gamma_\mu\tau_L)(\bar{e}_R\gamma^\mu e_R)$	$C_{\ell e}^{e\tau ee} + 2sin^2\theta_W\left(C_{\Phi\ell}^{(1)e\tau} + C_{\Phi\ell}^{(3)e\tau}\right)$
$(\bar{e}_L\gamma^\mu e_L)(\bar{e}_R\gamma_\mu\mu_R)$	$C_{\ell e}^{ee\mu e} + (2sin^2\theta_W - 1)C_{\Phi e}^{e\mu}$
$(\bar{\mu}_L\gamma^\mu\mu_L)(\bar{\mu}_R\gamma_\mu\tau_R)$	$C_{\ell e}^{\mu\mu\mu\tau} + (2sin^2\theta_W - 1)C_{\Phi e}^{\mu\tau}$
$(\bar{e}_L\gamma^\mu e_L)(\bar{e}_R\gamma_\mu\tau_R)$	$C_{\ell e}^{eee\tau} + (2sin^2\theta_W - 1)C_{\Phi e}^{e\tau}$
$(\bar{\mu}_L\gamma_\mu\tau_L)(\bar{e}_R\gamma^\mu e_R)$	$C_{\ell e}^{\mu\tau ee} + sin^2\theta_W\left(C_{\Phi\ell}^{(1)\mu\tau} + C_{\Phi\ell}^{(3)\mu\tau}\right)$
$(\bar{e}_L\gamma_\mu\tau_L)(\bar{\mu}_R\gamma^\mu\mu_R)$	$C_{\ell e}^{e\tau\mu\mu} + sin^2\theta_W\left(C_{\Phi\ell}^{(1)e\tau} + C_{\Phi\ell}^{(3)e\tau}\right)$
$(\bar{e}_L\gamma^\mu e_L)(\bar{\mu}_R\gamma_\mu\tau_R)$	$C_{\ell e}^{ee\mu\tau} + (2sin^2\theta_W - 1)C_{\Phi e}^{\mu\tau}$
$(\bar{\mu}_L\gamma^\mu\mu_L)(\bar{e}_R\gamma_\mu\tau_R)$	$C_{\ell e}^{\mu\mu e\tau} + (2sin^2\theta_W - 1)C_{\Phi e}^{e\tau}$
$(\bar{e}_L\gamma_\mu\tau_L)(\bar{e}_R\gamma^\mu\mu_R)$	$C_{\ell e}^{e\tau e\mu}$
$(\bar{\mu}_L\gamma_\mu e_L)(\bar{e}_R\gamma^\mu\tau_R)$	$C_{\ell e}^{\mu ee\tau}$
$(\bar{e}_L\gamma_\mu\tau_L)(\bar{e}_R\gamma^\mu\mu_R)$	$C_{\ell e}^{e\tau e\mu}$
$(\bar{e}_L\gamma_\mu\mu_L)(\bar{e}_R\gamma^\mu\tau_R)$	$C_{\ell e}^{e\mu e\tau}$
$(\bar{e}_L\gamma_\mu\mu_L)(\bar{\mu}_R\gamma^\mu\tau_R)$	$C_{\ell e}^{e\mu\mu\tau}$
$(\bar{\mu}_L\gamma_\mu\tau_L)(\bar{\mu}_R\gamma^\mu e_R)$	$C_{\ell e}^{\mu\tau\mu e}$
$(\bar{\mu}_L\gamma_\mu e_L)(\bar{\mu}_R\gamma^\mu\tau_R)$	$C_{\ell e}^{\mu e\mu\tau}$

Table 3.1: Vector LEFT coefficients in terms of the Wilson SMEFT coefficients at order $\frac{1}{\Lambda^2}$ and at tree level.

O_i	c_i
$(\bar{e}_L e_R)(\bar{\mu}_R e_L)$	$\frac{m_e v}{\sqrt{2} m_h^2}[L_e^\dagger C_{e\Phi 3}^\dagger R_e]_{\mu e}$
$(\bar{e}_R e_L)(\bar{\mu}_L e_R)$	$\frac{m_e v}{\sqrt{2} m_h^2}[L_e^\dagger C_{e\Phi 3}^\dagger R_e]_{e\mu}$
$(\bar{e}_L e_R)(\bar{\tau}_R e_L)$	$\frac{m_e v}{\sqrt{2} m_h^2}[L_e^\dagger C_{e\Phi 3}^\dagger R_e]_{\tau e}$
$(\bar{e}_R e_L)(\bar{\tau}_L e_R)$	$\frac{m_e v}{\sqrt{2} m_h^2}[L_e^\dagger C_{e\Phi 3}^\dagger R_e]_{e\tau}$
$(\bar{\mu}_L \mu_R)(\bar{\tau}_R \mu_L)$	$\frac{m_\mu v}{\sqrt{2} m_h^2}[L_e^\dagger C_{e\Phi 3}^\dagger R_e]_{\tau\mu}$
$(\bar{\mu}_R \mu_L)(\bar{\tau}_L \mu_R)$	$\frac{m_\mu v}{\sqrt{2} m_h^2}[L_e^\dagger C_{e\Phi 3}^\dagger R_e]_{\tau\mu}$

Table 3.2: Scalar LEFT coefficients in terms of the Wilson SMEFT coefficients at order $\frac{1}{\Lambda^2}$ and at tree level.

O_i	c_i
$(\bar{\mu}_L \sigma^{\mu\nu} e_R) F_{\mu\nu}$	$\frac{v}{\sqrt{2}}\left(cos\theta_W C_{eB}^{\mu e} - sin\theta_W C_{eW}^{\mu e}\right)$
$(\bar{\tau}_L \sigma^{\mu\nu} e_R) F_{\mu\nu}$	$\frac{v}{\sqrt{2}}\left(cos\theta_W C_{eB}^{\tau e} - sin\theta_W C_{eW}^{\tau e}\right)$
$(\bar{\tau}_L \sigma^{\mu\nu} \mu_R) F_{\mu\nu}$	$\frac{v}{\sqrt{2}}\left(cos\theta_W C_{eB}^{\tau \mu} - sin\theta_W C_{eW}^{\tau \mu}\right)$

Table 3.3: Dipole LEFT coefficients in terms of the Wilson SMEFT coefficients at order $\frac{1}{\Lambda^2}$ and at tree level.

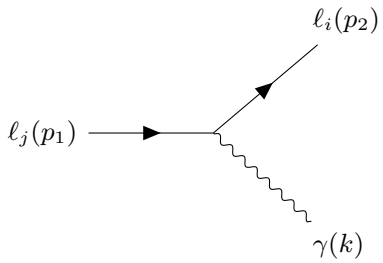

Figure 3.3: Feynman diagram contributing to $\ell_j \to \ell_i \gamma$.

and the corresponding amplitude reads:

$$i\mathcal{M} = i\frac{C_{e\gamma}^{ij}}{\Lambda^2} v\sqrt{2}\bar{u}_i(p_2)\sigma_{\mu\nu}P_R k^\nu u_j(p_1)\epsilon^{*\mu}(k) + i\frac{C_{e\gamma}^{ji*}}{\Lambda^2} v\sqrt{2}\bar{u}_i(p_2)\sigma_{\mu\nu}P_L k^\nu u_j(p_1)\epsilon^{*\mu}(k), \tag{3.12}$$

where a factor two has been taken into account due to the field strength $F^{\mu\nu}$ and $\epsilon^{*\mu}$ is the polarization of the photon. Squaring the amplitude, summing over the final polarization states and averaging on the initial ones we get the unpolarized squared amplitude:

$$|\mathcal{M}|^2 = 4m_j^4(|c_{e\gamma}^{ij}|^2 + |c_{e\gamma}^{ji}|^2). \tag{3.13}$$

As in the case of the Fermi theory in Chapter 1, the electron mass is neglected, therefore the energy of the electron and the photon are equal to one half the muon mass. The phase space evaluation is straightforward and brings to the final result

$$\Gamma(\mu \to e\gamma) = \frac{1}{16\pi}\frac{|\mathcal{M}|^2}{m_\mu} = \frac{m_\mu^3 v^2}{8\pi\Lambda^4}\left(|C_{e\gamma}^{e\mu}|^2 + |C_{e\gamma}^{\mu e}|^2\right). \tag{3.14}$$

From this calculation we can try to infer information either on the Wilson coefficient or on the new physics scale Λ:

- let us assume, for instance, as pointed out in the SM section, that the new energy scale is about $\Lambda \approx 1\,TeV$. Then comparing with the present bound on $\mu \to e\gamma$, we obtain $|C_{e\gamma}^{\mu e}| \lesssim 2.1 \cdot 10^{-10}$, therefore this scenario gives a very little prediction for the coefficient;

- taking, instead, a coefficient of order one $|C_{e\gamma}^{\mu e}| \approx 1$ we get $\Lambda \gtrsim 6.8 \cdot 10^4\,TeV$, that means that new particles lie at very high energy scales.

The same calculation can be repeated considering the processes $\tau \to e\gamma$ and $\tau \to \mu\gamma$ and the relative bounds are reported in Table 3.4.

	$\lvert C_a\rvert$ [$\Lambda = 1$ TeV]	Λ (TeV) [$\lvert C_a\rvert = 1$]	CLFV Process
$C_{e\gamma}^{\mu e}$	2.1×10^{-10}	6.8×10^4	$\mu \to e\gamma$
$C_{e\gamma}^{\tau\mu}$	2.7×10^{-6}	610	$\tau \to \mu\gamma$
$C_{e\gamma}^{\tau e}$	2.4×10^{-6}	650	$\tau \to e\gamma$

Table 3.4: Bounds on the coefficients of some of the flavor-violating operators of Table 2.1, exploiting the experimental constraints of Table 1.1, for $\Lambda = 1$ TeV, and corresponding bounds on Λ (in TeV) for $|C_a| = 1$.

The dipole operators contribute to the muon decay directly at tree level, but in the renormalizable theories beyond the SM, the operators Q_{eB} and Q_{eW} can only be generated at the loop level while other operators, like the effective four-lepton couplings, can already be generated at tree level. Thus, the radiative lepton decays contributions can come from other dimension-6 operators which contribute to such decays at 1-loop level. These contributions can be comparable or even dominant with tree level contributions and from them it is possible to infer bounds on other coefficients that does not appear in CLFV at tree level.

3.1.3 $\ell_i^\pm \to \ell_j^\pm \ell_l^\pm \ell_k^\mp$

Let us move to investigate the three-body decay of a heavy lepton into three lighter leptons. Before considering a set of operators, we find general expressions regarding the decay rate, starting from a generic amplitude. The diagram associated with such a decay can be either a four-fermion vertex like

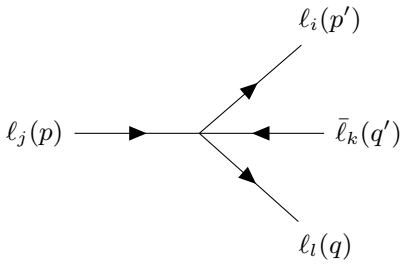

Figure 3.4: Feynman diagram contributing to $\ell_j \to \ell_i \bar{\ell}_k \ell_l$.

or a photon-exchange diagram like

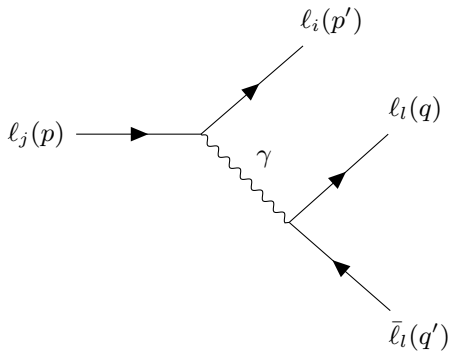

Figure 3.5: Feynman diagram contributing to $\ell_j \to \ell_i \bar{\ell}_l \ell_l$ thorough photon exchange.

In the first case the amplitude is given by the following expression:

$$i\mathcal{M} = iNc^X_{P_1P_2}\bar{u}_i(p')\Gamma_X P_1 u_j(p)\bar{u}_l(q)\Gamma_X P_2 v_k(q'), \tag{3.15}$$

where the coefficients $c^X_{P_1P_2}$ are the LEFT couplings reported in Tables 3.1 and 3.2. The superscript X can be $X = S, V$ representing either scalar or vector vertices and thus the corresponding Dirac structures Γ_X are:

$$\Gamma_S = 1, \qquad \Gamma_V = \gamma_\mu. \tag{3.16}$$

Moreover, P_1 and P_2 can be either left-handed or right-handed chirality projectors and comparing with the notation adopted in the previous subsections we recall that:

$$c^X_{P_LP_L} = c^X_{\ell\ell}, \qquad c^X_{P_LP_R} = c^X_{\ell e}, \qquad c^X_{P_RP_R} = c^X_{ee}. \tag{3.17}$$

In addition, according to the diagram we are considering, a symmetry factor N has been taken into account and can assume values $N = 1, 2$. Let us start from the vector interaction, first of all we have to distinguish between the case in which we have two projectors with the same chirality $P_1 = P_2 = P$ and the case in which we have opposite chirality $P_1 \neq P_2$. In the former case, the amplitude reads

$$i\mathcal{M} = iNc^V_{PP}\bar{u}_i(p')\gamma_\mu P u_j(p)\bar{u}_l(q)\gamma^\mu P v_k(q'). \tag{3.18}$$

Then squaring the amplitude, summing over final polarization states and averaging over the initial ones we get the unpolarized squared amplitude:

$$|\mathcal{M}|^2 = 8N^2|c^V_{PP}|^2(p\cdot q')(p'\cdot q). \tag{3.19}$$

While in the latter case the amplitude reads:

$$i\mathcal{M} = iNc^V_{P_1P_2}\bar{u}_i(p')\gamma_\mu P_1 u_j(p)\bar{u}_l(q)\gamma^\mu P_2 v_k(q'). \tag{3.20}$$

Then squaring the amplitude, summing over final polarisation states and averaging over the initial ones we get the unpolarised squared amplitude:

$$|\mathcal{M}|^2 = 8N^2|c^V_{P_1P_2}|^2(p\cdot q)(p'\cdot q'). \tag{3.21}$$

In the case of a three body decay, the phase space evaluation necessary to obtain the decay rate is not

as straightforward as in the two body decay. It can be evaluated through the Fermi Golden rule:

$$d\Gamma = \frac{1}{N_i}\frac{|\mathcal{M}|^2}{2m_j}\frac{d^3p'}{(2\pi)^3 2E'}\frac{d^3q}{(2\pi)^3 2Q}\frac{d^3q'}{(2\pi)^3 2Q'}(2\pi)^4\delta^{(4)}(p-p'-q-q'), \tag{3.22}$$

where E', Q, Q' are the energies of the final states and the factor $\frac{1}{N_i}$, in front, is there because in the final state one can have N_i indistinguishable particles. Since for the two amplitudes the procedure is the same, it is presented only for the one in Eq. (3.19). The differential decay rate can be recasted as follows:

$$d\Gamma = \frac{N^2}{4m_j(2\pi)^5 N_i}|c^V_{PP}|^2 p_\alpha p'_\beta \frac{d^3p'}{E'} I^{\alpha\beta}(k), \tag{3.23}$$

where

$$I^{\alpha\beta}(k) = \int \frac{d^3q}{Q}\frac{d^3q'}{Q'}\delta^{(4)}(p-p'-q-q')q'^\alpha q^\beta. \tag{3.24}$$

.
By Lorentz invariant argument, the integral can be rewritten as

$$I^{\alpha\beta}(k) = g^{\alpha\beta}A(k^2) + \frac{k^\alpha k^\beta}{k^2}B(k^2). \tag{3.25}$$

In order to determine the components of this tensor, one can solve the following system of equations:

$$g_{\alpha\beta}I^{\alpha\beta} = 4A + B, \qquad k^\alpha k^\beta I_{\alpha\beta} = k^2(A+B). \tag{3.26}$$

Being the last two quantities Lorentz invariant, they can be calculated in any reference frame. The evaluation of those integrals in the lab frame is straightforward and gives:

$$A(k^2) = \frac{\pi}{6}k^2, \qquad B(k^2) = \frac{\pi}{3}k^2. \tag{3.27}$$

Finally, the result is obtained integrating in d^3p' between the kinematic conditions $E'_{min} = 0$ and $E'_{max} = \frac{m_j}{2}$. Indeed, they corresponds to the case in which the $\ell_l\ell_k$ couple takes the entire energy and the case of $\ell_l\ell_k$ collinear emission, respectively. The decay rate is:

$$\Gamma_V = \frac{N^2}{N_i}|c^V_{PP}|^2\frac{m_j^5}{192\pi^3\cdot 8}. \tag{3.28}$$

Repeating the same calculation one finds that the same result is valid both in the case in which $P_1 \neq P_2$ and in the case $P_1 = P_2$.
Considering now the scalar case, we get the following amplitude:

$$\mathcal{M} = iN^2 c^S_{P_1P_2}\bar{u}_i(p')P_1u_j(p)\bar{u}_l(q)P_2v_k(q'), \tag{3.29}$$

then the unpolarized squared amplitude is

$$|\mathcal{M}|^2 = 2N^2|c^S_{P_1P_2}|^2(p\cdot p')(q'\cdot q'), \tag{3.30}$$

both if the two projectors are equal or different. Therefore, in the decay rate the difference with the

previous case is just a factor four:

$$\Gamma_S = \frac{N^2}{N_i}|c^S_{P_1P_2}|^2\frac{m_j^5}{192\pi^3\cdot 32}. \tag{3.31}$$

It is worth noting that, the different operator structures analyzed until now, cannot interfere and therefore have been analyzed separately. In the following the interference terms arising from photon exchange diagram are going to be evaluated through a Mathematica code, using the package *FeynCalc*. Through the three body CLFV muon decay, it is possible to constrain also the dipole operators. We consider the following diagram:

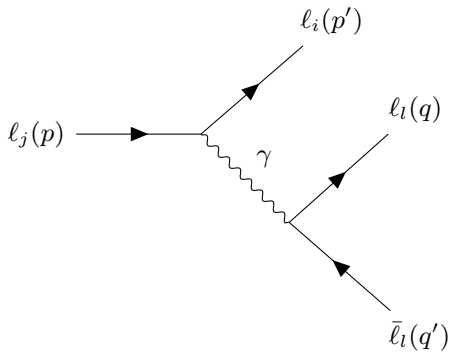

Figure 3.6: Feynman diagram contributing to $\ell_j \to \ell_i\bar{\ell}_l\ell_l$ thorough photon exchange.

that is obtained by photon-exchange through the dipole operators

$$\mathscr{L}_{eff} = \frac{C^{e\mu}_{e\gamma}}{\Lambda^2}\frac{v}{\sqrt{2}}\bar{e}\sigma_{\mu\nu}P_R\mu F^{\mu\nu} + \frac{C^{\mu e}_{e\gamma}}{\Lambda^2}\frac{v}{\sqrt{2}}\bar{\mu}\sigma_{\mu\nu}P_R e F^{\mu\nu} + h.c. \tag{3.32}$$

Clearly, in order to obtain a result suppressed by $\frac{1}{\Lambda^2}$ only one of the two vertices is effective, while the other one is a flavor conserving QED vertex. Therefore, there are two possibilities:

- If $i \neq j \neq l$, then the amplitude is given by:

$$i\mathcal{M} = i\frac{ev\sqrt{2}}{\Lambda^2}\bar{u}_i(p')\sigma_{\mu\alpha}(p-p')^\alpha\left(C^{ij}_{e\gamma}P_R + C^{ji*}_{e\gamma}P_L\right)u_j(p)\bar{u}_l(q)\gamma_\nu v_l(q')\frac{g^{\mu\nu}}{(p-p')^2}. \tag{3.33}$$

- If $i = l \neq j$ an additional term given by the exchange of i and l appears, with the usual minus sign due to the fermion exchange:

$$\begin{aligned} i\mathcal{M} = {} & i\frac{ev\sqrt{2}}{\Lambda^2}\bar{u}_i(p')\sigma_{\mu\alpha}(p-p')^\alpha\left(C^{ij}_{e\gamma}P_R + C^{ji*}_{e\gamma}P_L\right)u_j(p)\bar{u}_l(q)\gamma_\nu v_l(q')\frac{g^{\mu\nu}}{(p-p')^2} + \\ & - i\frac{ev\sqrt{2}}{\Lambda^2}\bar{u}_l(q)\sigma_{\mu\alpha}(p-q)^\alpha\left(C^{ij}_{e\gamma}P_R + C^{ji*}_{e\gamma}P_L\right)u_j(p)\bar{u}_l(p')\gamma_\nu v_l(q')\frac{g^{\mu\nu}}{(p-p')^2}. \end{aligned} \tag{3.34}$$

In this case the three body phase space evaluation is more lengthy, because all the external masses must be considered to avoid infrared divergencies of the photon propagator. In order to evaluate it, a Mathematica code has been implemented. Calling p_2, p_3 and p_4 the 4−momenta of the final states, the general formula to obtain the differential decay rate is:

$$d\Gamma = \frac{|\mathcal{M}|^2}{2m_j}\frac{d^3p_2}{(2\pi)^3 2E_2}\frac{d^3p_3}{(2\pi)^3 2E_3}\frac{d^3p_4}{(2\pi)^3 2E_4}(2\pi)^4\delta^{(4)}(p-p_2-p_3-p_4), \tag{3.35}$$

	$\lvert C_a\rvert$ [$\Lambda = 1$ TeV]	Λ (TeV) [$\lvert C_a\rvert = 1$]	CLFV Process
$C_{e\gamma}^{\mu e}$	4.0×10^{-9}	1.6×10^{4}	$\mu \to eee$
$C_{e\gamma}^{\tau e}$	2×10^{-5}	221	$\tau \to eee$
$C_{e\gamma}^{\tau \mu}$	3.7×10^{-5}	165	$\tau \to \mu\mu\mu$

Table 3.5: Bounds on the coefficients of some of the flavor-violating operators of Table 2.1, exploiting the experimental constraints of Table 1.1, for $\Lambda = 1$ TeV , and corresponding bounds on Λ (in TeV) for $|C_a| = 1$.

where E_1, E_2, and E_3 represent the zero component of the 4−momenta of the three final particles. Integrating the delta function one obtains the following formula for the decay rate[28]:

$$\Gamma\left(\ell_i \to \ell_j \ell_l \ell_l\right) = \int_{X_{\min}}^{X_{\max}} dX \int_{Y_{\min}}^{Y_{\max}} dY \frac{|\mathcal{M}|^2}{(2\pi)^3 32 m_j^3}.$$

The parameters, X, Y and Z, denote invariant masses m_{ij}^2 as

$$X = m_{12}^2 = \left(p' + q\right)^2, \tag{3.36}$$
$$Y = m_{23}^2 = \left(q + q'\right)^2, \tag{3.37}$$
$$Z = m_{13}^2 = m_j^2 + 2m_l^2 - X - Y, \tag{3.38}$$

which are kinematically limited by

$$\left(m_i + m_l\right)^2 \leq X \leq \left(m_j - m_l\right)^2, \tag{3.39}$$

$$Y_{\min,\max} = \left(E_q + E_{q'}\right)^2 - \left[\left(E_q^2 - m_l^2\right)^{\frac{1}{2}} \pm \left(E_{q'}^2 - m_l^2\right)^{\frac{1}{2}}\right]^2, \tag{3.40}$$

with

$$E_q = \frac{X - m_i^2 + m_l^2}{2m_{12}}, \qquad E_{q'} = \frac{m_j^2 - m_l^2 - X}{2m_{12}}. \tag{3.41}$$

The code used to perform this calculation is reported in Appendix B. The final result, in the case $i = l \neq j$ reads:

$$\Gamma(\ell_j \to \ell_i \ell_i \ell_i) = \frac{m_j^3 e^2 v^2}{96\pi^3 \Lambda^4} \left(\log \frac{m_j^2}{m_i^2} - \frac{11}{4}\right) \left(|C_{e\gamma}^{ij}|^2 + |C_{e\gamma}^{ji}|^2\right), \tag{3.42}$$

where the factor two, due to the identical particles in the final state, has been considered. Conversely, in the case $i \neq l \neq j$ the result is:

$$\Gamma(\ell_j \to \ell_i \ell_l \ell_l) = \frac{m_j^3 e^2 v^2}{96\pi^3 \Lambda^4} \left(\log \frac{m_j^2}{m_i^2} - 3\right) \left(|C_{e\gamma}^{ij}|^2 + |C_{e\gamma}^{ji}|^2\right). \tag{3.43}$$

Starting from these results and comparing them with the experimental constraints, we obtain bounds on the Wilson coefficients as we show in Table 3.5. The next step is to evaluate the interference terms. In order to do that, the previous Mathematica code is used again. The final expressions for the decay rates are reported in the following three different cases:

- Three leptons with the same flavor in the final state ($\Delta L = 1$):

$$\begin{aligned}\Gamma\left(\ell_j^\pm \to \ell_i^\pm \ell_i^\pm \ell_i^\mp\right) =& \frac{m_j^5}{16\cdot 192\pi^3\Lambda^4}\left[4|c_{\ell\ell}^{V,ijii}|^2 + 4|c_{ee}^{V,ijii}|^2 + |c_{\ell e}^{V,ijii}|^2 + |c_{\ell e}^{V,iiij}|^2\right] + \\ &+ \frac{m_j^5}{64\cdot 192\pi^3\Lambda^4}\left[4|c_{\ell\ell}^{S,ijii}|^2 + 4|c_{ee}^{S,ijii}|^2 + |c_{\ell e}^{S,ijii}|^2 + |c_{\ell e}^{S,iiij}|^2\right] + \\ &+ \frac{m_j^3 e^2 v^2}{192\pi^3\Lambda^4}\left(\log\frac{m_j^2}{m_i^2} - \frac{11}{4}\right)\left(|C_{e\gamma}^{ij}|^2 + |C_{e\gamma}^{ji}|^2\right) + \\ &- \frac{\sqrt{2}m_j^4 ev}{768\pi^3}\Re\left[\left(2c_{\ell\ell}^{V,ijii} + c_{\ell e}^{V,ijii} - \frac{1}{2}c_{\ell e}^{S,ijii}\right)C_{e\gamma}^{ij*} + \right. \\ &\left. - \left(2c_{ee}^{V,ijii} + c_{\ell e}^{V,iiij} - \frac{1}{2}c_{\ell e}^{S,iiij}\right)C_{e\gamma}^{ji}\right].\end{aligned} \tag{3.44}$$

- Two different leptons in the final state, with the electric charge of the decaying particle j equal to the one of the particle i ($\Delta L = 1$):

$$\begin{aligned}\Gamma\left(\ell_j^\pm \to \ell_i^\pm \ell_l^\pm \ell_l^\mp\right) =& \frac{m_j^5}{8\cdot 192\pi^3\Lambda^4}\left[|c_{\ell\ell}^{V,ijii}|^2 + |c_{ee}^{V,ijii}|^2 + |c_{\ell e}^{V,ijii}|^2 + |c_{\ell e}^{V,iiij}|^2\right] + \\ &+ \frac{m_j^5}{32\cdot 192\pi^3\Lambda^4}\left[|c_{\ell\ell}^{S,ijii}|^2 + |c_{ee}^{S,ijii}|^2 + |c_{\ell e}^{S,ijii}|^2 + |c_{\ell e}^{S,iiij}|^2\right] + \\ &+ \frac{m_j^3 e^2 v^2}{96\pi^3\Lambda^4}\left(\log\frac{m_j^2}{m_i^2} - 3\right)\left(|C_{e\gamma}^{ij}|^2 + |C_{e\gamma}^{ji}|^2\right) + \\ &- \frac{\sqrt{2}m_j^4 ev}{384\pi^3}\Re\left[\left(c_{\ell\ell}^{V,ijii} + c_{\ell e}^{V,ijii}\right)C_{e\gamma}^{ij*} + \right. \\ &\left. - \left(c_{ee}^{V,ijii} + c_{\ell e}^{V,iiij}\right)C_{e\gamma}^{ji}\right].\end{aligned} \tag{3.45}$$

- Two different leptons in the final state, with the electric charge of the decaying particle j different to the one of the particle i ($\Delta L = 2$):

$$\begin{aligned}\Gamma\left(\ell_j^\pm \to \ell_i^\mp \ell_l^\pm \ell_l^\pm\right) =& \frac{m_j^5}{16\cdot 192\pi^3\Lambda^4}\left[4|c_{\ell\ell}^{V,ijll}|^2 + 4|c_{ee}^{V,ijll}|^2 + |c_{\ell e}^{V,ijll}|^2 + |c_{\ell e}^{V,llij}|^2\right] + \\ &+ \frac{m_j^5}{64\cdot 192\pi^3\Lambda^4}\left[4|c_{\ell\ell}^{S,ijll}|^2 + 4|c_{ee}^{S,ijll}|^2 + |c_{\ell e}^{S,ijll}|^2 + |c_{\ell e}^{S,llij}|^2\right].\end{aligned} \tag{3.46}$$

Let us now end this subsection obtaining constraints on the Wilson coefficients of all the other operators. In particular, we switch off all the contributions but one, assuming that only one operator is responsible for new-physics. Then, in the following, also the interplay between different Wilson coefficients is studied. Let us start from the 4-lepton operators of the Table 2.1 $Q_{\ell\ell}$ and Q_{ee} which contributes directly to the vector coefficients. Thus, we can infer bounds on the coefficients and on the new physics scale not only for $\mu \to eee$ but also for $\tau \to eee$ and $\tau \to \mu\mu\mu$. This bounds are shown in Table 3.6.

	$\lvert C_a\rvert$ [$\Lambda = 1$ TeV]	Λ (TeV) [$\lvert C_a\rvert = 1$]	CLFV Process
$C^{e\mu ee}_{\ell\ell,ee}$	2.3×10^{-5}	207	$\mu \to eee$
$C^{\mu\tau\mu\mu}_{\ell\ell,ee}$	7.8×10^{-3}	11	$\tau \to \mu\mu\mu$
$C^{e\tau ee}_{\ell\ell,ee}$	9.2×10^{-3}	10	$\tau \to eee$

Table 3.6: Bounds on the coefficients of some of the flavor-violating operators of Table 2.1, exploiting the experimental constraints of Table 1.1, for $\Lambda = 1$ TeV, and corresponding bounds on Λ (in TeV) for $|C_a| = 1$.

The other set of operators contributing to the point-like interaction diagram are $Q_{\ell e}$ and the bounds for the corresponding coefficients are reported in Table 3.7.

	$\lvert C_a\rvert$ [$\Lambda = 1$ TeV]	Λ (TeV) [$\lvert C_a\rvert = 1$]	CLFV Process
$C^{e\mu ee, ee\mu e}_{\ell e}$	4.6×10^{-5}	146	$\mu \to eee$
$C^{\mu\tau\mu\mu, \mu\mu\mu\tau}_{\ell e}$	1.6×10^{-2}	8	$\tau \to \mu\mu\mu$
$C^{e\tau ee, eee\tau}_{\ell e}$	1.8×10^{-2}	7	$\tau \to eee$

Table 3.7: Bounds on the coefficients of some of the flavor-violating operators of Table 2.1, exploiting the experimental constraints of Table 1.1, for $\Lambda = 1$ TeV, and corresponding bounds on Λ (in TeV) for $|C_a| = 1$.

Moreover, there are other contributions arising from the Lepton-Higgs operators. The Feynman diagram that is associated to this contribution is a Z boson exchange, as we have seen in the previous subsection. The constraints are shown in Table 3.8.

	$\lvert C_a\rvert$ [$\Lambda = 1$ TeV]	Λ (TeV) [$\lvert C_a\rvert = 1$]	CLFV Process
$C^{e\mu}_{\Phi e}$	3.3×10^{-5}	174	$\mu \to eee$
$\lvert C^{(1)e\mu}_{\Phi\ell} + C^{(3)e\mu}_{\Phi\ell}\rvert$	3.3×10^{-5}	174	$\mu \to eee$
$C^{e\tau}_{\Phi e}$	1.2×10^{-2}	14	$\tau \to eee$
$\lvert C^{(1)e\tau}_{\Phi\ell} + C^{(3)e\tau}_{\Phi\ell}\rvert$	1.2×10^{-2}	14	$\tau \to eee$
$C^{\mu\tau}_{\Phi e}$	1.1×10^{-2}	14	$\tau \to \mu\mu\mu$
$\lvert C^{(1)\mu\tau}_{\Phi\ell} + C^{(3)\mu\tau}_{\Phi\ell}\rvert$	1.1×10^{-2}	14	$\tau \to \mu\mu\mu$

Table 3.8: Bounds on the coefficients of some of the flavor-violating operators of Table 2.1, exploiting the experimental constraints of Table 1.1, for $\Lambda = 1$ TeV, and corresponding bounds on Λ (in TeV) for $|C_a| = 1$.

In addition, from Eq. (2.30) we obtain an additional diagram involving the exchange of the Higgs boson. The constraints on the Wilson coefficients of the operators $Q_{e\Phi 3}$ are:

	$\lvert C_a\rvert$ [$\Lambda = 1$ TeV]	Λ (TeV) [$\lvert C_a\rvert = 1$]	CLFV Process
$[L^\dagger_e C^\dagger_{e\Phi 3} R_e]_{\mu e}$	0.07	3.9	$\mu \to eee$
$[L^\dagger_e C^\dagger_{e\Phi 3} R_e]_{\tau e}$	25	2.0	$\tau \to eee$
$[L^\dagger_e C^\dagger_{e\Phi 3} R_e]_{\tau\mu}$	0.11	3.0	$\tau \to \mu\mu\mu$

Table 3.9: Bounds on the coefficients of some of the flavor-violating operators of Table 2.1, exploiting the experimental constraints of Table 1.1, for $\Lambda = 1$ TeV, and corresponding bounds on Λ (in TeV) for $|C_a| = 1$.

3.1.4 $Z \to \ell_i^{\pm}\ell_f^{\mp}$

Another interesting CLFV decay is the Z boson into a lepton pair with different flavors. As pointed out in the previous section within SMEFT the W and Z couplings get modified and this decay can be induced already at tree level through the vertex:

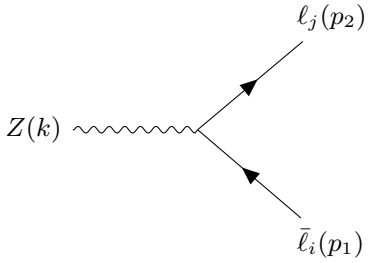

Figure 3.7: Feynman diagram contributing to the Z flavor violating decay.

Indeed, from lepton-Higgs operators and dipole operators one obtains flavor violating interactions as written in Eq. (2.34) and in Eq. (2.38). Therefore, the amplitude reads

$$\mathcal{M} = i\bar{u}_j(p_2)\not{\epsilon}(k)[a^Z_{ji}P_L + b^Z_{ji}P_R]v_i(p_1) - i\frac{\sqrt{2}v}{\Lambda^2}\bar{u}_j(p_2)\sigma^{\mu\nu}k_\nu\epsilon_\mu(k)u(k)[C^{ji}_{eZ}P_L + C^{ij*}_{eZ}P_R]v_i(p_1). \quad (3.47)$$

In order to obtain the unpolarized squared amplitude we sum over final polarizations and average over the three Z-boson polarization states, getting

$$|\mathcal{M}|^2 = \frac{2}{3\pi}M_Z^2\left[\frac{M_Z^2v^2}{\Lambda^4}(|C^{ji}_{eZ}|^2 + |C^{ij}_{eZ}|^2) + |a^Z_{ji}|^2 + |b^Z_{ji}|^2\right]. \quad (3.48)$$

Therefore, neglecting the final masses the decay rate is given by

$$\Gamma(Z \to \ell_i\ell_j) = \frac{1}{24\pi}M_Z\left[\frac{M_Z^2v^2}{\Lambda^4}(|C^{ji}_{eZ}|^2 + |C^{ij}_{eZ}|^2) + |a^Z_{ji}|^2 + |b^Z_{ji}|^2\right]. \quad (3.49)$$

This calculation is based on the fact that the final state is the fixed couple $\ell_i(p_1)$ and $\ell_f(p_2)$, but in experiments it is not possible to distinguish between the decay $Z \to e^-\mu^+$ and $Z \to e^+\mu^-$. Thus, to compare this result with experimental bounds, one should multiply by a factor two Eq. (3.49). The constraints obtained are presented in Table 3.10

3.1.5 $h \to \ell_i^{\pm}\ell_j^{\mp}$

Let us now move to study the Higgs flavor violating decays. We have already evaluated the Higgs coupling to leptons and the Higgs coupling to leptons and photon, the formulae are in Equations 2.33 and 2.34, respectively. Therefore, the Feynman diagram of the flavor violating Higgs decay is:

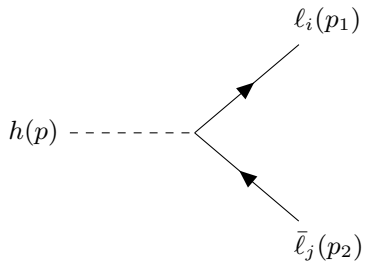

Figure 3.8: Feynman diagram contributing to the Higgs flavor violating decay.

	$\lvert C_a\rvert$ [$\Lambda = 1$ TeV]	Λ (TeV) [$\lvert C_a\rvert = 1$]	CLFV Process
$C_{\Phi e}^{e\mu}$	0.07	4	$Z \to e\mu$
$\lvert C_{\Phi \ell}^{(1)e\mu} + C_{\Phi \ell}^{(3)e\mu}\rvert$	0.07	4	$Z \to e\mu$
$C_{eZ}^{\mu e}$	0.06	4	$Z \to e\mu$
$C_{\Phi e}^{e\tau}$	0.16	3	$Z \to e\tau$
$\lvert C_{\Phi \ell}^{(1)e\tau} + C_{\Phi \ell}^{(3)e\mu}\rvert$	0.16	3	$Z \to e\tau$
$C_{eZ}^{\tau e}$	0.14	3	$Z \to e\tau$
$C_{\Phi e}^{\mu\tau}$	0.18	2	$Z \to \tau\mu$
$\lvert C_{\Phi \ell}^{(1)\mu\tau} + C_{\Phi \ell}^{(3)\mu\tau}\rvert$	0.18	2	$Z \to \tau\mu$
$C_{eZ}^{\tau\mu}$	0.16	3	$Z \to \tau\mu$

Table 3.10: Bounds on the coefficients of some of the flavor-violating operators of Table 2.1, exploiting the experimental constraints of Table 1.1, for $\Lambda = 1$ TeV, and corresponding bounds on Λ (in TeV) for $|C_a| = 1$.

The tree-level amplitude is easily obtained as:

$$i\mathcal{M} = i\frac{v^2}{\sqrt{2}\Lambda^2}[L_e^\dagger C_{e\Phi 3}^\dagger R_e]_{ij}\bar{u}_i(p_1)P_L v_j(p_2) + i\frac{v^2}{\sqrt{2}\Lambda^2}[L_e^\dagger C_{e\Phi 3}^\dagger R_e]_{ji}\bar{u}_i(p_1)P_R v_j(p_2), \tag{3.50}$$

in this case squaring the amplitude and performing the phase space evaluation is straightforward. The decay rate is

$$\Gamma\left(h \to \ell_i \ell_j\right) = \frac{m_h v^4}{32\pi\Lambda^4}\left(|[L_e^\dagger C_{e\Phi 3}^\dagger R_e]_{ij}|^2 + |[L_e^\dagger C_{e\Phi 3}^\dagger R_e]_{ji}|^2\right). \tag{3.51}$$

Then, as in the previous decay, to compare our result with the experimental bound we must consider that it is not possible to distinguish between the decays $h \to e^-\mu^+$ and $h \to e^+\mu^-$, thus to compare this result with experimental bounds, one should multiply by a factor two Eq. (3.51).
As far as the radiative flavor violating Higgs decay is concerned, we have three diagrams contributing:

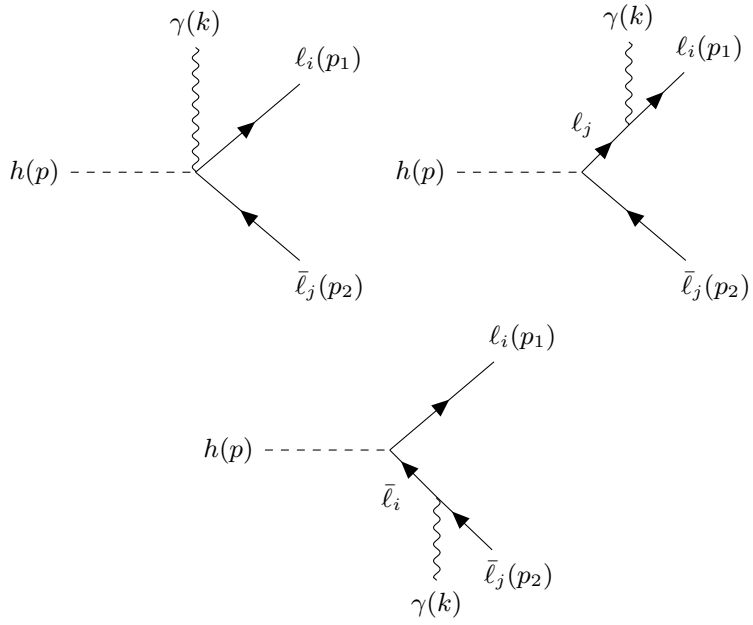

Figure 3.9: Feynman diagrams contributing to the Higgs flavor violating decay with photon emission.

Thus, the amplitude is given by:

$$\begin{aligned}
i\mathcal{M} =& i\frac{C_{e\gamma}^{ij}}{\Lambda^2}\sqrt{2}\bar{u}_i(p_1)\sigma_{\mu\nu}P_R k^\nu v_j(p_2)\epsilon^{*\mu}(k) + i\frac{C_{e\gamma}^{ji}}{\Lambda^2}\sqrt{2}\bar{u}_i(p_2)\sigma_{\mu\nu}P_L k^\nu v_j(p_1)\epsilon^{*\mu}(k) + \\
&+ i\frac{C_{e\gamma}^{ij}}{\Lambda^2}\sqrt{2}m_j\bar{u}_i(p_1)\sigma_{\mu\nu}P_R k^\nu \frac{1}{\not{p}-\not{p_2}-m_j}v_j(p_2)\epsilon^{*\mu}(k) \\
&+ i\frac{C_{e\gamma}^{ji}}{\Lambda^2}\sqrt{2}m_j\bar{u}_i(p_1)\sigma_{\mu\nu}P_L k^\nu \frac{1}{\not{p}-\not{p_2}-m_j}v_j(p_2)\epsilon^{*\mu}(k) \\
&+ i\frac{C_{e\gamma}^{ij}}{\Lambda^2}\sqrt{2}m_i\bar{u}_i(p_1)\frac{1}{\not{p}-\not{p_1}-m_i}\sigma_{\mu\nu}P_R k^\nu v_j(p_2)\epsilon^{*\mu}(k) \\
&+ i\frac{C_{e\gamma}^{ji}}{\Lambda^2}\sqrt{2}m_i\bar{u}_i(p_1)\frac{1}{\not{p}-\not{p_1}-m_i}\sigma_{\mu\nu}P_L k^\nu v_j(p_2)\epsilon^{*\mu}(k).
\end{aligned} \tag{3.52}$$

Then squaring the amplitude and performing the three body phase space integration with a Mathematica code similar to the one reported in Appendix B we obtain:

$$\Gamma\left(h\to\ell_i\ell_j\gamma\right) = \frac{m_h^5}{1536\Lambda^4\pi^3}\left(|C_{e\gamma}^{ij}|^2 + |C_{e\gamma}^{ji}|^2 + \mathcal{O}\left(\frac{m_{i,j}}{m_h}\right)\right). \tag{3.53}$$

Eventually, the usual factor two must be considered for the experimental comparison. The bounds obtained on the Wilson coefficients are given in the following table:

	$\lvert C_a\rvert$ [$\Lambda = 1$ TeV]	Λ (TeV) [$\lvert C_a\rvert = 1$]	CLFV Process
$[L_e^\dagger C_{e\Phi 3}^\dagger R_e]_{\mu e}$	1.3×10^{-2}	8.9	$h\to e\mu$
$[L_e^\dagger C_{e\Phi 3}^\dagger R_e]_{\tau e}$	3.1×10^{-2}	5.6	$h\to \tau e$
$[L_e^\dagger C_{e\Phi 3}^\dagger R_e]_{\tau \mu}$	2.6×10^{-2}	6.2	$h\to \tau\mu$

Table 3.11: Bounds on the coefficients of some of the flavor-violating operators of Table 2.1, exploiting the experimental constraints of Table 1.1, for $\Lambda = 1$ TeV, and corresponding bounds on Λ (in TeV) for $|C_a| = 1$.

3.1.6 CLFV decays through semileptonic operators

In the previous subsections, we have analyzed many constraints on the SMEFT operators. However, until now, we have no contribution of the 2-quark-2-lepton operators to the the considered decays. Therefore, it is important to take into account processes able to constrain also those operators. In order to do that, we consider pseudo-scalar meson decays. We define the decaying particle as $P = \bar{q}_i q_j$ and introduce its decaying constant as

$$\langle 0|\,\bar{q}_i\gamma^\mu\gamma_5 q_j\,|P(p)\rangle = i f_P p^\mu. \tag{3.54}$$

Following [29], the general expression of the decay rate for a purely leptonic meson decay is given by

$$\begin{aligned}
\Gamma(P\to\ell_k^-\ell_l^+) =& \frac{f_P^2 m_P m_{\ell_k}^2}{32\pi\Lambda^4}\left(1-\frac{m_{\ell_k}^2}{m_P^2}\right)^2 \\
&\times\left\{\left|\left(C_{\ell d}^{klij} - C_{\ell q}^{(1)klij} - C_{\ell q}^{(3)klij}\right) - \frac{C_{\ell edq}^{klij}\,m_P^2}{m_{\ell_k}(m_{q_i}+m_{q_j})}\right|^2 + (L\leftrightarrow R)\right\},
\end{aligned} \tag{3.55}$$

As far as neutral kaon decays are concerned this result must be modified as explained in [29]. Finally, when confronting theory with the experimental measurements one needs to account for the effect

$P \to M\ell_i\ell_j$	a_V^+	a_V^-	a_A^+	a_A^-	a_S^+	a_S^-	a_P^+	a_P^-	a_{VS}^+	a_{VS}^-	c_{AP}^+	c_{AP}^-
$B \to \pi e^+\mu^-$	5.7(4)	5.7(4)	0	0	8.1(5)	8.1(5)	0	0	0.50(3)	0.50(3)	0	0
$B \to \pi e^+\tau^-$	3.7(2)	3.7(2)	0	0	5.2(3)	5.2(3)	0	0	4.2(3)	4.2(3)	0	0
$B \to \pi \mu^+\tau^-$	3.6(2)	3.7(2)	0	0	5.0(3)	5.3(3)	0	0	3.8(2)	4.6(3)	0	0
$B \to K e^+\mu^-$	8.2(6)	8.2(6)	0	0	14.5(6)	14.5(6)	0	0	1.07(7)	1.09(7)	0	0
$B \to K e^+\tau^-$	5.3(2)	5.3(2)	0	0	8.4(3)	8.4(3)	0	0	8.1(3)	8.1(3)	0	0
$B \to K \mu^+\tau^-$	5.2(2)	5.2(2)	0	0	8.1(2)	8.7(3)	0	0	7.3(3)	8.9(4)	0	0

Table 3.12: Values for the multiplicative factors defined in Eq. (3.57) computed by using the form factor for the transitions $B \to \pi$, $B \to K$ through LQCD evaluations[29].

of oscillations in the $B_s - \bar{B}_s$ system because the time dependence of the B_s-decay rate has been integrated in experiment[30]. Therefore, the experimental decay rate is

$$\Gamma(B_s \to \ell_k^- \ell_l^+)_{exp} \approx \frac{1}{1-y_s}\Gamma(B_s \to \ell_k^- \ell_l^+), \tag{3.56}$$

where $y_s = \Delta\Gamma_{B_s}/(2\Gamma_{B_s}) \approx 0.061$.
In addition, we obtain constraints on the 2-quark-2-lepton operators also from the semileptonic meson decays. In this subsection, we consider $P \to M\ell_k\ell_l$ and its corresponding branching fraction is obtained as [29]

$$\begin{aligned}
\mathcal{B}(P \to M\ell_k^-\ell_l^+) = \frac{v^4}{\Lambda^4}\sum_\alpha \left[a_\alpha^+ \left|\mathscr{C}_{\alpha,L+R}\right|^2 + a_\alpha^- \left|\mathscr{C}_{\alpha,L-R}\right|^2\right] \\
+ \frac{v^4}{\Lambda^4} a_{VS}^+ \,\Re[\mathscr{C}_{V,L+R}\,(\mathscr{C}_{S,L+R})^*] \\
+ \frac{v^4}{\Lambda^4} a_{VS}^- \,\Re[\mathscr{C}_{V,L-R}\,(\mathscr{C}_{S,L-R})^*] \\
+ \frac{v^4}{\Lambda^4} a_{AP}^+ \,\Re[\mathscr{C}_{A,L+R}\,(\mathscr{C}_{P,L+R})^*] \\
+ \frac{v^4}{\Lambda^4} a_{AP}^- \,\Re[\mathscr{C}_{A,L-R}\,(\mathscr{C}_{P,L-R})^*]\,,
\end{aligned} \tag{3.57}$$

where the coefficients are defined as

$$\mathscr{C}_{(^S_P)R} = \frac{\pm C_{\ell edq}^{klij}}{2}, \tag{3.58}$$

$$\mathscr{C}_{(^V_A)L} = \frac{C_{\ell d}^{klij} \pm \left(C_{\ell q}^{(1)klij} + C_{\ell q}^{(3)klij}\right)}{2}, \tag{3.59}$$

$$\mathscr{C}_{(^V_A)R} = \frac{C_{ed}^{klij} \pm C_{qe}^{ijkl}}{2}, \tag{3.60}$$

$$\mathscr{C}_{(^S_P)L} = \frac{C_{\ell edq}^{klij*}}{2}\,, \tag{3.61}$$

and the multiplicative coefficients are reported in Table 3.12.

Another interesting process is the τ decay into a lepton $\ell = e, \mu$ and a meson. Here, we consider $\tau \to \ell\pi$. In order to evaluate the decay rate two steps are necessary. First, one should evaluate the perturbative matrix element and then the hadronization process must be considered[31]. The results we present are taken from [28]:

$$\Gamma\left(\tau^+ \to \ell^+\pi^0\right) = \frac{m_\tau^3}{256\pi\Lambda^4}\left(1 - \frac{m_\pi^2}{m_\tau^2}\right)^2 f_\pi^2\Big[\,|A_L^\pi|^2 + |A_R^\pi|^2\,\Big], \tag{3.62}$$

where f_π is the pion decay constant. $A_{L,R}^\pi$ is expressed by

$$\begin{aligned} A_L^\pi =& \Big(C_{\ell u} - C_{\ell q}^{(1)}\Big)^{\tau\ell uu} - \Big(C_{\ell d} - C_{\ell q}^{(1)}\Big)^{\tau\ell dd} \\ &+ \frac{m_\pi^2}{m_\tau\,(m_u + m_d)}\left[\Big(C_{lequ}^{(1)*} - C_{ledq}^*\Big)^{\ell\tau uu} - \Big(C_{lequ}^{(1)*} - C_{ledq}^*\Big)^{\ell\tau dd}\right], \end{aligned} \tag{3.63}$$

$$\begin{aligned} A_R^\pi =& \Big(C_{\ell u}\Big)^{uu\tau\ell} - \Big(C_{\ell q}^{(1)}\Big)^{\tau\ell uu} - \left[\Big(C_{\ell d}\Big)^{dd\tau\ell} - \Big(C_{\ell q}^{(1)}\Big)^{\tau\ell dd}\right] \\ &+ \frac{m_\pi^2}{m_\tau\,(m_u + m_d)}\left[\Big(C_{lequ}^{(1)} - C_{ledq}\Big)^{\tau\ell uu} - \Big(\Big(C_{lequ}^{(1)} - C_{ledq}\Big)^{\tau\ell dd}\right]. \end{aligned} \tag{3.64}$$

The bounds on the Wilson coefficients and on the NP scale are given in Table 3.13.

	$\lvert C_a\rvert$ [$\Lambda = 1$ TeV]	Λ (TeV) [$\lvert C_a\rvert = 1$]	CLFV Process
$C_{\ell u}^{\tau euu}$	1.9×10^{-2}	7.3×10^3	$\tau \to e\pi$
$C_{\ell u}^{\tau\mu uu}$	1.5×10^{-2}	8.1×10^3	$\tau \to \mu\pi$
$C_{lequ}^{(1)e\tau uu}$	1.8×10^{-3}	2.4×10^4	$\tau \to e\pi$
$C_{lequ}^{(1)\mu\tau uu}$	1.4×10^{-3}	2.7×10^4	$\tau \to \mu\pi$

Table 3.13: Bounds on the coefficients of some of the flavor-violating operators of Table 2.1, exploiting the experimental constraints of Table 1.1, for $\Lambda = 1$ TeV, and corresponding bounds on Λ (in TeV) for $|C_a| = 1$.

3.2 One-loop contributions to LFV decays

Until now many operators contribute to the three-body decay at tree level, however, only dipole operators generate the decay $\ell_i \to \ell_j\gamma$. The aim of this section is to obtain a modification of the dipole operators at the 1 loop level. In this way, several operators are constrained by the decay of $\ell_i \to \ell_j\gamma$. Moreover, these modified couplings also generate 1-loop contributions to other processes, such as the three-body LFV decays.

3.2.1 $\ell_i \to \ell_j\gamma$ at 1-loop induced by 4-fermion operators

As pointed out in the previous chapter, the general form of the effective lepton-photon vertex can be written in the following way:

$$V_{\ell\ell\gamma}^{ji\,\mu} = \frac{i}{\Lambda^2}\Big[\gamma^\mu(F_{VL}^{ji}P_L + F_{VR}^{ji}P_R) + (F_{SL}^{ji}P_L + F_{SR}^{ji}P_R)q^\mu + (F_{TL}^{ji}i\sigma^{\mu\nu}P_L + F_{TR}^{ji}i\sigma^{\mu\nu}P_R)q_\nu\Big]\ . \tag{3.65}$$

However, only the tensor form factors really enter the formula for the decay rate, as we saw in Eq. (1.36), while the other terms vanish on-shell. The generic topologies of Feynman diagrams that can contribute to $\ell_i \to \ell_j\gamma$ at one loop are the following[27]:

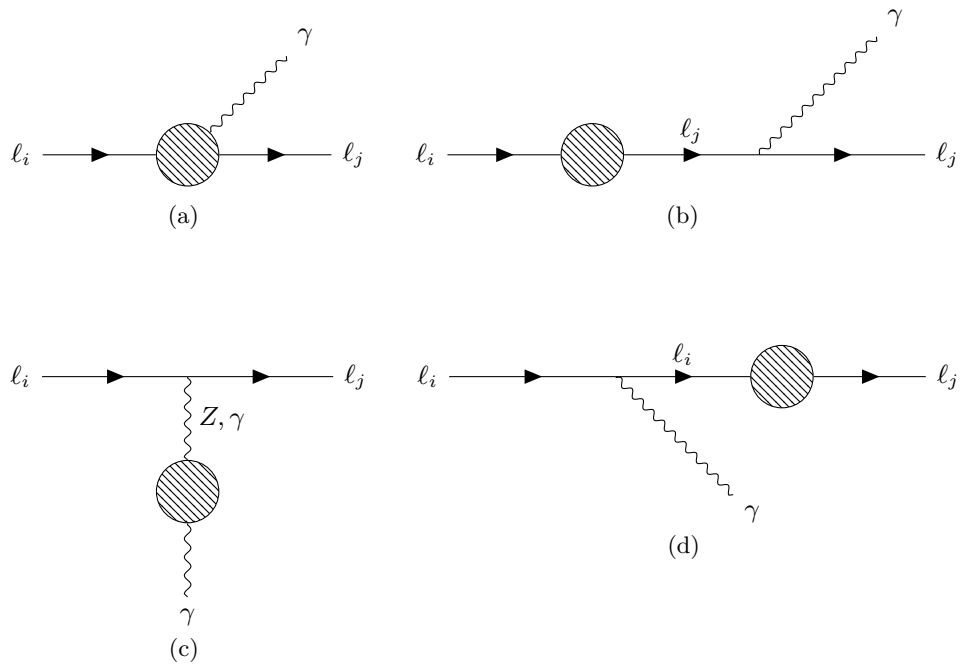

Figure 3.10: Generic topologies of diagram contributing to the radiative CLFV muon decay at one loop.

The gray discs represent either the self-energy insertion or the 1-particle irreducible three-point functions that can be obtained once we consider a certain set of operators. Let us start evaluating the graphs (b) and (d) in full generality to see that they cannot contribute to the tensor form factors entering the decay rate. We can decompose those self-energy contributions in terms of scalar, vector, pseudo-scalar, and pseudo-vector form factors:

$$\Sigma^{ij}(p) = \Sigma_V^{ij} \not{p} + \Sigma_A^{ij} \not{p} \gamma^5 + \Sigma_S^{ij} + \Sigma_p^{ij} \gamma^5. \tag{3.66}$$

Denoting the amplitude of the first diagram as $\mathcal{M}_1$ and the second diagram as $\mathcal{M}_2$ their explicit expressions read:

$$\begin{aligned} \mathcal{M}_1 &= ie\bar{u}_j(p-q)\Sigma^{ij}(p-q)\frac{\not{p}-\not{q}+m_i}{(p-q)^2-m_i^2}\gamma^\mu u_i(p)\epsilon_\mu^*(q), \\ \mathcal{M}_2 &= ie\bar{u}_j(p-q)\gamma^\mu \frac{\not{p}+m_j}{p^2-m_j^2}\Sigma^{ij}(p)u_i(p)\epsilon_\mu^*(q). \end{aligned} \tag{3.67}$$

To simplify these relations, we can use the Dirac equations

$$\bar{u}_j(p-q)(\not{p}-\not{q}) = m_j\bar{u}_j(p-q), \qquad \not{p}\bar{u}_i(p) = m_i\bar{u}_i(p). \tag{3.68}$$

Indeed, writing the explicit form of the self-energy reported in Eq. (3.66) and applying the four contributions on the spinors, one gets:

$$\mathcal{M}_1 + \mathcal{M}_2 = ie\bar{u}_j\left[\frac{A}{m_i-m_j}\gamma^\mu - \frac{B}{m_i+m_j}\gamma^\mu\gamma^5\right]u_i(p)\epsilon_\mu^*(q), \tag{3.69}$$

where A is given by

$$A = m_i\Sigma_V^{ij}(m_i^2) + \Sigma_S^{ij}(m_i^2) - m_j\Sigma_V^{ij}(m_j^2) - \Sigma_S^{ij}(m_j^2), \tag{3.70}$$

and B is

$$B = m_i \Sigma_P^{ij}(m_i^2) - \Sigma_A^{ij}(m_i^2) - m_j \Sigma_A^{ij}(m_j^2) - \Sigma_P^{ij}(m_j^2). \tag{3.71}$$

Thus, the self-energy contributions can modify only the vector invariant amplitudes, without participating in the evaluation of the decay rate. However, they are necessary to cancel relevant parts of other diagrams in order to make the total amplitude gauge invariant, and even if for on-shell photons their contribution is vanishing, they can contribute to the off-shell vertices. To obtain the SMEFT prediction for $\ell_i \to \ell_j \gamma$ we have to look to the 3-point 1-PI diagrams, and this will be done in the rest of the section.

Let us start considering the 2-quark 2-lepton operators; for this set of operators the calculation is quite straightforward and can be carried out completely by hand without the help of Mathematica. For this reason, the first evaluation is written in full detail to better understand the procedure and the main aspect of the results. The contribution of 2-quark 2-lepton operators to muon decay arises from the following one-loop diagram:

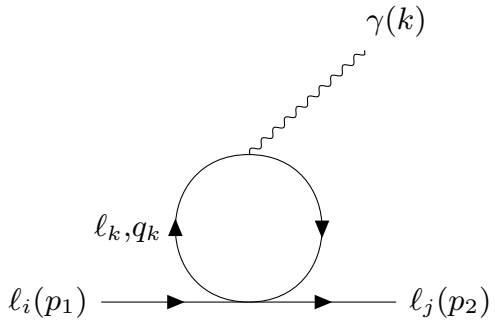

Figure 3.11: Feynman diagram contributing to the decay $\ell_i \to \ell_j \gamma$ at 1 loop, due to 2-quark 2-lepton and 4-lepton operators.

The operators that can be inserted into the diagram to form the loop are those reported in Table 2.1, in the second group. To show the calculation, we start by considering the first one, namely,

$$Q_{\ell q}^{(1)} = (\bar{L}_L \gamma_\mu L_L)(\bar{Q}_L \gamma^\mu Q_L). \tag{3.72}$$

The first thing that we can notice is that it does not contribute to the self-energy, indeed, the corresponding amplitude is

$$\Sigma^{ij} = \sum_l \gamma_\mu \mu^{4-d} \int \frac{d^d p}{(2\pi)^d} Tr\left[\frac{1}{\not{p} - m_{q_l}} \gamma^\mu\right] = \sum_l \gamma_\mu \mu^{4-d} \int \frac{d^d p}{(2\pi)^d} Tr\left[\frac{\not{p} + m_{q_l}}{p^2 - m_{q_l}^2} \gamma^\mu\right]. \tag{3.73}$$

However, the previous integration is vanishing, because taking the trace, since $Tr[\gamma^\mu] = 0$, the term that contains the mass is zero; while when we integrate on the other term, we have to integrate an odd function over an even domain, getting zero again. Therefore, the only diagram we have to evaluate is the first one reported in Figure 3.11 and the corresponding amplitude in dimensional regularization is given by

$$\mathcal{M} = -\sum_l \frac{Q_l e C_{\ell q}^{(1)ijll}}{\Lambda^2} \bar{u}_j(p_2) \gamma_\mu P_L u_i(p_1) \mu^{4-d} \int \frac{d^d p}{(2\pi)^d} Tr\left[\frac{1}{\not{p} - m_{q_l}} \gamma_\rho \frac{1}{\not{p} - \not{k} - m_{q_l}} \gamma^\mu P_L\right] \epsilon^{*\rho}(k), \tag{3.74}$$

where Q_l is the electric charge of the quark considered. The trace can be evaluated using the standard

traces for Dirac matrices reported in Appendix A and gives the following:

$$Tr\left[\frac{1}{\not p - m_{q_l}}\gamma^\rho \frac{1}{\not p - \not k - m_{q_l}}\gamma^\mu P_L\right] = \frac{2i\epsilon^{\mu\rho\alpha\beta}p_\alpha k_\beta - 2k^\mu p^\rho - 2p^\mu k^\rho + 4k^\mu k^\rho + \left(2m^2 - 2p^2 + 2k\cdot p\right) g^{\mu\rho}}{(p^2 - m_{q_l}^2)((p-k)^2 - m_{q_l}^2)}. \tag{3.75}$$

Since this kind of loop integrals is going to be evaluated many times in this chapter, for this first diagram all the steps are presented in full detail. First, the denominator must be rewritten using the Feynman parameterization:

$$\frac{1}{AB} = \int_0^1 \frac{dx}{[xA + (1-x)B]^2}. \tag{3.76}$$

Giving

$$\frac{1}{(p^2 - m_{q_l}^2)((p-k)^2 - m_{q_l}^2)} = \int_0^1 \frac{dx}{[(p^2 - m_{q_l}^2)(1-x) + ((p-k)^2 - m_{q_l}^2)x]^2}. \tag{3.77}$$

Completing the square in the denominator, one obtains:

$$\frac{1}{(p^2 - m_{q_l}^2)((p-k)^2 - m_{q_l}^2)} = \int_0^1 \frac{dx}{[(p-kx)^2 - C]^2}, \tag{3.78}$$

where $C = k^2x(x-1) + m_{q_l}^2$. Since the integration domain in d^4p is the entire space-time one can shift the momentum setting $p' = p - kx$ obtaining:

$$\int \frac{d^dp}{(2\pi)^d}\frac{1}{(p^2 - m_{q_l}^2)((p-k)^2 - m_{q_l}^2)} = \int \frac{d^dp}{(2\pi)^d}\int_0^1 \frac{dx}{(p^2 - C)^2}. \tag{3.79}$$

If in the numerator there are no powers of p, then one can directly use the master formula for loop integrals in dimensional regularization, that is:

$$I_{r,m} = \int \frac{d^dp}{(2\pi)^d}\frac{(k^2)^r}{[k^2 - C]^m} = i\frac{(-1)^{r-m}}{(4\pi)^2}\left(\frac{4\pi}{C}\right)^{\frac{\epsilon}{2}} C^{2+r-m}\frac{\Gamma(2 + r - \frac{\epsilon}{2})}{\Gamma(2 - \frac{\epsilon}{2})}\frac{\Gamma(m - r - 2 + \frac{\epsilon}{2})}{\Gamma(m)}, \tag{3.80}$$

where Γ is the Euler Gamma function. Applying this formula, we get:

$$\int \frac{d^dp}{(2\pi)^d}\frac{1}{(p^2 - m_{q_l}^2)((p-k)^2 - m_{q_l}^2)} = \int_0^1 dx \frac{i}{(4\pi)^2}\left(\frac{4\pi}{C}\right)^{\frac{\epsilon}{2}}\Gamma\left(\frac{\epsilon}{2}\right). \tag{3.81}$$

The last step requires us to expand the Gamma function using the well-known series:

$$\begin{aligned}\Gamma(\epsilon - 1) &= -\frac{1}{\epsilon} - 1 + \gamma + \mathcal{O}(\epsilon)\\ \Gamma(\epsilon) &= \frac{1}{\epsilon} - \gamma + \mathcal{O}(\epsilon),\end{aligned} \tag{3.82}$$

where $\gamma \approx 0.557216$ is the Euler-Mascheroni constant. Keeping only the leading terms in ϵ one obtains:

$$\int \frac{d^dp}{(2\pi)^d}\frac{1}{(p^2 - m_{q_l}^2)((p-k)^2 - m_{q_l}^2)} = \int_0^1 dx \frac{i}{(4\pi)^2}\left(\frac{2}{\epsilon} - \gamma + log(4\pi) + log\frac{\mu^2}{C^2}\right). \tag{3.83}$$

The last thing to do is perform the integral in the variable x and this can be done analytically

expanding in the external momenta obtaining:

$$\int \frac{d^dp}{(2\pi)^d}\frac{1}{(p^2-m_{q_l}^2)((p-k)^2-m_{q_l}^2)} = \frac{i}{(4\pi)^2}\left(\frac{2}{\epsilon}-\gamma+log(4\pi)+log\frac{\mu^2}{m_{q_l}^2}+\frac{k^2}{6m_{q_l}^2}+\frac{(k^2)^2}{60m_{q_l}^4}+\mathcal{O}\left((k^2)^2\right)\right). \tag{3.84}$$

If we are interested only in the case in which the photon is on-shell, then the final result becomes very simple and reads:

$$\int \frac{d^dp}{(2\pi)^d}\frac{1}{(p^2-m_{q_l}^2)((p-k)^2-m_{q_l}^2)} = \frac{i}{(4\pi)^2}\left(\frac{2}{\epsilon}-\gamma+log(4\pi)+log\frac{\mu^2}{m_{q_l}^2}\right) \tag{3.85}$$

Differently, in the case where in the numerator there is a dependence on the integration variable p one should perform the shift on it, cancel all odd powers because they are odd integrand functions on an even domain, and then use the formula in Eq. (3.80). Eventually, one obtains the following results for the remaining two integrals:

$$\int \frac{d^dp}{(2\pi)^d}\frac{p^\mu}{(p^2-m_{q_l}^2)((p-k)^2-m_{q_l}^2)} = \frac{ik^\mu}{2(4\pi)^2}\left(\frac{2}{\epsilon}-\gamma+log(4\pi)+log\frac{\mu^2}{m_{q_l}^2}+\frac{k^2}{6m_{q_l}^2}+\mathcal{O}\left((k^2)^2\right)\right), \tag{3.86}$$

$$\int \frac{d^dp}{(2\pi)^d}\frac{p^2}{(p^2-m_{q_l}^2)((p-k)^2-m_{q_l}^2)} = \frac{i}{(4\pi)^2}\left[2m_{q_l}^2\left(\frac{2}{\epsilon}-\gamma+log(4\pi)+log\frac{\mu^2}{m_{q_l}^2}\right)+m_{q_l}^2+\frac{k^2}{6}\right]+\mathcal{O}\left((k^2)^2\right). \tag{3.87}$$

Substituting the integration results into Eq. (3.75) we obtain the final expression for the amplitude, that is:

$$\begin{aligned}\mathcal{M} = &\sum_l \frac{iQ_l e C_{\ell q}^{(1)ijll}}{(4\pi)^2\Lambda^2}\bar{u}_j(p_2)\gamma_\mu P_L u_i(p_1)\left[\left(-\frac{2}{3}k^\mu k_\rho\epsilon^{*\rho}(k)\left(\frac{2}{\epsilon}-\gamma+log(4\pi)+log\frac{\mu^2}{m_{q_l}^2}\right)\right)+\right.\\ &\left.+\left(\frac{2}{3}k^2\epsilon^{*\mu}(k)\left(\frac{2}{\epsilon}-\gamma+log(4\pi)+log\frac{\mu^2}{m_{q_l}^2}\right)\right)\right].\end{aligned} \tag{3.88}$$

Calling now $\Delta = \frac{2}{\epsilon}-\gamma+log(4\pi)$ and distinguishing between down-type quarks (d_i) and up-type quarks (u_i) we can write the final expression for the form factors that are:

$$\begin{aligned}F_{VL}^{ji,4f} &= \frac{4ek^2}{9(4\pi)^2}\sum_{l=1}^{3}\left(C_{\ell q}^{(1)jill}\right)\left(\Delta-\log\frac{m_{u_l}^2}{\mu^2}\right)-\frac{2ek^2}{9(4\pi)^2}\sum_{l=1}^{3}\left(C_{\ell q}^{(1)jill}\right)\left(\Delta-\log\frac{m_{d_l}^2}{\mu^2}\right),\\ F_{TL}^{ji,4f} &= 0,\\ F_{SL}^{ji,4f} &= \frac{4e}{9(4\pi)^2}\sum_{l=1}^{3}m_l\left(C_{\ell q}^{(1)jill}\right)\left(\Delta-\log\frac{m_{u_l}^2}{\mu^2}\right)-\frac{2e}{9(4\pi)^2}\sum_{l=1}^{3}m_j\left(C_{\ell q}^{(1)jill}\right)\left(\Delta-\log\frac{m_{d_l}^2}{\mu^2}\right).\end{aligned}$$

In the last equation the electron mass comes out because of the Dirac equation; indeed, when we have $\bar{u}_j(p_2)\gamma_\mu P_L u_i(p_1)k^\mu$ we can rewrite it as:

$$\bar{u}_j(p_2)(\not{p}_1-\not{p}_2)P_L u_i(p_1) = \bar{u}_j(p_2)(-m_e P_L+m_\mu P_R)u_i(p_1). \tag{3.89}$$

For this reason, to obtain $F_{SR}^{4f\,ji}$ one can simply exchange $m_j \leftrightarrow m_i$ and change the sign.
The first thing to notice is that this operator does not contribute to $F_{TL}^{4f\,ji}$ and therefore does not induce muon decay with the final photon on-shell, but it induces a vertex with the photon off-shell. It is interesting to notice that if the final photon is on-shell, namely $k^2 = 0$, the vector form factor is vanishing and this represents an important check for our calculation because the Gauge invariance requires exactly the cancelation of $F_{VL}^{4f\,ji}$. The same procedure has been repeated for all operators reported in Table 2.1 for what concerns the 2-quark 2-lepton operators. The final result is given by

$$\begin{aligned}
F_{VL}^{ji,4f} &= \frac{4ek^2}{9(4\pi)^2}\sum_{l=1}^{3}\left(C_{\ell q}^{(1)jill} - C_{\ell q}^{(3)jill} + C_{\ell u}^{jill}\right)\left(\Delta - \log\frac{m_{u_l}^2}{\mu^2}\right), \\
&- \frac{2ek^2}{9(4\pi)^2}\sum_{l=1}^{3}\left(C_{\ell q}^{(1)jill} + C_{\ell q}^{(3)jill} + C_{\ell d}^{jill}\right)\left(\Delta - \log\frac{m_{d_l}^2}{\mu^2}\right), \\
F_{VR}^{ji,4f} &= \frac{4ek^2}{9(4\pi)^2}\sum_{l=1}^{3}\left(C_{eq}^{jill} + C_{eu}^{(3)jill}\right)\left(\Delta - \log\frac{m_{u_l}^2}{\mu^2}\right), \\
&- \frac{2ek^2}{9(4\pi)^2}\sum_{l=1}^{3}\left(C_{eq}^{jill} + C_{ed}^{(3)jill}\right)\left(\Delta - \log\frac{m_{d_l}^2}{\mu^2}\right), \\
F_{SL}^{ji,4f} &= \frac{4e}{9(4\pi)^2}\sum_{l=1}^{3}\left(m_j\left(C_{\ell q}^{(1)jill} - C_{\ell q}^{(3)jill} + C_{\ell u}^{jill}\right) - m_i\left(C_{eq}^{jill} + C_{eu}^{(3)jill}\right)\right)\left(\Delta - \log\frac{m_{u_l}^2}{\mu^2}\right), \\
&- \frac{2e}{9(4\pi)^2}\sum_{l=1}^{3}\left(m_j\left(C_{\ell q}^{(1)jill} + C_{\ell q}^{(3)jill} + C_{\ell d}^{jill}\right) - m_i\left(C_{eq}^{jill} + C_{ed}^{(3)jill}\right)\right)\left(\Delta - \log\frac{m_{d_l}^2}{\mu^2}\right), \\
F_{SR}^{ji,4f} &= -F_{SL}^{ji,4f}(m_j \leftrightarrow m_i), \\
F_{TL}^{ji,4f} &= -\frac{16e}{3\cdot(4\pi)^2}\sum_{l=1}^{3} C_{\ell equ}^{(3)ijll*} m_{u_l}\left(\Delta - \log\frac{m_{u_l}^2}{\mu^2}\right), \\
F_{TR}^{ji,4f} &= -\frac{16e}{3\cdot(4\pi)^2}\sum_{l=1}^{3} C_{\ell equ}^{(3)ijll} m_{u_l}\left(\Delta - \log\frac{m_{u_l}^2}{\mu^2}\right).
\end{aligned} \tag{3.90, 3.91}$$

Once again the vector form factors vanish in the on-shell limit, but this time we have a contribution to the tensor form factors from the operator $Q_{\ell equ}^{(3)}$ that gives a non-vanishing decay rate for $\mu \to e\gamma$ according to Eq. (3.13). For this important result, let us see the main steps involved in the evaluation of the tensor form factors. The corresponding amplitude in dimensional regularization is given by:

$$\mathcal{M} = -\sum_{l=1}^{3}\frac{2eC_{\ell equ}^{(3)ijll}}{3\Lambda^2}\bar{u}_j(p_2)\sigma_{\mu\nu}P_R u_i(p_1)\mu^{4-d}\int\frac{d^dp}{(2\pi)^d}Tr\left[\frac{1}{\not{p} - m_{u_l}}\gamma_\rho\frac{1}{\not{p} - \not{k} - m_{u_l}}\sigma^{\mu\nu}P_R\right]\epsilon^{*\rho}(k), \tag{3.92}$$

where p is the momentum flowing in the loop and μ the 't Hooft parameter.
The trace can be evaluated using the standard traces for Dirac matrices reported in Appendix A and gives:

$$Tr\left[\frac{1}{\not{p} - m_{u_l}}\gamma^\rho\frac{1}{\not{p} - \not{k} - m_{u_l}}\sigma^{\mu\nu}P_R\right] = \frac{2m_{u_l}k^\nu g^{\mu\rho} - 2m_{u_l}k^\mu g^{\nu\rho} + 2im_{u_l}\epsilon^{\nu\rho\mu\sigma}k_\sigma}{(p^2 - m_{u_l}^2)((p-k)^2 - m_{u_l}^2)}. \tag{3.93}$$

Since this trace is contracted with the skew-symmetric tensor $\sigma_{\mu\nu}$ we can swap those indices changing

sign and use the identity $\sigma_{\mu\nu} = \frac{i}{2}\epsilon^{\mu\nu\alpha\beta}\sigma_{\alpha\beta}\gamma_5$ to get:

$$Tr\left[\frac{1}{\not{p} - m_{u_l}}\gamma^\rho \frac{1}{\not{p} - \not{k} - m_{u_l}}\sigma^{\mu\nu}P_R\right] = \frac{8m_{u_l}k^\nu g^{\mu\rho}}{(p^2 - m_{u_l}^2)((p-k)^2 - m_{u_l}^2)}. \tag{3.94}$$

Finally, by integrating as explained above, the result reported in Eq. (3.91) is achieved. It is worth noting that the obtained result is divergent in the limit $\epsilon \to 0$, this divergence can be understood looking at a UV completion; indeed, directly calculating the contributions to the amplitude in the full theory one would obtain a finite result[27] because the divergence is canceled by a counterterm to Q_{eW} and Q_{eB}.

A very similar calculation can be repeated for the 4-lepton operators in Table 2.1. In this case the main differences are two:

- The electric charge of the particle running in the loop is different from the previous case: $Q = 1$ for charged leptons;
- The Feynman rule for what concerns the operators $Q_{\ell\ell}$ and Q_{ee} requires an additional factor two for the symmetry of the vertex as reported in [32].

Taking into account these differences, it is straightforward to use the previous expressions to obtain the results for the 4-lepton operators that are:

$$\begin{aligned}
F_{VL}^{ji,4\ell} &= -\frac{2ek^2}{3(4\pi)^2}\sum_{l=1}^{3}\left((2C_{\ell\ell}^{jill} + C_{\ell e}^{jill})\left(\Delta - \log\frac{m_{\ell_l}^2}{\mu^2}\right)\right), \\
F_{VR}^{ji,4\ell} &= -\frac{2ek^2}{3(4\pi)^2}\sum_{l=1}^{3}\left((2C_{ee}^{jill} + C_{\ell e}^{llji})\left(\Delta - \log\frac{m_{\ell_l}^2}{\mu^2}\right)\right), \\
F_{SL}^{ji,4\ell} &= -\frac{2e}{3(4\pi)^2}\sum_{l=1}^{3}\left((2C_{\ell\ell}^{jill}m_e - 2C_{ee}^{jill}m_\mu - (C_{\ell e}^{llji}m_\mu - C_{\ell e}^{jill}m_\mu))\left(\Delta - \log\frac{m_{\ell_j}^2}{\mu^2}\right)\right), \\
F_{SR}^{ji,4\ell} &= -F_{SL}^{ji,4\ell}(m_j \leftrightarrow m_i).
\end{aligned} \tag{3.95, 3.96}$$

Particular attention is required in the calculation regarding the operator $Q_{\ell e}^{jlli}$: in this case, the loop is closed between leptons belonging to different currents in the operator. Consequently, Fierz identities must be used to rewrite that operator with both off-shell leptons in the same vertex.

Evaluating the loop integration one obtains a non-vanishing tensor form factor:

$$F_{TL}^{ji,4\ell} = \frac{2em_i}{16\pi^2}C_{\ell e}^{illj}, \tag{3.97}$$

and as far as the right amplitude is concerned we get the following result:

$$F_{TR}^{ji,4\ell} = \frac{2em_i}{16\pi^2}C_{\ell e}^{lijl}. \tag{3.98}$$

In particular, we observe that the mass appearing in the final result is the mass of the particle that is flowing in the loop. Therefore, this allows us to infer bounds on several coefficients, as shown in the following Table 3.14.

	$\lvert C_a\rvert$ [$\Lambda = 1$ TeV]	Λ (TeV) [$\lvert C_a\rvert = 1$]	CLFV Process
$C_{\ell e}^{\mu eee,eee\mu}$	3.7×10^{-2}	5	$\mu \to e\gamma$ [1-loop]
$C_{\ell e}^{\mu\mu\mu e,e\mu\mu\mu}$	1.8×10^{-4}	75	$\mu \to e\gamma$ [1-loop]
$C_{\ell e}^{\mu\tau\tau e,e\tau\tau\mu}$	1.0×10^{-5}	312	$\mu \to e\gamma$ [1-loop]
$C_{\ell e}^{\tau eee,eee\tau}$	418	0.05	$\tau \to e\gamma$ [1-loop]
$C_{\ell e}^{\tau\mu\mu e,e\mu\mu\tau}$	2	0.7	$\tau \to e\gamma$ [1-loop]
$C_{\ell e}^{\tau\tau\tau e,e\tau\tau\tau}$	0.12	3	$\tau \to e\gamma$ [1-loop]
$C_{\ell e}^{\tau ee\mu,\mu ee\tau}$	482	0.05	$\tau \to \mu\gamma$ [1-loop]
$C_{\ell e}^{\tau\mu\mu\mu,\mu\mu\mu\tau}$	2.3	0.7	$\tau \to \mu\gamma$ [1-loop]
$C_{\ell e}^{\tau\tau\tau\mu,\mu\tau\tau\tau}$	0.14	3	$\tau \to \mu\gamma$ [1-loop]

Table 3.14: Bounds on the coefficients of some of the flavor-violating operators of Table 2.1, exploiting the experimental constraints of Table 1.1, for $\Lambda = 1$ TeV, and corresponding bounds on Λ (in TeV) for $|C_a| = 1$.

3.2.2 $\ell_i \to \ell_j\gamma$ induced by Higgs modified couplings

We have shown in Eq. (2.33) how a flavor violating Higgs-lepton interaction is generated. Thus, at the one-loop level, we obtain a diagram for the radiative decay with the Higgs boson running in the loop[1]:

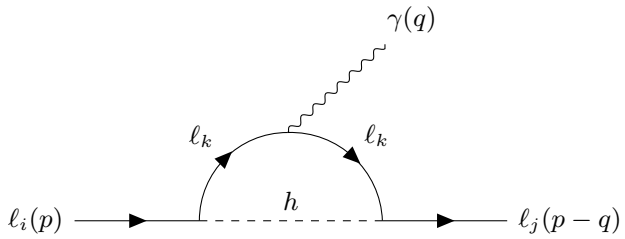

Figure 3.12: Feynman diagram contributing to the decay $\ell_i \to \ell_j\gamma$ at 1 loop, due to modified Higgs interactions.

In particular, only one of the two Higgs-lepton vertices is effective, the other one is a Standard Model vertex. Therefore, the amplitude is given by:

$$\mathcal{M} = \mu^{4-d} \int \frac{d^d k}{(2\pi)^d} \frac{N}{(k^2 - m_k^2)[(k-q)^2 - m_k^2][(k-p)^2 - m_h^2]}, \tag{3.99}$$

where the numerator

$$N = \frac{e m_i v}{\sqrt{2}\Lambda^2} \bar{u}_j(p-q) \left([L_e^\dagger C_{e\Phi 3}^\dagger R_e]_{ji} P_R + L_e^\dagger C_{e\Phi 3}^\dagger R_e]_{ij}^* P_L \right) (\not{k} - \not{q} + m_k)\gamma^\mu (\not{k} + m_k) u_i(p) \epsilon_\mu^*(q). \tag{3.100}$$

It is worth noting that one can exchange the two vertices, obtaining another contribution to the amplitude. However, it would be suppressed by the mass of the final lepton, and thus we neglect it. In addition, it is important to consider the self-energy contributions, which cannot contribute to the decay with the photon on-shell, but give a contribution to vector and scalar form factors. On the contrary, the diagram (c) in Figure 3.10 is vanishing. Evaluation of the loop integrals with three propagators is much more difficult and lengthy; thus, a Mathematica program has been implemented with *Package-X*. This tool is able to translate the loop integral into a combination of Passarino-Veltman functions,

[1] We neglect cases where photon vertex is flavor violating because this process would be induced at tree level.

	$\lvert C_a\rvert$ [$\Lambda = 1$ TeV]	Λ (TeV) [$\lvert C_a\rvert = 1$]	CLFV Process
$[L_e^\dagger C_{e\Phi 3}^\dagger R_e]_{\mu e}$	3.9×10^{-2}	5	$\mu \to e\gamma$
$[L_e^\dagger C_{e\Phi 3}^\dagger R_e]_{\tau e}$	4.8×10^{-10}	46×10^3	$\tau \to e\gamma$
$[L_e^\dagger C_{e\Phi 3}^\dagger R_e]_{\tau \mu}$	5.5×10^{-10}	43×10^3	$\tau \to \mu\gamma$

Table 3.15: Bounds on the coefficients of some of the flavor-violating operators of Table 2.1, exploiting the experimental constraints of Table 1.1, for $\Lambda = 1$ TeV, and corresponding bounds on Λ (in TeV) for $|C_a| = 1$.

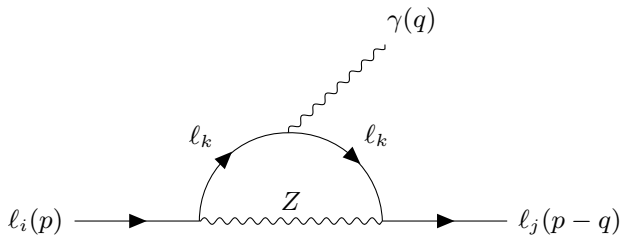

Figure 3.13: Feynman diagram contributing to the decay $\ell_i \to \ell_j\gamma$ at 1 loop, due to modified Z interactions.

and then the expansion in terms of light lepton masses is straightforward. The program to compute the final result is reported in Appendix B. Once again, as an important check of the calculation, the vector form factors must vanish on-shell due to Gauge invariance, and this is also proved in Appendix B.

The results for the tensor form factors entering the decay rate are the following:

$$\begin{aligned} F_{TL}^{ji,H} &= \frac{e}{16\pi^2}\frac{m_i^2 v}{\sqrt{2}m_h^2}\left(log\left(\frac{m_h^2}{m_i^2}\right) - \frac{4}{3}\right)[L_e^\dagger C_{e\Phi 3}^\dagger R_e]_{ij}^*, \\ F_{TR}^{ji,H} &= \frac{e}{16\pi^2}\frac{m_i^2 v}{\sqrt{2}m_h^2}\left(log\left(\frac{m_h^2}{m_i^2}\right) - \frac{4}{3}\right)[L_e^\dagger C_{e\Phi 3}^\dagger R_e]_{ji}. \end{aligned} \tag{3.101}$$

While the expressions for the vector and scalar form factors are given by:

$$\begin{aligned} F_{VL}^{ji,H} &= \frac{e}{16\pi^2}\frac{q^2 m_i v}{3\sqrt{2}m_h^2}\left(log\left(\frac{m_h^2}{m_i^2}\right) - \frac{4}{3}\right)[L_e^\dagger C_{e\Phi 3}^\dagger R_e]_{ij}^*, \\ F_{VR}^{ji,H} &= \frac{e}{16\pi^2}\frac{q^2 m_i v}{3\sqrt{2}m_h^2}\left(log\left(\frac{m_h^2}{m_i^2}\right) - \frac{4}{3}\right)[L_e^\dagger C_{e\Phi 3}^\dagger R_e]_{ji}, \\ F_{SL}^{ji,H} &= -\frac{e}{32\pi^2\sqrt{2}}\left(\frac{1}{2} + \Delta + 2log\left(\frac{\mu^2}{m_h^2}\right)\right)[L_e^\dagger C_{e\Phi 3}^\dagger R_e]_{ij}^*, \\ F_{SR}^{ji,H} &= \frac{e}{32\pi^2\sqrt{2}}\left(\frac{1}{2} + \Delta + 2log\left(\frac{\mu^2}{m_h^2}\right)\right)[L_e^\dagger C_{e\Phi 3}^\dagger R_e]_{ji}. \end{aligned} \tag{3.102}$$

Therefore, we compare the decay rate with the experimental limits and obtain the constraints of Table 3.15.

3.2.3 $\ell_i \to \ell_j\gamma$ at 1-loop induced by Z and W modified couplings

Thanks to the modification of the weak interaction couplings, evaluated in Equations 2.38 and 2.40, we obtain flavor mixing Z and W couplings. These interactions generate a $1-$ loop diagram that contributes to the muon radiative decay. The graph is given in Figure 3.13.

In the case in which the dipole operator coefficients are nonvanishing, the radiative flavor violating muon decay is already induced at the tree level by the photon dipole. Thus, the contribution of the Z

dipole operator to the one-loop diagram is neglected, and therefore in the effective vertices only the coefficients a_{ij}^Z and b_{ij}^Z are considered. From now on for the sake of simplicity, the apex Z is omitted. An important observation is that in the limit of large momenta the propagators of the Z and W bosons are divergent in the unitary gauge. Because of this, all the following calculations are performed in a generic $R-\xi$ Gauge, where the divergencies disappear. However, there is a price to pay, which consists of adding the contribution of the Goldstone bosons. The expression for the amplitude in a generic $R-\xi$ Gauge can be expressed as the sum between the ξ-independent part and a ξ-dependent part $\mathcal{M} = \mathcal{M}_0 + \mathcal{M}_\xi$ and reads

$$\mathcal{M}_0 = \mu^{4-d} \int \frac{d^d k}{(2\pi)^d} \frac{N_0}{(k^2 - m_k^2)[(k-q)^2 - m_k^2][(k-p)^2 - M_Z^2]}, \tag{3.103}$$

where

$$N_0 = -e\bar{u}_j(p-q)\gamma_\alpha(a_{jk}^* P_L + b_{jk}^* P_R)(\not{k} - \not{q} + m_k)\gamma^\mu(\not{k} + m_k)\gamma^\alpha(a_{ki}P_L + b_{ki}P_R)u_i(p)\epsilon_\mu^*(q), \tag{3.104}$$

while the ξ-dependent part is:

$$\mathcal{M}_\xi = \mu^{4-d} \int \frac{d^d k}{(2\pi)^d} \frac{N_\xi}{(k^2 - m_k^2)[(k-q)^2 - m_k^2][(k-p)^2 - M_Z^2][(k-p)^2 - \xi M_Z^2]}, \tag{3.105}$$

with

$$N_\xi = (1-\xi)e\bar{u}_j(p-q)(\not{k} - \not{p})(a_{jk}^* P_L + b_{jk}^* P_R)(\not{k} - \not{q} + m_k)\gamma^\mu(\not{k} + m_k)(\not{k} - \not{p})(a_{ki}P_L + b_{ki}P_R)u_i(p)\epsilon_\mu^*(q). \tag{3.106}$$

Working on the numerator of the amplitude $\mathcal{M}_0$, referred to as N_0, we obtain a simplified expression:

$$\begin{aligned} N_0 = &-e\bar{u}_j(p-q)(a_{jk}^* P_R + b_{jk}^* P_L)[2(k^2 - m_k^2 - 2k\cdot q)\gamma^\mu + 8m_k k^\mu \\ &-4k^\mu \not{k} - 4m_k q^\mu + 4k^\mu \not{q} + 2\gamma^\mu \not{q}\not{k}](a_{ki}P_L + b_{ki}P_R)u_i(p)\epsilon_{\mu *}(q), \end{aligned} \tag{3.107}$$

and, as far as the ξ-dependent amplitude is concerned, the numerator can be rewritten as:

$$\begin{aligned} N_\xi = &e(1-\xi)\bar{u}_j(p-q)(a_{jk}^* P_R + b_{jk}^* P_L)\{k^4\gamma^\mu - m_k^2 k^2\gamma^\mu + 2m_k^2 k^\mu \gamma\cdot k - m_k^2((\gamma\cdot k)\gamma^\mu(\gamma\cdot p)) + \\ &- m_k^2(\gamma\cdot p)\gamma^\mu(\gamma\cdot k) + m_k k^2\gamma^\mu(\gamma\cdot k) + m_k k^2(\gamma\cdot k)\gamma^\mu - 2m_k k^\mu(\gamma\cdot k)(\gamma\cdot p) + \\ &- 2m_k k^\mu(\gamma\cdot p)(\gamma\cdot k) + m_k p^2\gamma^\mu(\gamma\cdot k) + m_k p^2(\gamma\cdot k)\gamma^\mu + m_k(\gamma\cdot k)(\gamma\cdot q)\gamma^\mu(\gamma\cdot p) + \\ &+ m_k(\gamma\cdot p)(\gamma\cdot q)\gamma^\mu(\gamma\cdot k) - 2m_k(k\cdot q)\gamma^\mu(\gamma\cdot k) + 2m_k k^\mu(\gamma\cdot q)(\gamma\cdot k) - m_k k^2(\gamma\cdot q)\gamma^\mu + \\ &+ k^2 p^2\gamma^\mu + 4k^\mu(k\cdot p)\gamma\cdot p - k^2\gamma^\mu(\gamma\cdot k)(\gamma\cdot p) - k^2(\gamma\cdot p)(\gamma\cdot k)\gamma^\mu - 2k^2 p^\mu\gamma\cdot p + \\ &- 2p^2 k^\mu\gamma\cdot k - 2(k\cdot p)(\gamma\cdot q)\gamma^\mu(\gamma\cdot p) + 2(k\cdot q)\gamma^\mu(\gamma\cdot k)(\gamma\cdot p) - 2(p\cdot q)\gamma^\mu(\gamma\cdot k)(\gamma\cdot p) + \\ &- 2k^\mu(\gamma\cdot q)(\gamma\cdot k)(\gamma\cdot p) + 2p^\mu(\gamma\cdot q)(\gamma\cdot k)(\gamma\cdot p) + k^2(\gamma\cdot p)(\gamma\cdot q)\gamma^\mu + k^2(\gamma\cdot q)\gamma^\mu(\gamma\cdot p) + \\ &+ p^2(\gamma\cdot q)\gamma^\mu(\gamma\cdot k) - k^2(\gamma\cdot k)(\gamma\cdot q)\gamma^\mu - m_k^2 p^2\gamma^\mu + 2m_k^2 p^\mu\gamma\cdot p - 2m_k(p\cdot q)\gamma^\mu(\gamma\cdot p) + \\ &+ 2m_k p^\mu(\gamma\cdot q)(\gamma\cdot p) - m_k p^2(\gamma\cdot q)\gamma^\mu\} \times (a_{ki}P_L + b_{ki}P_R)u_i(p)\epsilon_{\mu *}(q). \end{aligned} \tag{3.108}$$

From now on the calculation is very tedious, not only due to the lengthy expression of N_ξ, but also due to the loop integrals involving three and four terms in the denominator. For this reason to obtain the final result a Mathematica program has been implemented and to verify its correctness there are two main checks that can be done:

- The vector form factors must vanish in the on-shell limit;
- The final result must be ξ-independent.

For the evaluation of the final result, a program very similar to that in Appendix B was used. First, considering that the ratios between the external lepton masses and the mass of the Z boson are small, an expansion has been performed in terms of m_i and m_j. Then, also an expansion in the lepton mass running in the loop has been adopted. Substituting the expressions for a and b written in Eq. (2.38), the final result is finally obtained and reads:

$$F_{TL}^{ji,Z} = \frac{4e\left[\left(C_{\Phi\ell}^{(1)ji} + C_{\Phi\ell}^{(3)ji}\right) m_j(1 + sin\theta_W^2) - C_{\Phi e}^{ji} m_i(\frac{3}{2} - sin\theta_W^2)\right]}{3(4\pi)^2}, \tag{3.109}$$

and

$$F_{TR}^{ji,Z} = \frac{4e\left[\left(C_{\Phi\ell}^{(1)ji} + C_{\Phi\ell}^{(3)ji}\right) m_i(1 + sin\theta_W^2) - C_{\Phi e}^{ji} m_j(\frac{3}{2} - sin\theta_W^2)\right]}{3(4\pi)^2}. \tag{3.110}$$

For the evaluation of the other form factors we should work more, because in this case we have other contributions arising from the self-energy of the lepton and from the diagram (c) in Figure 3.10.

In particular, the self-energy contribution follows again the code in Appendix B, while for what concerns the amplitude of diagram (c)in Figure 3.10 we get:

$$\mathcal{M} = -\bar{u}_j(p-q)(a^{ji*}P_L + b^{ji*}P_R)\gamma_\mu u_i(p)\frac{g^{\mu\nu}}{q^2 - M_Z^2}\Sigma_{\nu\rho}^{Z\gamma}(q^2)\epsilon^{\rho*}(q), \tag{3.111}$$

where $\Sigma_{\nu\rho}^{Z\gamma}(q^2)$ is the Z-γ self-energy, but since a flavor violating photon is not considered in this analysis because if it were present, the tree-level contribution to the muon decay would be dominant, then it corresponds exactly to the Standard Model Z-γ self energy. As we can see, this diagram cannot contribute to the tensor form factors and therefore modifies only the vector and scalar form factors. When collecting all contributions, the final result regarding the form factors reads

$$\begin{aligned}
F_{VL}^{ji,Z} &= \frac{2e(1-2sin\theta_W^2)q^2}{9(4\pi)^2}\left(C_{\Phi\ell}^{(1)ji} + C_{\Phi l}^{(3)ji}\right)\left(1 - 6\log\frac{m_i m_j}{M_Z^2}\right), \\
F_{VR}^{ji,Z} &= -\frac{4esin\theta_W^2 q^2}{9(4\pi)^2}C_{\Phi e}^{ji}\left(1 - 6\log\frac{m_i m_j}{M_Z^2}\right), \\
F_{SL}^{ji,Z} &= \frac{2e}{9(4\pi)^2}\left[m_j(1-2sin\theta_W^2)\left(C_{\Phi\ell}^{(1)ji} + C_{\Phi l}^{(3)ji}\right) + 2m_i sin\theta_W^2 C_{\Phi e}^{ji}\right]\left(1 - 6\log\frac{m_i m_j}{M_Z^2}\right), \\
F_{SR}^{ji,Z} &= -F_{SL}^{ji,Z}(m_j \leftrightarrow m_i).
\end{aligned} \tag{3.112}$$

The bounds obtained from this 1-loop amplitude are given in Table 3.16

	$\lvert C_a\rvert$ [$\Lambda = 1$ TeV]	Λ (TeV) [$\lvert C_a\rvert = 1$]	CLFV Process
$C_{\Phi e}^{e\mu}$, $\lvert C_{\Phi\ell}^{(1)e\mu} + C_{\Phi\ell}^{(3)e\mu}\rvert$	2.1×10^{-4}	69	$\mu \to e\gamma$ [1-loop]
$C_{\Phi e}^{e\tau}$, $\lvert C_{\Phi\ell}^{(1)e\tau} + C_{\Phi\ell}^{(3)e\tau}$	0.14	3	$\tau \to e\gamma$ [1-loop]
$C_{\Phi e}^{\mu\tau}$, $\lvert C_{\Phi\ell}^{(1)\mu\tau} + C_{\Phi\ell}^{(3)\mu\tau}\rvert$	0.16	2	$\tau \to \mu\gamma$ [1-loop]

Table 3.16: Bounds on the coefficients of some of the flavor-violating operators of Table 2.1, exploiting the experimental constraints of Table 1.1, for $\Lambda = 1$ TeV, and corresponding bounds on Λ (in TeV) for $|C_a| = 1$.

Not only the Z-boson interactions, but also the W-boson ones get modification from the Lepton-

Higgs operators. Effective vertices are reported in Eq. (2.40). The other vertices that can contribute, in the $R-\xi$ Gauge, to this decay are:

- The Goldston-Lepton-Neutrino coupling

$$i\Gamma_{G_1,ji} = i\left(b^G_{jl}\not{p} - \frac{\sqrt{2}}{v}\delta_{jl}m_\ell\right)U_{li}P_L, \tag{3.113}$$

  where

$$b^G_{jl} = -\frac{v\sqrt{2}}{\Lambda^2}C^{(3)jl}_{\phi\ell}. \tag{3.114}$$

- The 2-Lepton-Goldston-W coupling given by

$$i\Gamma^\mu_{G_2,ji} = i\gamma^\mu\left(c^G_{ji}P_L + c^G_{ji}P_R\right), \tag{3.115}$$

  where

$$c^G_{ji} = -\frac{ev}{\Lambda^2 sin\theta_W}C^{(1)ji}_{\phi\ell}, \qquad d^G_{ji} = -\frac{ev}{\Lambda^2 sin\theta_W}C^{ji}_{\phi e}. \tag{3.116}$$

The last Feynman rule that we need is the Goldstone propagator in the R-ξ Gauge that is:

$$\Delta_G(k^2) = \frac{i}{k^2 - \xi_G M_W^2}. \tag{3.117}$$

The diagrams associated with the muon decay mediated by these interactions combined with the Standard Model interactions are:

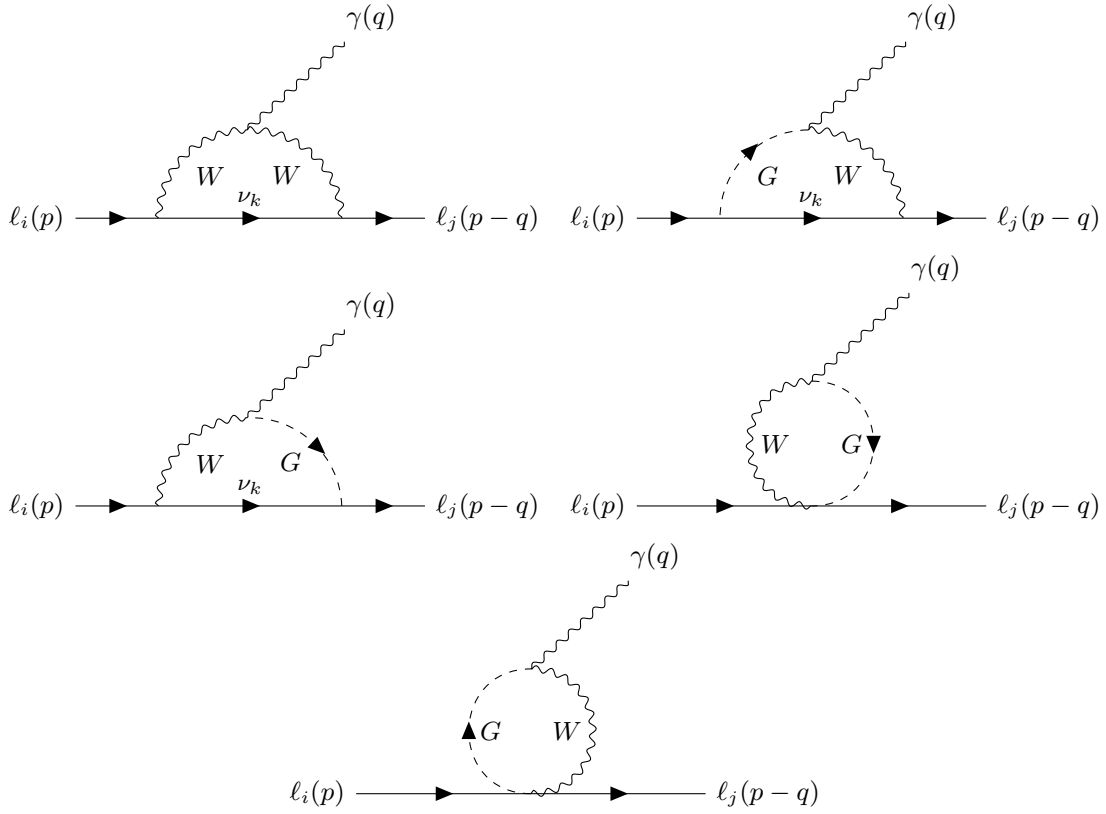

Figure 3.14: Feynman diagram contributing to the decay $\ell_i \to \ell_j\gamma$ at 1 loop, due to modified W interactions.

	$\lvert C_a\rvert$ [$\Lambda = 1$ TeV]	Λ (TeV) [$\lvert C_a\rvert = 1$]	CLFV Process
$C_{\Phi\ell}^{(3)e\mu}$	1.1×10^{-4}	95	$\mu \to e\gamma$ [1-loop]
$C_{\Phi\ell}^{(3)e\tau}$	7.2×10^{-2}	4	$\tau \to e\gamma$ [1-loop]
$C_{\Phi\ell}^{(3)\mu\tau}$	8.3×10^{-2}	4	$\tau \to \mu\gamma$ [1-loop]

Table 3.17: Bounds on the coefficients of some of the flavor-violating operators of Table 2.1, exploiting the experimental constraints of Table 1.1, for $\Lambda = 1$ TeV, and corresponding bounds on Λ (in TeV) for $|C_a| = 1$.

The procedure adopted for the evaluation of this set of amplitudes is the same as the one presented for the case of the Z modified couplings, and the results as far as the tensor form factors are concerned are

$$\begin{aligned} F_{TL}^{ji,W} &= -\frac{10em_i C_{\Phi\ell}^{(3)ji}}{3(4\pi)^2}, \\ F_{TR}^{ji,W} &= -\frac{10em_j C_{\Phi\ell}^{(3)ji}}{3(4\pi)^2}. \end{aligned} \tag{3.118}$$

While the expressions for the vector and scalar form factors are given by:

$$\begin{aligned} F_{VL}^{ji,W} &= -\frac{2eq^2}{9(4\pi)^2}\left[16C_{\Phi\ell}^{(3)ji} + 6cos\theta_W^2\left(C_{\Phi\ell}^{(1)ji} + C_{\Phi\ell}^{(3)ji}\right)\right. \\ &+ \left. 3cos\theta_W^2\left(15C_{\Phi\ell}^{(1)ji} + 16C_{\Phi\ell}^{(3)ji}\right)\left(\Delta - \log\frac{M_W^2}{\mu^2}\right)\right], \\ F_{VR}^{ji,W} &= -\frac{2ecos\theta_W^2 q^2}{3(4\pi)^2} C_{\Phi e}^{ji}\left[2 + 15\left(\Delta - \log\frac{M_W^2}{\mu^2}\right)\right], \\ F_{SL}^{ji,W} &= \frac{e}{9(4\pi)^2}\left[12cos\theta_W^2(m_i C_{\Phi e}^{ji} - m_j(C_{\Phi\ell}^{(1)ji} + C_{\Phi\ell}^{(3)ji})) - 32m_j C_{\Phi\ell}^{(3)ji}\right. \\ &+ \left. 3\left(15cos\theta_W^2(m_i C_{\Phi e}^{ji} - m_j(C_{\Phi\ell}^{(1)ji} + C_{\Phi\ell}^{(3)ji})) - 2m_j C_{\Phi\ell}^{(3)ji}\right)\left(\Delta - \log\frac{M_W^2}{\mu^2}\right)\right], \\ F_{SR}^{ji,W} &= -F_{SL}^{ji,W}(m_j \leftrightarrow m_i). \end{aligned} \tag{3.119}$$

As already done in the previous cases, let us infer numerical bounds on the Wilson coefficients and on the scale Λ of new physics. To obtain the decay rate, Eq. (3.13) was used and compared with the present bounds, we obtain the values shown in Table 3.17.

3.2.4 One loop matching of SMEFT into LEFT for dipole operators

In the previous subsection, we evaluated several contributions at the one-loop level to dipole operators. In Table 3.18 we report the final results of the matching to LEFT. Furthermore, as we have seen before, only the tensor form factors contribute to the radiative muon LFV decay. However, the other parts of the amplitude that we have evaluated in the previous part of the section generate an effective vertex for the off-shell photon. Let us show this by considering the vector form factors. In this case, we obtain the following three-point interaction:

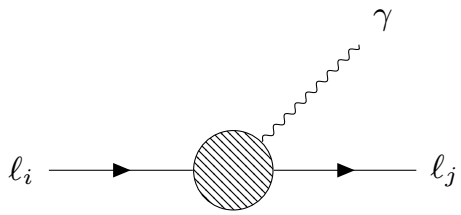

Figure 3.15: Modified off-shell photon-leptons vertex at one loop.

$$V^{ji\,\mu}_{\ell\ell\gamma} = \frac{i}{\Lambda^2}\left[\gamma^\mu(F^{ji}_{VL}P_L + F^{ji}_{VR}P_R)\right], \tag{3.120}$$

where the left-handed coefficient, called k the momentum in the photon propagator, is given by:

$$\begin{aligned}
F^{ji}_{VL} =& -\frac{4ek^2}{9(4\pi)^2}\sum_{l=1}^{3}\left(C^{(1)jill}_{\ell q} - C^{(3)jill}_{\ell q} + C^{jill}_{\ell u}\right)\log\frac{m^2_{u_l}}{\mu^2} + \frac{2ek^2}{9(4\pi)^2}\sum_{l=1}^{3}\left(C^{(1)jill}_{\ell q} + C^{(3)jill}_{\ell q} + C^{jill}_{\ell d}\right)\log\frac{m^2_{d_l}}{\mu^2} \\
&+ \frac{2ek^2}{3(4\pi)^2}\sum_{l=1}^{3}\left((2C^{jill}_{\ell\ell} + C^{jill}_{\ell e})\log\frac{m^2_{\ell_l}}{\mu^2}\right) + \frac{2e(1-2sin\theta^2_W)k^2}{9(4\pi)^2}\left(C^{(1)ji}_{\Phi\ell} + C^{(3)ji}_{\Phi l}\right)\left(1 - 6\log\frac{m_i m_j}{M^2_Z}\right) \\
&- \frac{2ek^2}{9(4\pi)^2}\left[16C^{(3)ji}_{\Phi\ell} - 6cos\theta^2_W\left(C^{(1)ji}_{\Phi\ell} + C^{(3)ji}_{\Phi\ell}\right)3cos\theta^2_W\left(15C^{(1)ji}_{\Phi\ell} + 16C^{(3)ji}_{\Phi\ell}\right)\log\frac{M^2_W}{\mu^2}\right] + \\
&+ \frac{e}{16\pi^2}\frac{q^2 m_i v}{3\sqrt{2}m^2_h}\left(log\left(\frac{m^2_h}{m^2_i}\right) - \frac{4}{3}\right)[L^\dagger_e C^\dagger_{e\Phi 3} R_e]^*_{ij},
\end{aligned} \tag{3.121}$$

while the right one is:

$$\begin{aligned}
F^{ji}_{VR} =& -\frac{4ek^2}{9(4\pi)^2}\sum_{l=1}^{3}\left(C^{jill}_{eq} + C^{(3)jill}_{eu}\right)\log\frac{m^2_{u_l}}{\mu^2} + \frac{2ek^2}{9(4\pi)^2}\sum_{l=1}^{3}\left(C^{jill}_{eq} + C^{(3)jill}_{ed}\right)\log\frac{m^2_{d_l}}{\mu^2} \\
&+ \frac{2ek^2}{3(4\pi)^2}\sum_{l=1}^{3}\left((2C^{jill}_{ee} + C^{lljl}_{\ell e})\log\frac{m^2_{\ell_j}}{\mu^2}\right) - \frac{4esin\theta^2_W k^2}{9(4\pi)^2}C^{ji}_{\Phi e}\left(1 - 6\log\frac{m_i m_j}{M^2_Z}\right) \\
&- \frac{2ecos\theta^2_W k^2}{3(4\pi)^2}C^{ji}_{\Phi e}\left[2 - 15\log\frac{M^2_W}{\mu^2}\right] \\
&+ \frac{e}{16\pi^2}\frac{q^2 m_i v}{3\sqrt{2}m^2_h}\left(log\left(\frac{m^2_h}{m^2_i}\right) - \frac{4}{3}\right)[L^\dagger_e C^\dagger_{e\Phi 3} R_e]_{ji}.
\end{aligned} \tag{3.122}$$

But now, using an electromagnetic vertex, we can have a diagram contributing to the three-body LFV decay such as:

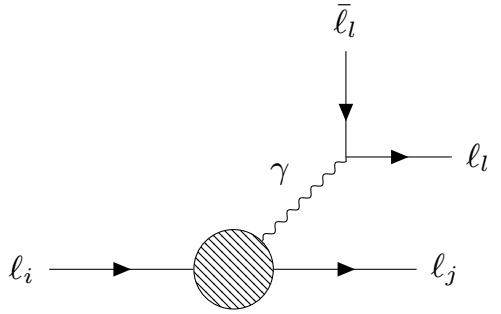

Figure 3.16: Feynman diagram contributing to $\ell_i \to \ell_l\bar{\ell}_l\ell_j$

And the corresponding amplitude is then obtained as:

$$i\mathcal{M} = iV_{\ell\ell\gamma}^{ji\,\mu}\frac{1}{k^2}\bar{u}_l\gamma_\mu v_l. \tag{3.123}$$

It is worth noting that the dependence on the propagator momentum cancels out. Eventually, one can adopt the renormalization group improved perturbation theory to eliminate the dependence on the scale μ and use the expressions of the previous section to get the 1-loop decay rate for the three-body LFV decay.

O_i	c_i
$(\bar{\mu}_L\sigma^{\mu\nu}e_R)F_{\mu\nu}$	$\frac{16e}{3\cdot(4\pi)^2}\sum_{i=1}^{3}C_{\ell equ}^{(3)\mu eii}m_{u_i}\log\frac{m_{u_i}^2}{\mu^2}+\sum_{i=1}^{3}\frac{2em_i}{16\pi^2}C_{\ell e}^{i\mu ei}-\frac{10em_eC_{\Phi\ell}^{(3)e\mu}}{3(4\pi)^2}+$ $+\frac{4e\left[\left(C_{\Phi\ell}^{(1)e\mu}+C_{\Phi\ell}^{(3)e\mu}\right)m_\mu(1+sin\theta_W^2)-C_{\Phi e}^{e\mu}m_e(\frac{3}{2}-sin\theta_W^2)\right]}{3(4\pi)^2}$ $+\frac{e}{16\pi^2}\frac{m_i^2v}{\sqrt{2}m_h^2}\left(log\left(\frac{m_h^2}{m_i^2}\right)-\frac{4}{3}\right)[L_e^\dagger C_{e\Phi 3}^\dagger R_e]_{ji}$
$(\bar{\mu}_R\sigma^{\mu\nu}e_L)F_{\mu\nu}$	$\frac{16e}{3\cdot(4\pi)^2}\sum_{i=1}^{3}C_{\ell equ}^{(3)\mu eii^*}m_{u_i}\log\frac{m_{u_i}^2}{\mu^2}+\sum_{i=1}^{3}\frac{2em_i}{16\pi^2}C_{\ell e}^{\mu iie}-\frac{10em_\mu C_{\Phi\ell}^{(3)e\mu}}{3(4\pi)^2}+$ $+\frac{4e\left[\left(C_{\Phi\ell}^{(1)e\mu}+C_{\Phi\ell}^{(3)e\mu}\right)m_e(1+sin\theta_W^2)-C_{\Phi e}^{e\mu}m_\mu(\frac{3}{2}-sin\theta_W^2)\right]}{3(4\pi)^2}$ $+\frac{e}{16\pi^2}\frac{m_i^2v}{\sqrt{2}m_h^2}\left(log\left(\frac{m_h^2}{m_i^2}\right)-\frac{4}{3}\right)[L_e^\dagger C_{e\Phi 3}^\dagger R_e]_{ij}^*$

Table 3.18: 1-loop matching to the LEFT dipole operators arising from the diagrams in Figure 3.10.

Chapter 4

High-energy probes of Lepton Flavor Violation

4.1 LFV scatterings

Muon colliders and FCC-ee colliders have great potential for high-energy physics. They can offer collisions of point-like particles at very high energies. In particular since muons can be accelerated in a ring without limitation from synchrotron radiation[33], a 14 TeV muon collider provides an effective energy reach similar to that of the 100 TeV FCC, and potentially the c.o.m. energy in colliding muons can go well beyond. Therefore, it is important to consider in our study also CLFV processes in future high energy colliders. Furthermore, we also present the results for LFV scatterings in existing colliders such as LHC and we evaluate the cross section for the lepton flavor conversion in the scattering with a nucleus.

4.1.1 $\ell_i\ell_i \to \ell_j\ell_k$

In order to study a CLFV muon collision we consider the general case of a lepton-antilepton scattering into a flavor violating lepton pair. The diagrams contributing to this high-energy CLFV scattering are:

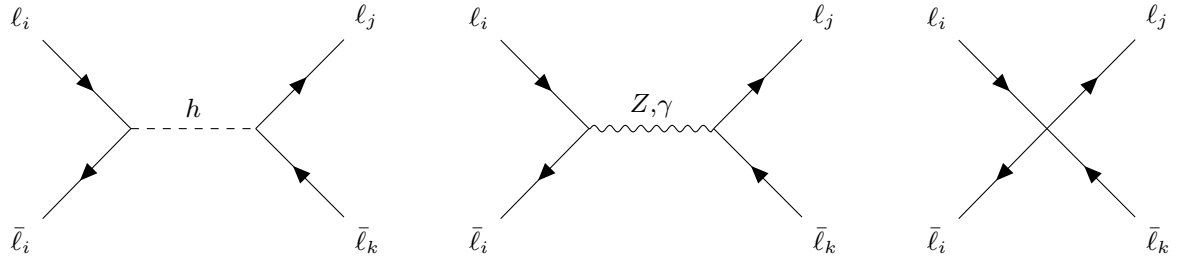

Figure 4.1: Tree-level diagrams contributing to the CLFV lepton-antilepton scattering in the s-channel.

In this case, we have several contributions:

- The photon-exchange diagram is induced by the photon-dipole operator and a QED vertex;
- The Z-exchange diagram is induced by either the Z-dipole or the modified weak couplings due to the lepton-Higgs operators and a SM Z-vertex;
- The Higgs-exchange diagram is induced by the modified Yukawa couplings due to the lepton-Higgs operators, and a flavor conserving SM vertex;

- The point-like interaction diagram is induced by four lepton operators.

Furthermore, we also consider the t-channel in each of the above diagrams:

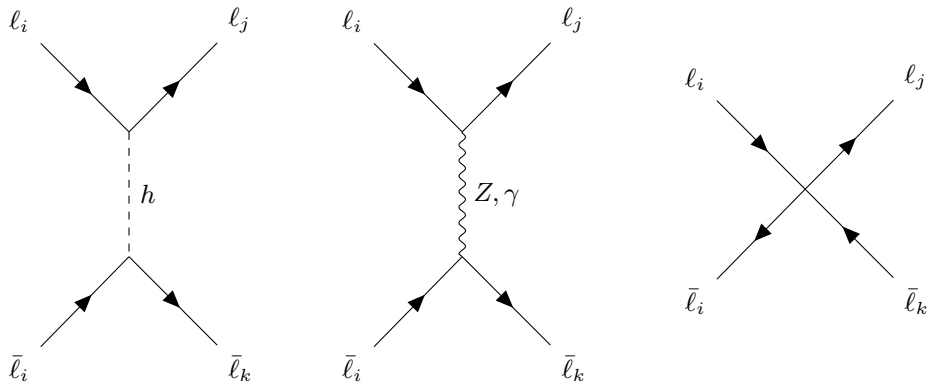

Figure 4.2: Tree-level diagrams contributing to the CLFV lepton-antilepton scattering in the t-channel.

In addition to the usual SMEFT power counting, it is also convenient to introduce a second power counting in $\frac{v}{\sqrt{s}}$. The final result for the cross section is:

$$
\begin{aligned}
\sigma(\ell_i\ell_i \to \ell_j\ell_i) = \frac{s}{12\pi\Lambda^4}\Bigg\{ & |C_{\ell e}^{iiji}|^2 + |C_{\ell e}^{jiii}|^2 + |C_{\ell\ell}^{iiji} + C_{\ell\ell}^{jiii}|^2 + |C_{ee}^{iiji} + C_{ee}^{jiii}|^2 + \mathcal{O}\left(\frac{m_{i,j}^2}{s}\right) + \\
& + \frac{9v^2m_i^2}{16s^2}\left[|[L_e^\dagger C_{e\Phi 3}^\dagger R_e]_{ij}|^2 + |[L_e^\dagger C_{e\Phi 3}^\dagger R_e]_{ji}|^2 + \mathcal{O}\left(\frac{m_h^2}{s}\right)\right] + \\
& + \frac{3vm_i}{8\sqrt{2}s}\left[\Re\left\{\left(C_{\ell e}^{jiii*} - 2C_{\ell e}^{iiji*}\right)[L_e^\dagger C_{e\Phi 3}^\dagger R_e]_{ji} + \left(C_{\ell e}^{jiii} - 2C_{\ell e}^{iiji}\right)[L_e^\dagger C_{e\Phi 3}^\dagger R_e]_{ij}\right\} + \right. \\
& \left. + \mathcal{O}\left(\frac{m_h^2}{s}\right)\right] + \frac{v^2}{s}e^2\left(|C_{e\gamma}^{ij}|^2 + |C_{e\gamma}^{ji}|^2\right)\left(3log\frac{s}{m_i^2} - 1\right) + \\
& + \frac{v^2}{s}\frac{g_2^2}{4cos\theta_W^2}\left[|C_{eZ}^{ji}|^2\left(6(g_L^2+g_R^2)log\frac{s}{M_Z^2} - 5g_R^2 - 11g_L^2\right) + \right. \\
& \left. + |C_{eZ}^{ij}|^2\left(6(g_L^2+g_R^2)log\frac{s}{M_Z^2} - 5g_L^2 - 11g_R^2\right) + \mathcal{O}\left(\frac{M_Z^2}{s}\right)\right] \\
& + \frac{v^2}{s}\frac{eg_2}{2cos\theta_W}\left[\Re\{C_{eZ}^{ij}C_{e\gamma}^{ij*}\}\left(6(g_L+g_R)log\frac{s}{M_Z^2} + g_L - 5g_R\right)\right. \\
& \left. + \Re\{C_{eZ}^{ji}C_{e\gamma}^{ji*}\}\left(6(g_L+g_R)log\frac{s}{M_Z^2} + g_R - 5g_L\right) + \mathcal{O}\left(\frac{M_Z^2}{s}\right)\right]\Bigg\} + \\
& + \frac{g_2^2}{16\pi M_Z^2 cos\theta_W^2}\left(g_R^2(a_{ij}^{Z2} + b_{ij}^{Z2}) + g_L^2(a_{ij}^{Z2} + b_{ij}^{Z2})\right) + \frac{g_2}{24\pi cos\theta_W\Lambda^2}\Re\left\{C_{\ell e}^{jiii*}g_R a_{ij}^Z\right\} + \\
& - \frac{g_2}{8\pi cos\theta_W\Lambda^2}log\frac{s}{M_Z^2}\Re\left\{C_{\ell e}^{iiji*}g_R a_{ij}^Z + C_{\ell e}^{jiii*}g_L b_{ij}^Z\right\} + \frac{g_2}{24\pi cos\theta_W\Lambda^2}\Re\left\{C_{\ell e}^{iiji*}g_L b_{ij}^Z\right\} + \\
& + \mathcal{O}\left(\frac{M_Z^2}{s}\right),
\end{aligned}
\tag{4.1}
$$

where $g_L = -\frac{1}{2} + \sin\theta_W^2$ and $g_R = \sin\theta_W^2$ and the coefficients a^Z, b^Z are defined in Eq. (2.38). As in the case of the Z decay, in order to compare the result to the experimental bounds, we should consider a factor two which accounts for charged conjugate final states:

$$
\sigma_{ji} = \sigma(\ell_i\ell_i \to \ell_j\ell_k + \ell_k\ell_i) = 2\sigma(\ell_i\ell_i \to \ell_j\ell_k). \tag{4.2}
$$

It is worth noting that for 4-fermion operators contributing to this scattering the cross section grows with s, the centre of mass energy squared, in contrast with other effective operator contributions. This is an important feature with respect to LFV decay processes. In the latter case the relevant energy scale of the process is fixed by the mass of the decaying particle. Thus, this enhancement due to the energy implies that the more energy there is, the bigger the cross section.
It is interesting to compute the forward-backward asymmetry when dealing with this process. The definition of the FB asymmetry is:

$$A_{FB} = \frac{\int_0^1 \frac{d\sigma}{d\cos\theta} d\cos\theta - \int_{-1}^0 \frac{d\sigma}{d\cos\theta} d\cos\theta}{\sigma}. \tag{4.3}$$

For the flavor-violating scattering, in the limit of large s, the asymmetry reads:

$$\begin{aligned} A_{FB}\left(\ell_i\ell_i \to \ell_j\ell_i\right) =& \frac{s}{64\pi\Lambda^4\sigma}\left[-|C_{\ell e}^{iiji}|^2 - |C_{\ell e}^{jiii}|^2 + 4|C_{\ell\ell}^{iiji} + C_{\ell\ell}^{jiii}|^2 + 4|C_{ee}^{iiji} + C_{ee}^{jiii}|^2\right] + \\ &- \frac{g_2}{8\pi cos\theta_W\Lambda^2\sigma} log\frac{s}{M_Z^2}\Re\left\{C_{\ell e}^{iiji*} g_R a_{ij}^Z + C_{\ell e}^{jiii*} g_L b_{ij}^Z\right\} + \\ &+ \frac{v^2}{4\pi\Lambda^4\sigma} e^2\left(|C_{e\gamma}^{ij}|^2 + |C_{e\gamma}^{ji}|^2\right) log\frac{s}{m_i^2} + \\ &+ \frac{v^2 g_2^2}{8\pi cos\theta_W^2\Lambda^2\sigma} log\frac{s}{M_Z^2}\left[|C_{eZ}^{ji}|^2\left(g_L^2 + g_R^2\right) + |C_{eZ}^{ij}|^2\left(\left(g_L^2 + g_R^2\right)\right)\right] + \\ &+ \frac{v^2 e g_2}{4\pi cos\theta_W\Lambda^2\sigma} log\frac{s}{M_Z^2}\left[\Re\{C_{eZ}^{ij} C_{e\gamma}^{ij*} + C_{eZ}^{ji} C_{e\gamma}^{ji*}\}\left(g_L + g_R\right)\right]. \end{aligned} \tag{4.4}$$

In particular, the contributions coming from four-lepton operators of the kind $C_{\ell e}$ and $C_{\ell\ell,ee}$ present an opposite sign as far as the asymmetry is concerned.

4.1.2 $\ell + N \to \tau + X$

We now move to study the scattering between a lepton $\ell = e, \mu$ and a nucleus. In the final state the flavor number is violated by the τ lepton and another generic hadronic state is present. Let P, p, p', k, and k' be the momenta of initial nucleon, initial quark/final antiquark, final quark/initial antiquark, initial lepton, and final lepton, respectively. The set of invariant Mandelstam variables defining the kinematics of the quark/antiquark lepton scattering is given by

$$\begin{aligned} \hat{s} &= (k+p)^2 = (k+xP)^2\,, \\ \hat{t} &= (k-k')^2\,, \\ \hat{u} &= (k-p')^2\,, \end{aligned} \tag{4.5}$$

obeying the condition $\hat{s}+\hat{t}+\hat{u} = 0$ for zero masses of quarks and nucleon in comparison with large value of initial lepton energy[34]. Here x is the Bjorken variable (the fraction of the nucleon momentum carried by q_i or $\bar{q}_i$): $x = Q^2/(q\cdot P)$. The inelasticity parameter is usually defined as $y = (q\cdot P)/(k\cdot P)$. The set $(\hat{s}, \hat{t}, \hat{u})$ is related to the total energy $s = (k+P)^2 \simeq 2m_N E_\ell$, where m_N is the nucleon mass and E_ℓ is the lepton beam energy. The following relations hold:

$$\begin{aligned} \hat{s} &= sx\,, \\ \hat{t} &= q^2 = -Q^2 = -sxy\,, \\ \hat{u} &= -sx(1-y)\,. \end{aligned} \tag{4.6}$$

The total cross section of the $l-\tau$ conversion on a nucleus can be approximated by the sum over the corresponding cross section on its constituent nucleons[34][31]:

$$\sigma(\ell+(A,Z)\to\tau+X) \;=\; Z\;\sigma(\ell+p\to\tau+X)+(A-Z)\;\sigma(\ell+n\to\tau+X), \tag{4.7}$$

where $N=p,n$. The total cross section is then obtained as

$$\begin{aligned}\sigma(\ell+N\to\tau+X) \;&=\; \sum_{if}\int_0^1 dx\int_0^1 dy\;\left[\frac{d^2\hat\sigma}{dxdy}(\ell+q_i\to\tau+q_f)\,q_i^N(x,Q^2)\right.\\ &+\;\left.\frac{d^2\hat\sigma}{dxdy}(\ell+\bar q_f\to\tau+\bar q_i)\,\bar q_f^N(x,Q^2)\right],\end{aligned} \tag{4.8}$$

where $q_i^N(x,Q^2)$ and $\bar q_i^N(x,Q^2)$ are quark and antiquark PDFs, respectively. The next step requires to evaluate the partonic cross section for the process $\ell+q_i\to\tau+q_f$. In particular, we consider the 2-quark 2-lepton operators of Table 2.1; they give the following Feynman diagrams:

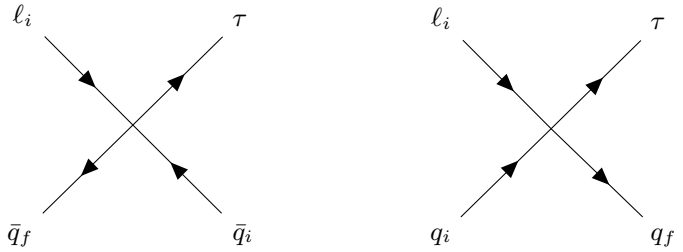

Figure 4.3: Tree-level diagrams contributing to the partonic cross section in $\ell+N\to\tau+X$

The elementary differential cross sections are given by

$$\frac{d^2\hat\sigma}{dxdy}(\ell+q_i\to\tau+q_f) \;=\; \sum_I \frac{|C_{I,if}|^2}{\Lambda^4}\frac{\hat s f_I(y)}{64\pi}\,, \tag{4.9}$$

$$\frac{d^2\hat\sigma}{dxdy}(\ell+\bar q_f\to\tau+\bar q_i) \;=\; \sum_I \frac{|C_{I,if}|^2}{\Lambda^4}\frac{\hat s g_I(y)}{64\pi}\,. \tag{4.10}$$

Where the functions $f_I(y)$ and $g_I(y)$ are reported in Table 4.1 for each operator.

Substituting (4.9), (4.10) into (4.8) and (4.7) we find

$$\sigma(\ell+(A,Z)\to\tau+X) \;=\; \sum_{I,if}\frac{|C_{I,if}|^2 Q^A_{I,if}}{\Lambda^4}, \tag{4.11}$$

with

$$Q^A_{I,if} \;=\; \frac{s}{64\pi}\int_0^1 dx\int_0^1 dy\;\left[x\,f_I(y)\,q_i^A(x,sxy)\;+\;x\,g_I(y)\,\bar q_f^A(x,sxy)\right]. \tag{4.12}$$

In particular, focusing on up and down quarks, the corresponding PDFs in a nucleus with atomic

C_I	$f_I(y)$	$g_I(y)$
$C_{\ell q}^{(1)}$	4	$4(1-y)^2$
$C_{\ell q}^{(3)}$	4	$4(1-y)^2$
C_{eq}	$4(1-y)^2$	4
$C_{\ell d}$	$4(1-y)^2$	4
C_{ed}	4	$4(1-y)^2$
$C_{\ell u}$	$4(1-y)^2$	4
C_{eu}	4	$4(1-y)^2$
C_{ledq}	y^2	y^2
$C_{lequ}^{(1)}$	y^2	y^2
$C_{lequ}^{(3)}$	$16(2-y)^2$	$16(2-y)^2$

Table 4.1: Functions f_I and g_I in terms of inelasticity y for some of the operators of Table 2.1.

number Z and mass number A are

$$\begin{aligned}
&u^A(x,Q^2) = Zu^p(x,Q^2) + (A-Z)d^p(x,Q^2)\,,\\
&d^A(x,Q^2) = Zd^p(x,Q^2) + (A-Z)u^p(x,Q^2)\,,\\
&u^A(x,Q^2) + d^A(x,Q^2) = A\left(u^p(x,Q^2) + d^p(x,Q^2)\right),\\
&\bar{u}^A(x,Q^2) = A\bar{u}^p(x,Q^2)\,,\\
&\bar{d}^A(x,Q^2) = A\bar{d}^p(x,Q^2).
\end{aligned} \tag{4.13}$$

where the functions with the superscript p are the partonic PDFs. In order to go on with the calculation, we follow [31] using the Mathematica package *ManeParse*[35]. This package provides fits for quark PDFs allowing to solve numerically the integral in Eq. (4.9). In this work, we consider both an electron and a muon beam, with energy $E_e = 100\,GeV$ and $E_\mu = 150\,GeV$ respectively, colliding into a Pb target. These results are given in Tables 4.2 and 4.3.
Regarding ℓ–τ conversion in nuclei, there are no experimental limits yet. However, for the numerical analysis we consider the expected sensitivity of the NA64 experiment [34]. This can be further translated in terms of the limits on the physical observables of our interest as

$$R_{\ell\tau} = \frac{\sigma(\ell\mathcal{N} \to \tau\, X)}{\sigma(\ell\mathcal{N} \to \ell\, X)} < 10^{-13} - 10^{-12}\,. \tag{4.14}$$

Here, the denominator is the dominant contribution to the inclusive $\ell + \mathcal{N}$ process: the lepton bremsstrahlung on nuclei, that we take from [34].

4.1.3 $pp \to \ell_k \ell_l$

Another interesting high energy probe is the scattering between two protons giving in the final state a flavor violating lepton couple. This kind of process is tested at LHC and now we show the procedure to obtain the prediction for the cross section.
First of all, with a calculation very similar to the one reported in the previous subsection, we obtain the partonic cross section for the quark-antiquark scattering. It is convenient to split the cross section into the down-type quark case and up-type case, because they arise independently in the SMEFT. In particular, following [29], we assume that the down-type quark Yukawas are diagonal and thus their

C_I	$Q_{I,uf}[GeV^2]$	$Q_{I,df}[GeV^2]$
$C_{\ell q}^{(1)}$	154.9	177.8
$C_{\ell q}^{(3)}$	154.9	177.8
C_{eq}	73.2	85.5
$C_{\ell d}$	73.2	85.5
C_{ed}	154.9	177.8
$C_{\ell u}$	73.2	85.5
C_{eu}	154.9	177.8
C_{ledq}	13.4	15.6
$C_{lequ}^{(1)}$	13.4	15.6
$C_{lequ}^{(3)}$	1610.3	1856.3

Table 4.2: Values for the parameter $Q_{I,if}$, defined in Eq. (4.12), considering an electron beam with energy $E_e = 100\,GeV$ scattering with a Pb nucleus.

C_I	$Q_{I,uf}[GeV^2]$	$Q_{I,df}[GeV^2]$
$C_{\ell q}^{(1)}$	227.5	261.1
$C_{\ell q}^{(3)}$	227.5	261.1
C_{eq}	108.2	125.9
$C_{\ell d}$	108.2	125.9
C_{ed}	227.5	261.1
$C_{\ell u}$	108.2	125.9
C_{eu}	227.5	261.1
C_{ledq}	19.9	23.1
$C_{lequ}^{(1)}$	19.9	23.1
$C_{lequ}^{(3)}$	2365.1	2723.3

Table 4.3: Values for the parameter $Q_{I,if}$, defined in Eq. (4.12), considering a muon beam with energy $E_\mu = 150\,GeV$ scattering with a Pb nucleus.

cross section reads

$$\sigma\left(d_i d_j \to \ell_k \ell_l\right) = \frac{\hat{s}}{144\pi\Lambda^4}\left[\left|C_{\ell q}^{(1)klij} + C_{\ell q}^{(3)klij}\right|^2 + \left|C_{ed}^{ijkl}\right|^2 + \left|C_{qe}^{ijkl}\right|^2 + \left|C_{\ell d}^{ijkl}\right|^2 + \frac{3}{4}\left|C_{\ell edq}^{ijkl}\right|^2 + \right.$$
$$\left. + \frac{3}{4}\left|C_{\ell edq}^{jikl}\right|^2\right], \tag{4.15}$$

while, denoting with V^{CKM} the Cabibbo-Kobayashi-Maskawa matrix, the up-type quarks cross section is given by:

$$\sigma\left(u_i u_j \to \ell_k \ell_l\right) = \frac{\hat{s}}{144\pi\Lambda^4}\left[\left|V_{ip}^{CKM} V_{jr}^{CKM*}\left(C_{\ell q}^{(1)klpr} - C_{\ell q}^{(3)klpr}\right)\right|^2 + \left|C_{eu}^{ijkl}\right|^2 + \left|V_{ip}^{CKM} V_{jr}^{CKM*} C_{qe}^{prkl}\right|^2 + \right.$$
$$+ \left|C_{\ell u}^{klij}\right|^2 + \frac{3}{4}\left|V_{ip}^{CKM} C_{\ell equ}^{(1)klpj}\right|^2 + 4\left|V_{ip}^{CKM} C_{\ell equ}^{(3)klpj}\right|^2 +$$
$$\left. + \frac{3}{4}\left|V_{jp}^{CKM} C_{\ell equ}^{(1)klpi}\right|^2 + 4\left|V_{jp}^{CKM} C_{\ell equ}^{(3)klpi}\right|^2\right], \tag{4.16}$$

where $\hat{s}$ denotes the c.o.m. energy of the partons. It is worth noting that in the previous result the fermion masses are neglected, this leads to the cancellation of the interference terms. In addition, since in the previous subsection we learned that the leading high-energy contributions come from four-fermion operators, in this process all other contributions are neglected.
In order to obtain the proton-proton cross section, the partonic cross-section should be convoluted with the relevant parton-parton luminosities [29], which is defined by the dimensionless functions

$$\mathcal{L}_{q_i\bar{q}_j}(\tau) = \tau \int_\tau^1 \frac{\mathrm{d}x}{x}\left[f_{q_i}(x,\mu_F) f_{\bar{q}_j}(\tau/x,\mu_F) + (q_i \leftrightarrow \bar{q}_j)\right], \tag{4.17}$$

where f_{q_i} denotes the quark q_i parton distribution functions (PDF), μ_F is the factorization scale and $\sqrt{s}$ stands for the proton-proton center-of-mass energy, with $\tau = \hat{s}/s$.

The hadronic cross-section is then given by the expression

$$\sigma(pp \to \ell_k^- \ell_l^+) = \sum_{ij} \int \frac{\mathrm{d}\tau}{\tau} \mathcal{L}_{q_i \bar{q}_j}(\tau) \left[\hat{\sigma}(\tau s)\right]_{ijkl}, \tag{4.18}$$

where q denotes both down and up-type quarks. The summation extends over all quark flavors, with the exception of the top quark which only contributes at one-loop to this process [29]. Notice that if the partonic cross-section $\hat{\sigma}$ is a linear function in τ, as it is our case, then the only dependence on τ of the integrand in Eq. (4.18) comes from the luminosity functions defined in Eq. (4.17).
In order to explain the next steps, we focus in what follows on a single effective coefficient, which we choose to be

$$\mathcal{L}_{\text{eff}} \supset \sum_{ijkl} \frac{C_{q_i q_j}^{\ell_k \ell_l}}{v^2} \left(\bar{q}_{Li} \gamma_\mu q_{Lj}\right) \left(\bar{\ell}_{Lk} \gamma^\mu \ell_{Ll}\right), \tag{4.19}$$

where i, j are flavor indices of down (d, s, b) or u-type quarks (u, c), and k, l of charged leptons (e, μ, τ), in the mass basis.

The relevant observable for probing the LFV operators is the high-mass tail of the invariant mass spectrum $m_{\ell_k \ell_l}$ of the final state dilepton[29]. For instance, for the set of left-handed effective operators defined in Eq. (4.19), this observable is computed from the differential hadronic cross-section (Eq. (4.18)), which is integrated over a fixed interval $\tau \in [\tau_{\min}, \tau_{\max}]$,

$$\begin{aligned} \left[\sigma(pp \to \ell_k^\mp \ell_l^\pm)\right]_{\tau_{\min}}^{\tau_{\max}} = & \frac{s}{144\pi\, v^4} \sum_{i \leq j} \int_{\tau_{\min}}^{\tau_{\max}} \mathrm{d}\tau\, \mathcal{L}_{q_i \bar{q}_j}(\tau) \\ & \times \left[|C_{q_i q_j}^{\ell_k \ell_l}|^2 + |C_{q_i q_j}^{\ell_l \ell_k}|^2\right], \end{aligned} \tag{4.20}$$

where we have used the fact LHC searches do not distinguish the charges of the final lepton states. The integration interval is chosen to map a specific invariant mass window into the tail of the dilepton distribution, far away from the SM resonance poles, and we have summed over the lepton charges, i.e. $\ell_k^\pm \ell_l^\mp \equiv \ell_k^+ \ell_l^- + \ell_k^- \ell_l^+$. The choice of the invariant mass windows should ultimately correspond to the most sensitive mass bins in the experiment.

Chapter 5

Numerical analysis

In this chapter, the bounds obtained on the SMEFT operators are studied carefully, with the aim of understanding which probe is the most sensitive for CLFV. In particular, we focus first on the comparison and the correlations between Wilson coefficients obtained in the decay processes and then also on the comparison between low- and high-energy constraints.

5.1 Low energy analysis

As we have seen in the previous chapters, very strong constraints on CLFV couplings have been obtained by studying decays of μ and τ leptons, with current upper limits on the branching fractions in the 10^{-13} and 10^{-8} ballparks, respectively. Let us start our comparison with the decay $\ell_j \to \ell_i \gamma$. In Figure 5.1, we report the bounds obtained through the aforementioned process on several coefficients. On the left histogram the bars represent the allowed values for the Wilson coefficients setting the new physics scale at $\Lambda = 1\,TeV$, while on the right, assuming a coefficient of order one, the lowest bounds for the new physics scale Λ are estimated. It is clear from the left histogram how the strongest bounds

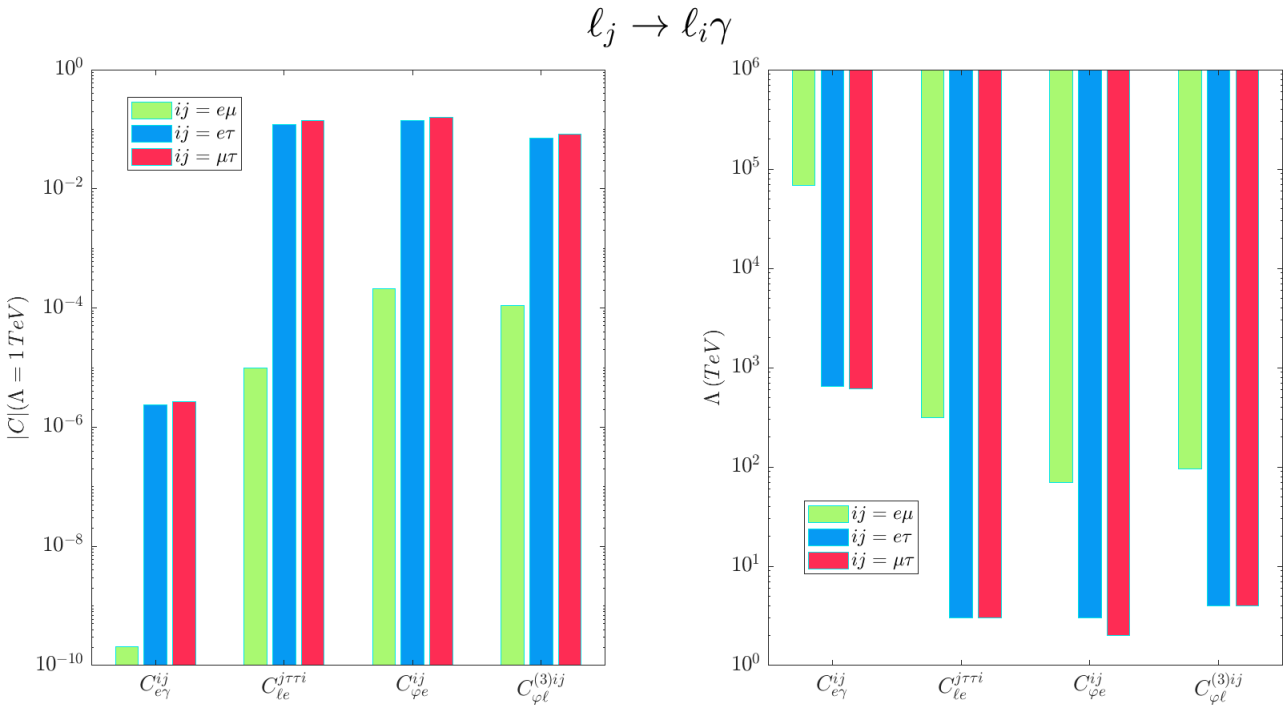

Figure 5.1: Histogram showing bounds on several Wilson coefficients obtained through $\ell_j \to \ell_i \gamma$ decay.

are for the photon-dipole operators. The reason is that this process is induced at the tree level only by these operators, while all other contributions emerge only at one loop level. Furthermore, the green bars, which are associated with $\mu \to e\gamma$ are always lower than the others. This is due to the fact that the experimental bounds for those processes are much stronger. Therefore, LFV effects at high energy might be especially important for $\tau - \mu$ and $\tau - e$ conversions. From the histogram on the right, we can see how the NP scale lower-bounds from the dipole operators are all around or above the $10^3\,TeV$ scale. On the other hand, the above lower bounds are much lower in the case of all other contributions stemming from non-dipoles operators. The situation is different when we consider the process $\ell_j \to \ell_i\ell_i\ell_i$. In this case, the bounds for the four-lepton and Higgs-lepton operators ($C_{\Phi e}$) are improved, as can be seen in Figure 5.2.

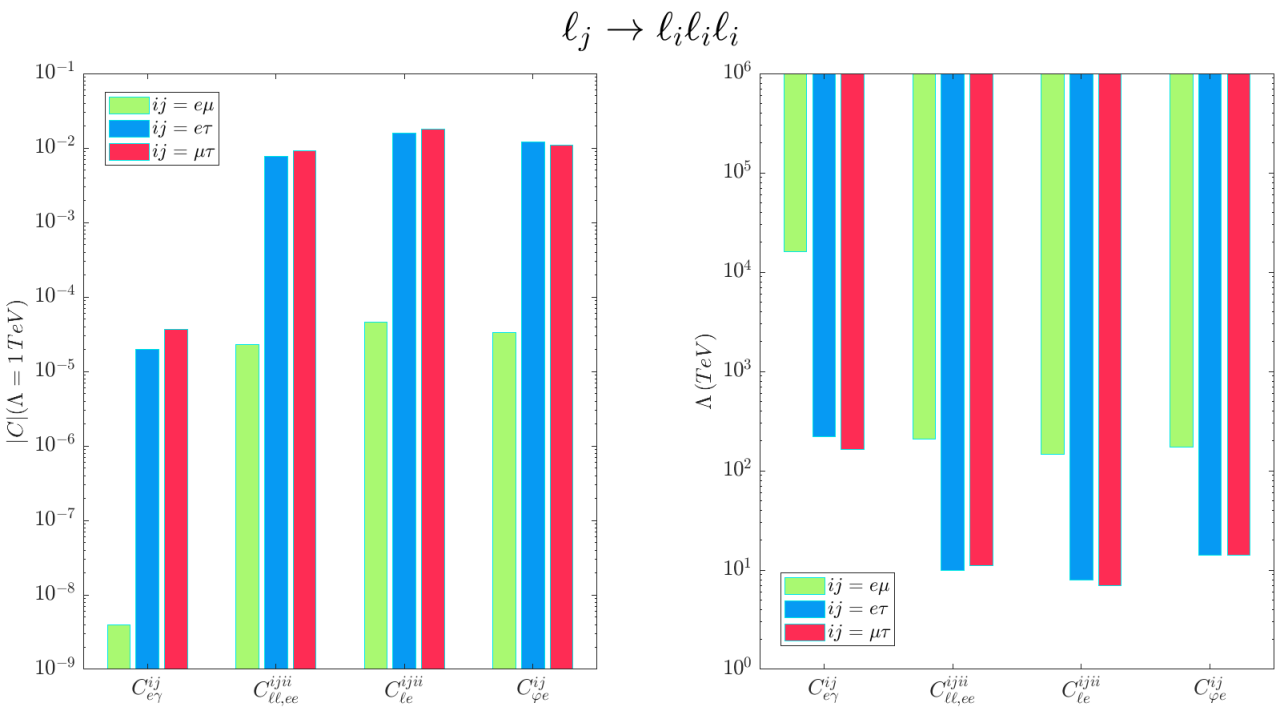

Figure 5.2: Histogram showing bounds on several Wilson coefficients obtained through $\ell_j \to \ell_i\ell_i\ell_i$ decay.

As we can see from the left diagram, the bounds on the lepton-Higgs operators arising from $\ell_j \to \ell_i\ell_i\ell_i$ processes are stronger than those obtained from $\ell_j \to \ell_i\gamma$ processes. This is due to the fact that $\ell_j \to \ell_i\gamma$ is induced only at one loop level by the lepton-Higgs operators. In addition, as can be seen in Table 1.1, the projections for the Mu3e experiment are going to lower the bounds on the $\ell_j \to \ell_i\ell_i\ell_i$ by four orders of magnitude. The comparison for the Z boson decay is not reported because the bounds are much weaker because of the low experimental sensitivity. However, the bounds on this process will improve of almost one order of magnitude in future LHC running [36].
Until now we have considered only one operator at a time. However, if we consider two processes induced by two different operators, we can better constrain the Wilson coefficients. Many dimension-6 operators contribute to both radiative LFV decays and three-body LFV decays. Thus, their decay rates can be correlated. Consider, as first example, the decays $\ell_j \to \ell_i\gamma$ and $\ell_j \to \ell_i\ell_i\ell_i$ induced by both dipole operators and 4-lepton operators. The bounds on the two-dimensional parameter space are represented by ellipses, the intersection of which gives the allowed region for the Wilson coefficients.

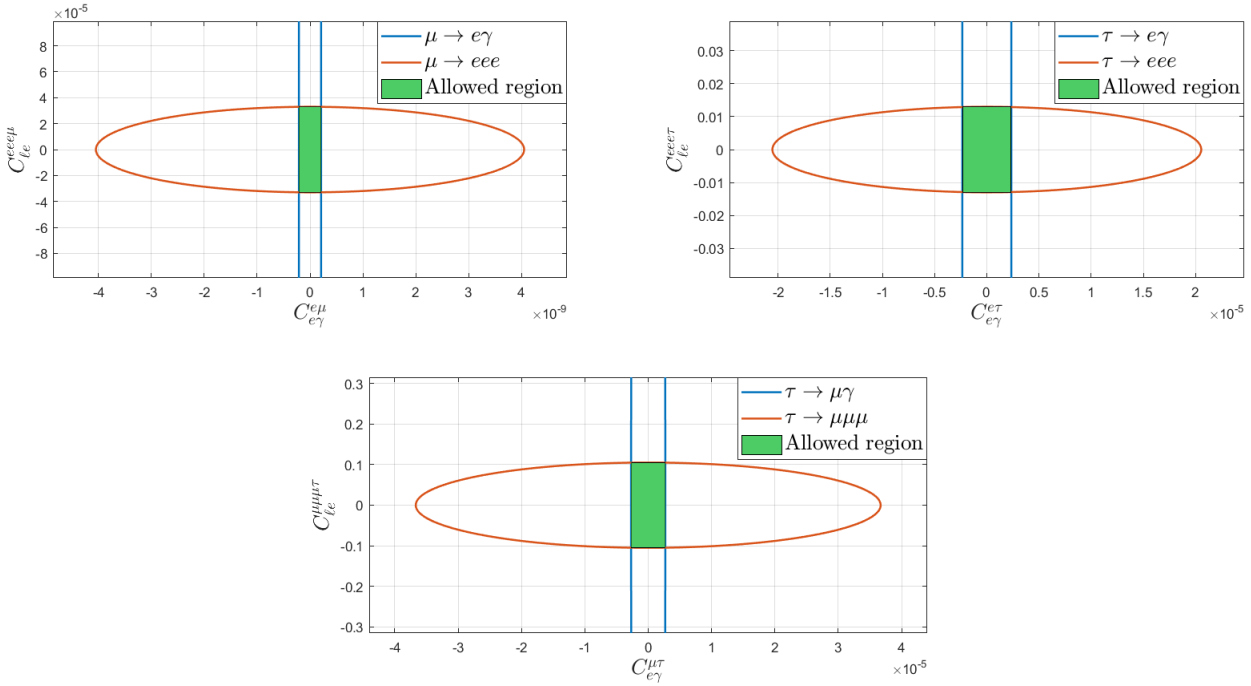

Figure 5.3: Correlation in the two dimensional parameter space between the coefficients $C_{e\gamma}$ and $C_{\ell e}$.

It is clear from Figure 5.3 that the constraining power of two different operators at a time is much stronger. For example, the bounds on the dipole operators are around one order of magnitude smaller than what we obtain in the single-operator analysis. In Figures 5.4 and 5.5 other correlations are shown. In the former, we consider the dipole operator C_{eW} and the lepton-Higgs operator $C_{\Phi e}$, which contribute to the radiative and three-body LFV decays. In the latter case, we show how the dipole operators C_{eW} and C_{eB} can be better constrained when we also consider the decay of the Z boson.

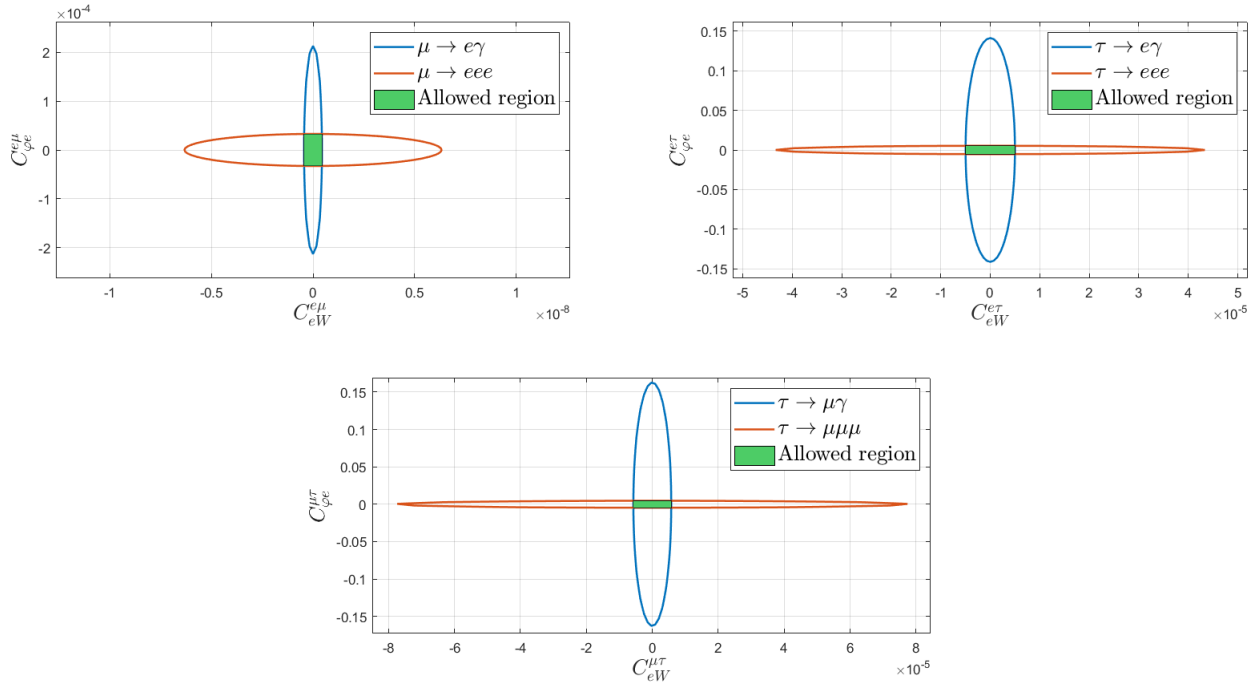

Figure 5.4: Correlation in the two dimensional parameter space between the coefficients C_{eW} and $C_{\Phi e}$.

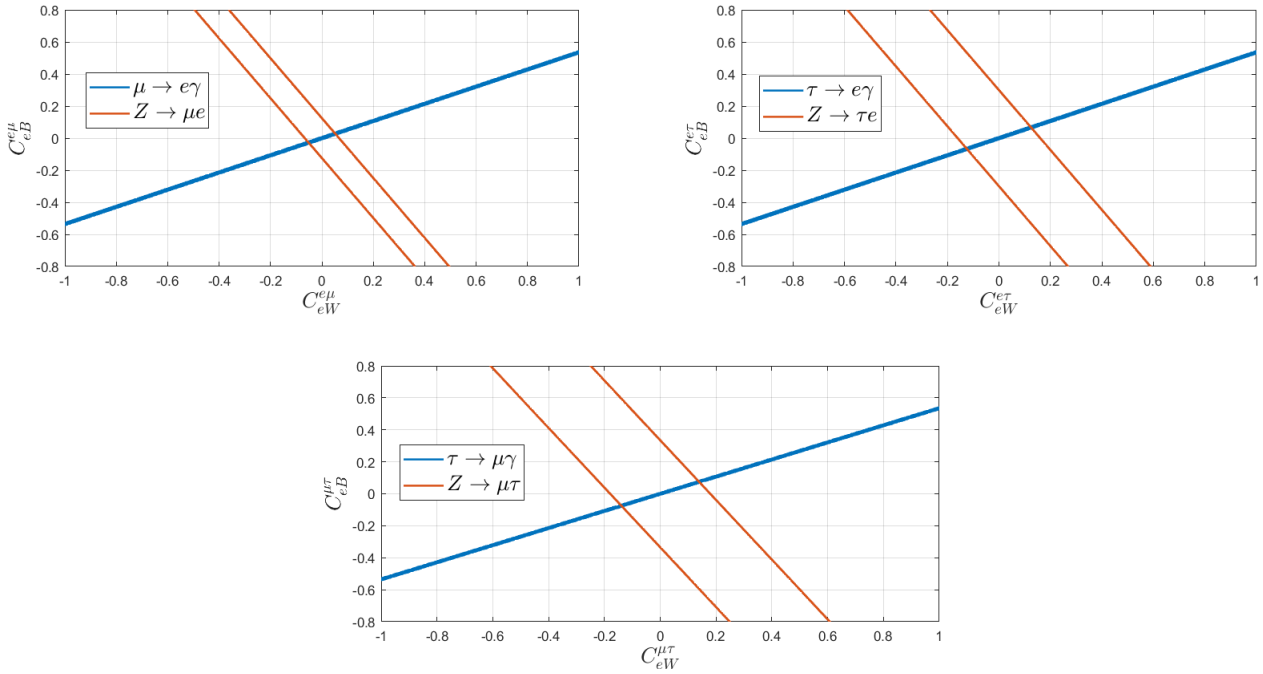

Figure 5.5: Correlation in the two dimensional parameter space between the coefficients C_{eW} and C_{eB}.

As is well known in the literature (see in particular [27]), in the case of the dipole operators dominance it turns out that the ratio

$$R = \frac{\Gamma\left(\ell_j \to \ell_i \gamma\right)}{\Gamma\left(\ell_j \to \ell_i \ell_i \ell_i\right)} = \left(\frac{\alpha}{3\pi}\left(\log\frac{m_j^2}{m_i^2} - 11/4\right)\right)^{-1} \tag{5.1}$$

depends only on SM parameters. Therefore, if any experiment were able to measure this ratio, any deviation from the above value should be attributed to other operators. This is shown in Figure 5.6. In particular, we find an important dependence on the four-lepton operator $C_{\ell e}^{j\tau\tau i}$ and the lepton-Higgs operator $C_{e\Phi}^{ji}$.

5.2 High-energy analysis

In the previous section, we have seen how, through LFV decays, it is possible to obtain very strong bounds on the Wilson coefficients. However, their energy scale is fixed by the mass of the decaying particle. Conversely, when we consider scattering processes, we have seen that for some operators, the cross section is proportional to s, the c.o.m. energy squared of the collision. Thus, it is interesting to understand which energy is required to future colliders to challenge the strong bounds obtained through the decays. In particular, the lepton decay limits translate into requirements on the luminosity, energy, and efficiency for a collider to be competitive. We formulate the criterion as follows [28]: for $\ell = \tau, \mu$, we require that the number of expected signal events in a given decay channel $\ell \to eY$, denoted by N_S^{decay}, and in a collider process, indicated by N_S^{scatt}, are comparable. For definiteness, we will phrase our discussion in terms of the collider process $\mu\mu \to \ell X$, relevant for muon colliders.

Searches for $\ell \to eY$ typically analyze a sample of charged N_ℓ leptons produced either by e^+e^- machines or by hadronic decays in a fixed-target experiment. These searches are also characterized by a signal efficiency ϵ_d, so that

$$N_S^{decay} = \epsilon_d \, N_\ell \, \mathrm{BR}_{\ell\to eY} = \epsilon_d \, N_\ell \, \Gamma_{\ell\to eY} \, \tau_\ell \ , \tag{5.2}$$

where τ_ℓ is the ℓ lepton lifetime. For example, in the case of both BaBar and Belle, $N_\tau \sim 10^9$ and ϵ_d is in the $2.5\% \to 6\%$ range depending on the decay channel considered. Currently, from experimental analysis one can infer only $\mathcal{O}(1)$ upper limits on N_S^{decay}, from which one deduces upper limits (UL) on the BRs

$$\mathrm{BR}^{UL}_{\ell\to eY} \sim \frac{1}{\epsilon_d\, N_\ell}\ , \tag{5.3}$$

where the symbol $\sim$ is used to indicate that analysis-dependent $\mathcal{O}(1)$ factors are missing on the RHS.

In contrast, in a collider setup, the relevant quantities are integrated luminosity $\mathcal{L}$, total signal efficiency ϵ_s (including selection and reconstruction) and cross section $\sigma_{\mu\mu\to\ell X}$, leading to

$$N_S^{scatt} = \epsilon_s\, \sigma_{\mu\mu\to\ell X}\, \mathcal{L}\ . \tag{5.4}$$

Equating N_S^{scatt} and N_S^{decay} one gets

$$\epsilon_s\, \mathcal{L} = (\epsilon_d\, N_\ell)\ \tau_\ell\, \frac{\Gamma_{\ell\to eY}}{\sigma_{\mu\mu\to\ell X}} \sim \frac{1}{\mathrm{BR}^{UL}_{\ell\to eY}}\, \tau_\ell\, \frac{\Gamma_{\ell\to eY}}{\sigma_{\mu\mu\to\ell X}}\ , \tag{5.5}$$

where in the last step we used (5.3). In Eq. (5.5) the ratio $\Gamma_{\ell\to eY}/\sigma_{\mu\mu\to\ell X}$ depends in principle on the underlying new-physics parameters. However, when considering a single dominant source of LFV (i.e. one SMEFT operator at a time), the dependence on new-physics parameters cancels completely in the ratio, which then depends only on the relevant masses, collider energy, phase-space factors and non-perturbative matrix elements. As we have seen in Eq. (4.1), the operators that are most sensitive to the c.o.m. energy s are the four lepton operators. Therefore, we expect to obtain strong bounds on them through the high energy scattering. A detailed design of a 14 TeV center-of-mass muon collider design is not yet complete; however, to estimate the potential of these machines, we use the projection from [37] and [38]. Thus, we consider as reference values a $\sqrt{s} = 10\,TeV$ muon collider with integrated luminosity of $\mathcal{L} = 10\,ab^{-1}$. In this analysis we evaluate the required integrated luminosity of the muon

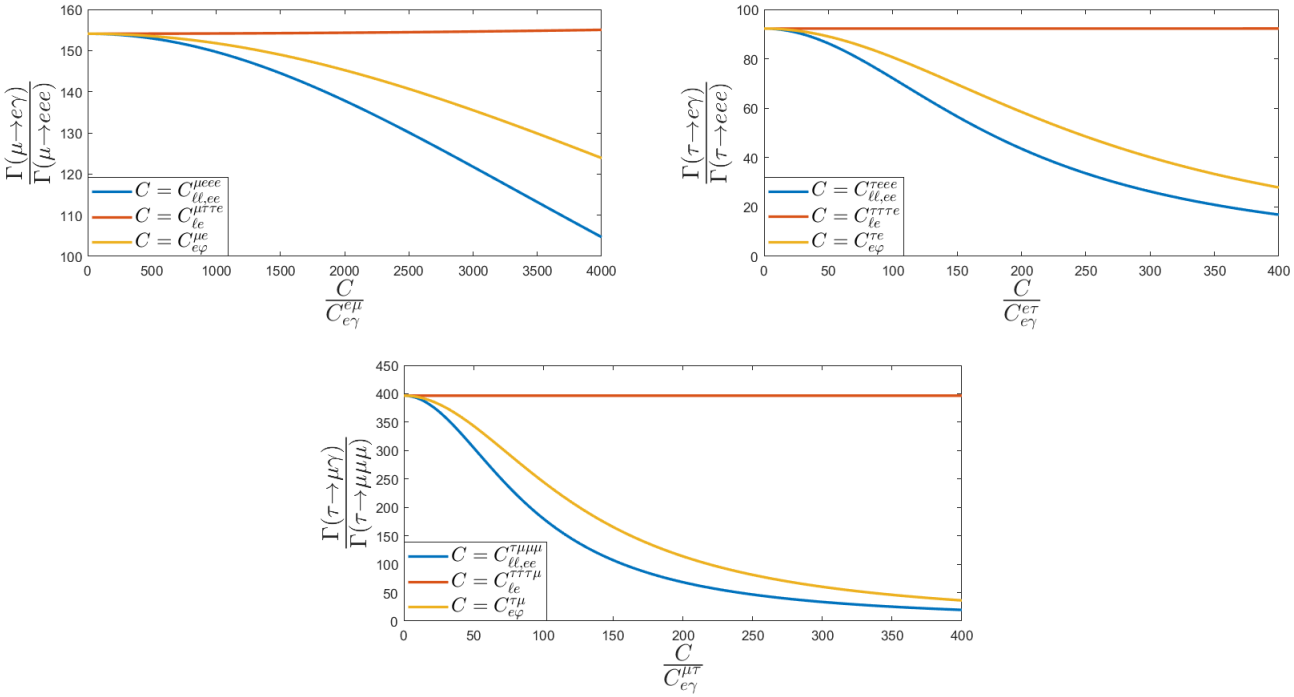

Figure 5.6: Dependence on some Wilson coefficients for what concerns the ratio R.

collider to be competitive with low-energy constraints. The results obtained are shown in Table 5.1.

$\mu\mu \to \tau\mu$ vs $\tau \to \mu\mu\mu$	
$C_{\ell e}^{\tau\mu\mu\mu}$	$\epsilon_s \mathcal{L} = 1.6 \times 10^{-5}\, ab^{-1}$
$C_{e\gamma}^{\tau\mu}$	$\epsilon_s \mathcal{L} = 4.4 \times 10^{2}\, ab^{-1}$
$\mu\mu \to \tau\mu$ vs $\tau \to \mu\gamma$	
$C_{\ell e}^{\tau\mu\mu\mu}$	$\epsilon_s \mathcal{L} = 7.8 \times 10^{-10}\, ab^{-1}$
$C_{e\gamma}^{\tau\mu}$	$\epsilon_s \mathcal{L} = 1.9 \times 10^{5}\, ab^{-1}$

Table 5.1: Integrated luminosities required to obtain, through a muon collision, competitive bounds on the considered Wilson coefficients.

As expected, since the bounds on the dipole operators, obtained through low-energy processes are very strong, a muon collider, in order to be competitive, should have values for the luminosity which are far away from the present projects. Conversely, recalling that the cross sections induced by four lepton operators grows with s, a muon collider could be able to constrain them strongly. Indeed, even considering a reasonable efficiency $\epsilon_s \approx 10^{-2}$, the luminosity required is much lower than the predicted values for muon colliders. Even if dipole operators cannot be well constrained by scattering, we recall that they are extremely constrained by radiative decay $\ell_i \to \ell_j \gamma$. Therefore, considering both the low-energy and high-energy processes, we are able to shrink the allowed parameter space to a small region. With the aim of obtaining a constraint on the Wilson coefficients through the scattering, we make the following assumptions:

- In the scattering experiment, none of these LFV processes is observed, thus $\sigma^{UL}_{\mu\mu\to\ell X} = \frac{1}{\epsilon_s \mathcal{L}}$.
- The reference value considered for the integrated luminosity is $\mathcal{L} = 10\, ab^{-1}$ and for the efficiency $\epsilon_s = 10^{-2}$.
- The new physics scale is set, as in the previous chapter, to $\Lambda = 1\, TeV$.

The graph showing the correlation is reported in Figure 5.7.

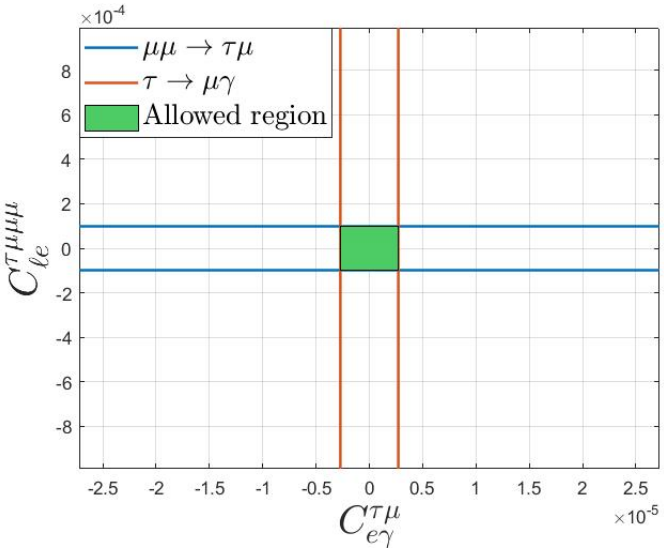

Figure 5.7: Correlation in the two dimensional parameter space between the coefficients $C_{e\gamma}$ and $C_{\ell e}$.

The high-energy scattering presents correlation not only with the radiative flavor violating decay, but also with the three body decay. Once again, the scattering strongly constrains the four-lepton

operators, whereas the Higgs-lepton operators are better constrained by the decay $\ell_i \to \ell_j \ell_j \ell_j$. This is shown in Figure 5.8.

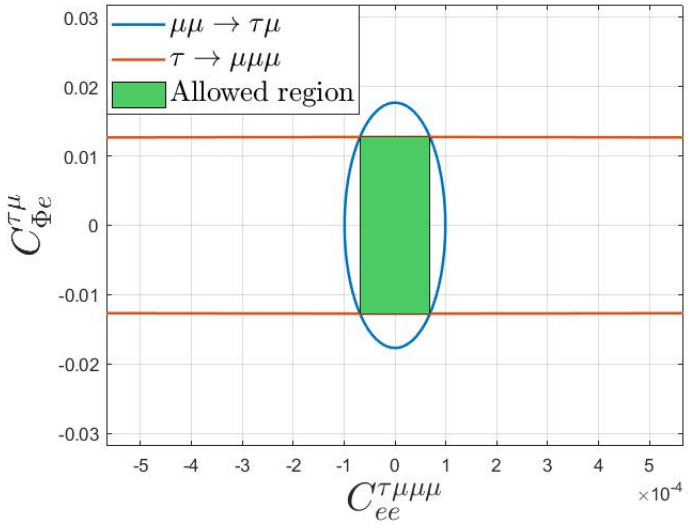

Figure 5.8: Correlation in the two dimensional parameter space between the coefficients $C_{\Phi e}$ and C_{ee}.

Let us now move to compare the constraints between the low energy τ decays and the lepton-τ conversion in nuclei. The first process is characterized by a very high experimental precision at Belle II, while the second one is interesting because of the enhancement with the beam energy and the proportionality to the atomic number of the nucleus. As currently there are no experimental limits for the latter process, we will consider the most conservative expected sensitivity of the NA64 experiment as explained in the previous chapter. The bounds obtained through the scattering process are shown in Table 5.2.

	$\lvert C_a\rvert$ [$\Lambda = 1$ TeV]	Λ (TeV) [$\lvert C_a\rvert = 1$]	CLFV Process
$C^{\tau euu}_{\ell u}$	11.1	0.3	$e + (A, Z) \to \tau + \pi$
$C^{\tau\mu uu}_{\ell u}$	8×10^{-2}	3.6	$\mu + (A, Z) \to \tau + \pi$
$C^{(1)e\tau uu}_{lequ}$	31.0	0.2	$e + (A, Z) \to \tau + \pi$
$C^{(1)\mu\tau uu}_{lequ}$	0.2	2.4	$\mu + (A, Z) \to \tau + \pi$

Table 5.2: Bounds on the coefficients of some of the flavor-violating operators of Table 2.1, exploiting the experimental constraints of Table 1.1, for $\Lambda = 1$ TeV, and corresponding bounds on Λ (in TeV) for $|C_a| = 1$.

Comparing these bound with those in Table 3.13 one can see how the NA64 experiment cannot challenge the strong bounds obtained through the decay processes. It is not until we reach $R_{\ell\tau} \sim 10^{-15}$ that $\mu - \tau$ plays a significant role in the analysis. In addition, the decay process constrains better the scalar operators with respect to the vector ones, while the scattering constrains better the vector operators. Therefore, once again we see the complementarity between high and low energy probes in LFV processes.

Conclusion

In the last few years the experimental improvements of MEG, Mu3e, and Belle pushed the upper bounds for the branching fractions of LFV decays to very small values. In addition, several future collider projects aim to investigate LFV at high energy. Because LFV in the SM is extremely suppressed, these channels have triggered great interest in the search for NP. In this dissertation, we have analyzed both LFV decays and scatterings in a model-independent way, assuming that NP originates at a scale $\Lambda \approx 1\,TeV$. We started by building the NP Lagrangian by selecting a group of six-dimensional operators of the SMEFT. Then we derived the low-energy effective Lagrangian at tree-level in order to obtain the decay rate for the considered low-energy processes. In addition, we evaluated the 1-loop modification of the dipole operators, obtaining loop contributions to the LFV decays. Eventually, we derived the cross section for the high-energy scattering with flavor violating final states. In the last part of the work, we analyzed numerically the obtained results, understanding which are the channels providing the strongest bounds on the Wilson coefficients. In particular, we compared the high-energy and low-energy results showing that, for the $4-$lepton operators, a muon collider could obtain stronger constraints with respect to decay processes. On the other hand, the experimental sensitivity to LFV in fixed target experiments is not comparable to that obtained through τ decays. Finally, we also found correlations, not only at low energy but also between high and low-energy processes through which the Wilson coefficients are more and more constrained.

Appendix A

Useful formulas

- **Dirac gamma relations**

$$\begin{aligned}
&\{\gamma^\mu, \gamma^\nu\} = 2g^{\mu\nu} \\
&\gamma^\mu\gamma^\nu\gamma_\mu = -2\gamma^\nu \\
&\gamma^\mu\gamma^\nu\gamma^\rho\gamma_\mu = 4g^{\nu\rho} \\
&\gamma^\mu\gamma^\nu\gamma^\rho\gamma^\sigma\gamma_\mu = -2\gamma^\sigma\gamma^\rho\gamma^\nu \\
&\gamma^\mu\gamma^\alpha\gamma^\nu = g^{\mu\alpha}\gamma^\nu + g^{\alpha\nu}\gamma^\mu - g^{\mu\nu}\gamma^\alpha + i\epsilon^{\mu\alpha\nu\rho}\gamma_\rho\gamma^5 \\
&\sigma_{\mu\nu} = \frac{i}{2}\epsilon^{\mu\nu\alpha\beta}\sigma_{\alpha\beta}\gamma_5
\end{aligned} \tag{A.1}$$

- **Trace identities**

$$\begin{aligned}
&Tr[\gamma^\mu\gamma^\nu] = 4g^{\mu\nu} \\
&Tr[\gamma^\mu\gamma^\nu\gamma^\rho\gamma^\sigma] = 4(g^{\mu\nu}g^{\rho\sigma} - g^{\mu\rho}g^{\nu\sigma} + g^{\mu\sigma}g^{\nu\rho}) \\
&Tr[\gamma^5] = 0 \\
&Tr[\gamma^5\gamma^\mu\gamma^\nu] = 0 \\
&Tr[\gamma^5\gamma^\mu\gamma^\nu\gamma^\rho\gamma^\sigma] = -4i\epsilon^{\mu\nu\rho\sigma} \\
&Tr[\gamma^{\alpha^1}...\gamma^{\alpha^{2n+1}}] = 0 \\
&Tr[\gamma^5\gamma^{\alpha^1}...\gamma^{\alpha^{2n+1}}] = 0
\end{aligned} \tag{A.2}$$

- **Feynman parametrisation**

$$\begin{aligned}
&\frac{1}{AB} = \int_0^1 \frac{dx}{[xA + (1-x)B]^2} \\
&\frac{1}{ABC} = 2\int_0^1 \frac{dx\,dy\,dz\,\delta(x+y+z-1)}{[Ax+By+Cz]^3}
\end{aligned} \tag{A.3}$$

- **Loop integral general formula**

$$I_{r,m} = \int \frac{d^dp}{(2\pi)^d}\frac{(k^2)^r}{[k^2-C]^m} = i\frac{(-1)^{r-m}}{(4\pi)^2}\left(\frac{4\pi}{C}\right)^{\frac{\epsilon}{2}} C^{2+r-m}\frac{\Gamma(2+r-\frac{\epsilon}{2})}{\Gamma(2-\frac{\epsilon}{2})}\frac{\Gamma(m-r-2+\frac{\epsilon}{2})}{\Gamma(m)} \tag{A.4}$$

- **Gordon identities**

$$\bar{u}(p')\gamma^\mu u(p) = \bar{u}(p')\left[\frac{(p+p')^\mu}{2m} + i\sigma^{\mu\nu}\frac{(p'-p)_\nu}{2m}\right]u(p)$$

$$p^\mu \bar{u}_j(p-q)P_{L,R}u_i(p) = \frac{1}{2}q^\mu \bar{u}_j(p-q)P_{L,R}u_i(p) + \frac{1}{2}\bar{u}_j(p-q)\sigma^{\mu\nu}q_\nu P_{L,R}u_i(p) + \frac{i}{2}q^\mu \bar{u}_j(p-q)(P_{L,R}m_j + P_{R,L}m_i)u_i(p) \tag{A.5}$$

- **Fierz identities**

$$\begin{aligned}
(\bar{a}P_L b)\,(\bar{c}P_L d) &= \frac{1}{2}\,(\bar{a}P_L d)\,(\bar{c}P_L b) + \frac{1}{8}\,(\bar{a}\sigma_{\mu\nu}P_L d)\,(\bar{c}\sigma^{\mu\nu}P_L b)\\
(\bar{a}P_L b)\,(\bar{c}P_R d) &= \frac{1}{2}\,(\bar{a}\gamma_\mu P_R d)\,(\bar{c}\gamma^\mu P_L b)\\
(\bar{a}\gamma_\mu P_L b)\,(\bar{c}\gamma^\mu P_L d) &= -\,(\bar{a}\gamma_\mu P_L d)\,(\bar{c}\gamma^\mu P_L b)\\
(\bar{a}\gamma_\mu P_L b)\,(\bar{c}\gamma^\mu P_R d) &= 2\,(\bar{a}P_R d)\,(\bar{c}P_L b)\\
(\bar{a}\sigma^{\mu\nu}P_L b)\,(\bar{c}\sigma_{\mu\nu}P_L d) &= 6\,(\bar{a}P_L d)\,(\bar{c}P_L b) - \frac{1}{2}\,(\bar{a}\sigma_{\mu\nu}P_L d)\,(\bar{c}\sigma^{\mu\nu}P_L b)
\end{aligned} \tag{A.6}$$

Appendix B

Mathematica codes

In this appendix, we present the Mathematica codes used for the evaluation of the observables starting from the amplitude and for the loop integrals. But before seeing the programs, let us introduce the package used:

- *FeynCalc* is a Mathematica package for algebraic calculations in high-energy physics. The basic idea of FeynCalc is to provide convenient tools for radiative corrections in the standard model. The input for FeynCalc, the analytical expressions for the diagrams, can be entered by hand or can be taken directly from the output of another package, *FeynArts*, which produces all diagrams for a given process. The user can provide certain additional information about the process under consideration, i.e., the kinematics and the choice of the standard matrix elements may be defined. Once this is done, FeynCalc performs the algebraic calculations like tensor algebra, tensor integral decomposition and reduction, yielding a polynomial in standard matrix elements, special functions, kinematical variables and scalars.

- *Package-X* is a Mathematica package for the analytic computation of one-loop integrals dimensionally regulated near 4 spacetime dimensions. *Package-X* computes arbitrarily high rank tensor integrals with up to three propagators, and gives compact expressions of UV divergent, IR divergent, and finite parts for any kinematic configuration involving real-valued external invariants and internal masses. Output expressions can be readily evaluated numerically and manipulated symbolically with built-in Mathematica functions. The emphasis is on the speed of evaluation, the readability of the results, and especially the user-friendliness. Also included is a routine to compute traces of products of Dirac matrices, and a collection of projectors to facilitate the computation of fermion form factors at one loop.

As far as *FeynCalc* is concerned, the function that is used in the code below is:

– **FermionSpinSum**[*exp*] that is capable of converting products of closed spinor chains in *exp* into Dirac traces.

Regarding *Package-X*, we use the following functions:

– **LoopIntegrate**[*num*, *k*, $\{q_0, m_0\}, \{q_1, m_1\}$, **...**] which expresses the one-loop tensor integral over integration variable k with numerator *num* and denominator factors $(q_0^2 - m_0^2)(q_1^2 - m_1^2)$ in terms of Passarino-Veltman coefficient functions.

– **LoopRefineSeries**[f,s,s_0,n] which generates a Taylor series expansion of f containing Passarino-Veltman functions about the point $s = s_0$ to order $(s - s_0)^n$.

Three body phase space evaluation for $\tau \to e\mu\mu$

Calling the package FeynCalc

In[ ]:=
```
Needs["FeynCalc`"];
```

FeynCalc 9.3.1 (stable version). For help, use the documentation center, check out the wiki or visit the forum.

To save your and our time, please check our FAQ for answers to some common FeynCalc questions.

See also the supplied examples. If you use FeynCalc in your research, please cite

- V. Shtabovenko, R. Mertig and F. Orellana, Comput.Phys.Commun. 256 (2020) 107478, arXiv:2001.04407.
- V. Shtabovenko, R. Mertig and F. Orellana, Comput.Phys.Commun. 207 (2016) 432–444, arXiv:1601.01167.
- R. Mertig, M. Böhm, and A. Denner, Comput. Phys. Commun. 64 (1991) 345–359.

Definition of the amplitude

All the masses are considered in order to avoid the divergence of the photon propagator.

In[29]:=
```
M1 = a1 / (m^2 + m1^2 - 2 * SP[p, p1]) * SpinorUBar[Momentum[p1], m1].
     DiracSigma[DiracGamma[LorentzIndex[μ]], DiracGamma[Momentum[p - p1]]].
     DiracGamma[6].SpinorU[Momentum[p], m].SpinorUBar[Momentum[p2], m2].
     DiracGamma[LorentzIndex[μ]].SpinorV[Momentum[p3], m3];
```

Matrix element squaring and sum over polarizations

In particular, we average on the initial state spins and we sum over the final state polarizations.

In[30]:=
```
M2 = M1 * ComplexConjugate[M1];
M3 = 1 / 2 * DiracSimplify[FermionSpinSum[M2]];
```

Definition of the kinematic conditions and integration limits

The integration limits are defined as ex1 and ex2.

In[32]:=
```
SP[p, p1] = 1 / 2 * (m^2 + m1^2 - m23);
SP[p, p2] = 1 / 2 * (m^2 + m2^2 - m13);
SP[p, p3] = 1 / 2 * (m^2 + m3^2 - m12);
SP[p2, p3] = 1 / 2 * (-m3^2 - m2^2 + m23);
SP[p1, p3] = 1 / 2 * (-m3^2 - m1^2 + m13);
SP[p1, p2] = 1 / 2 * (-m2^2 - m1^2 + m12);
SP[p, p] = m^2;
SP[p1, p1] = m1^2;
SP[p2, p2] = m2^2;
SP[p3, p3] = m3^2;
```

Final result for the matrix element

In particular, we average on the initial state spins and we sum over the final state polarizations.

In[42]:=
```
Simplify[M3]
```

Out[42]=
$$\frac{1}{\text{m23}^2}\text{a1}^2\left(-m^2\left(-2\,\text{m1}^2\left(4\,\text{m12}+4\,\text{m13}-4\,\text{m2}^2-4\,\text{m2}\,\text{m3}+\text{m23}-4\,\text{m3}^2\right)+5\,\text{m1}^4+\text{m12}^2+2\,\text{m12}\left(\text{m13}-2\,\text{m3}^2\right)+\text{m13}^2-4\,\text{m13}\,\text{m2}^2+\text{m2}^2\,\text{m23}+4\,\text{m2}^2\,\text{m3}^2+2\,\text{m2}\,\text{m23}\,\text{m3}-\text{m23}^2+\text{m23}\,\text{m3}^2\right)-m^4\left(5\,\text{m1}^2-4\,\text{m2}\,\text{m3}+\text{m23}\right)+m^6-\text{m1}^2\left(\text{m12}^2+2\,\text{m12}\left(\text{m13}-2\,\text{m2}^2\right)+\text{m13}^2-4\,\text{m13}\,\text{m3}^2+\text{m2}^2\,\text{m23}+4\,\text{m2}^2\,\text{m3}^2+2\,\text{m2}\,\text{m23}\,\text{m3}-\text{m23}^2+\text{m23}\,\text{m3}^2\right)-\text{m1}^4\left(\text{m23}-4\,\text{m2}\,\text{m3}\right)+\text{m1}^6+\text{m23}\left(\text{m12}^2-2\,\text{m12}\,\text{m13}+\text{m13}^2+\text{m23}\left(\text{m2}^2-2\,\text{m2}\,\text{m3}-\text{m23}+\text{m3}^2\right)\right)\right)$$

Definition of the differential decay rate and phase space integration

The integration limits are defined as ex1 and ex2.

```
dΓ0 = M5 / (2 * Pi^3 * 32 * m^3);
E2 = (m12 - m1^2 + m2^2) / (2 * Sqrt[m12]);
E3 = (m^2 - m12 - m3^2) / (2 * Sqrt[m12]);
ex1 = (E2 + E3)^2 - (Sqrt[E2^2 - m2^2] + Sqrt[E3^2 - m3^2])^2;
ex2 = (E2 + E3)^2 - (Sqrt[E2^2 - m2^2] - Sqrt[E3^2 - m3^2])^2;
dΓ1 =
  Simplify[Integrate[dΓ0, {m23, ex1, ex2}, Assumptions → {m1 > 0, m2 > 0, m3 > 0, m > 0, m12 > 0}]];
dΓ2 = Simplify[Integrate[dΓ1, {m12, (m1 + m2)^2, (m - m3)^2},
    Assumptions → {m1 > 0, m2 > 0, m3 > 0, m > 0}]];
```

Final result for the decay rate

Only after the phase space integration we expand at the leading order in the final masses

In[54]:=
```
Γ = Series[dΓ2, {m, Infinity, 0}] // Normal
```

Out[54]=
$$\frac{\text{a1}^2\,m^3\left(\log\left(\frac{m^2}{\text{m2}^2}\right)-3\right)}{192\,\pi^3}$$

$\mu \to e\gamma$ at 1-loop induced by modified Higgs couplings

Call Package X

In[3]:=
```
Needs["X`"];
```

```
Package-X v2.1.1, by Hiren H. Patel
For more information, see the guide
```

Define the kinematic conditions

Momenta of the leptons are on-shell, while the photon is kept off-shell for the evaluation of the vector form factors.

In[4]:=
```
onShell = {p.p → mμ^2, p.q → (mμ^2 - me^2 + q.q) / 2};
```

Compute the integral extracting the tensor form factors

The second tensor form factor (obtained projecting with G2) include also the fifth gamma matrix.

```
FT1 =
  LoopIntegrate[Spur[ℙR, (p - k - q).γ + ml 𝟙, LTensor[γ, μ], (p - k).γ + ml * 𝟙, Projector["F2", μ][
      {p, mμ}, {p - q, me}]], k, {p - k - q, ml}, {p - k, ml}, {k, mh}] /. onShell;
FT2 = LoopIntegrate[Spur[ℙR, (p - k - q).γ + ml 𝟙, LTensor[γ, μ],
    (p - k).γ + ml * 𝟙, Projector["G2", μ][{p, mμ}, {p - q, me}]],
   k, {p - k - q, ml}, {p - k, ml}, {k, mh}] /. onShell;
```

Expansion of the Passarino-Veltman functions

The previous integrals are expanded in terms of the ratio between external lepton masses and the Higgs mass.

In[•]:=
```
EFT1 = Series[LoopRefineSeries[FT1 /. q.q → 0, {me, 0, 0}, Analytic → True],
    {mμ, 0, 2}, {ml, 0, 1}, {mh, Infinity, 2}] // C0Expand // LoopRefine;
```

In[•]:=
```
Simplify[EFT1 /. ml → mμ]
```

Out[•]=
$$\left(\frac{\frac{1}{6}\left(4-3\,\text{Log}\left[\frac{mh^2}{m\mu^2}\right]\right)m\mu^2+O[m\mu]^3}{mh^2}+O\left[\frac{1}{mh}\right]^3\right)+O[me]^1$$

In[•]:=
```
EFT2 = Series[LoopRefineSeries[FT2 /. q.q → 0, {me, 0, 0}, Analytic → True],
    {mμ, 0, 2}, {ml, 0, 1}, {mh, Infinity, 2}] // C0Expand // LoopRefine;
```

In[•]:=
```
Simplify[EFT1 /. ml → mμ]
```

Out[•]=
$$\left(\frac{\frac{1}{6}\left(4-3\,\text{Log}\left[\frac{mh^2}{m\mu^2}\right]\right)m\mu^2+O[m\mu]^3}{mh^2}+O\left[\frac{1}{mh}\right]^3\right)+O[me]^1$$

Final result for the right tensor form factors

Eventually, we have to add the loop factor, and to adapt the Package X conventions to the ones of the dissertation. The coupling constants are still omitted.

In[11]:=
```
Simplify[-2 * % / (16 * Pi^2 * mμ)]
```

Out[•]=
$$\left(\left(\frac{-4+3\,\text{Log}\left[\frac{mh^2}{m\mu^2}\right]}{48\,\pi^2\,mh^2}+O\left[\frac{1}{mh}\right]^3\right)m\mu+O[m\mu]^2\right)+O[me]^1$$

Verify Gauge invariance

It is an interesting test for the code to verify if the sum of the vector form factors vanish on shell.

In[•]:=
```
FV1 =
  LoopIntegrate[Spur[ℙR, (p - k - q).γ + ml 𝟙, LTensor[γ, μ], (p - k).γ + ml * 𝟙, Projector["F1", μ][
      {p, mμ}, {p - q, me}]], k, {p - k - q, ml}, {p - k, ml}, {k, mh}] /. onShell;

FV2 = LoopIntegrate[Spur[LTensor[γ, μ], (p).γ + me 𝟙, ℙR, (p - k).γ + ml * 𝟙,
    Projector["F1", μ][{p, mμ}, {p - q, me}]], k, {p - k, ml}, {k, mh}] / (mμ^2);

FV3 = -LoopIntegrate[Spur[ℙR, (p - k - q).γ + ml * 𝟙, (p - q).γ + mμ 𝟙, LTensor[γ, μ],
     Projector["F1", μ][{p, mμ}, {p - q, me}]], k, {p - k - q, ml}, {k, mh}] / (mμ^2);

Series[LoopRefineSeries[(FV1 + FV2 + FV3) /. q.q → 0, {mμ, 0, 2}, {me, 0, 0}, Analytic → True],
   {ml, 0, 2}, {mh, Infinity, 2}] // C0Expand // LoopRefine;

Simplify[% /. ml → mμ] // Normal
```

Out[•]=
```
0
```

Vector form factor

However, for the photon off-shell the vector form factors are non vanishing and can be evaluated. The code for the scalar form factors are the same but using the F3 projector.

In[•]:=
```
Series[LoopRefineSeries[(FV1 + FV2 + FV3), {q.q, 0, 1}, {mμ, 0, 2}, {me, 0, 0}, Analytic → True],
    {ml, 0, 2}, {mh, Infinity, 2}] // C0Expand // LoopRefine;

Simplify[% /. ml → mμ] // Normal
```

Out[•]=
$$\frac{q.q\left(4-3\,\text{Log}\left[\frac{mh^2}{m\mu^2}\right]\right)}{18\,mh^2}$$

Bibliography

[1] Wilfried Buchmüller and Christoph Lüdeling. Field theory and standard model. *arXiv preprint hep-ph/0609174*, 2006.

[2] Guido Altarelli. The higgs and the excessive success of the standard model, 2014.

[3] Juan Maldacena. Gravity, particle physics and their unification. *arXiv preprint hep-ph/0002092*, 2000.

[4] M Concepción González-Garciá and Yosef Nir. Neutrino masses and mixing: Evidence and implications. *Reviews of Modern Physics*, 75(2):345, 2003.

[5] Leonard S Kisslinger and Debasish Das. A brief review of dark matter. *International Journal of Modern Physics A*, 34(27):1930013, 2019.

[6] Roberto D. Peccei. The strong CP problem and axions. In *Lecture Notes in Physics*, pages 3–17. Springer Berlin Heidelberg, 2008.

[7] AD Sakharov. Cp invariance and baryon asymmetry of the universe. *Sov. Phys. Usp*, 34:392, 1991.

[8] David H Lyth and Antonio Riotto. Particle physics models of inflation and the cosmological density perturbation. *Physics Reports*, 314(1-2):1–146, 1999.

[9] Hyun Min Lee. Lectures on physics beyond the standard model. *Journal of the Korean Physical Society*, may 2021.

[10] R. D. Peccei. Qcd, strong cp and axions, 1996.

[11] Stefania Gori. Tasi lectures on flavor physics. *Proceedings, Theoretical Advanced Study Institute in Elementary Particle Physics: Theory in an Era of Data (TASI 2018): Boulder, Colorado, USA, June 4-29, 2018*, 2019.

[12] Sara Celani. Lepton flavour universality tests and lepton flavour violation searches at lhcb, 2021.

[13] Alex Keshavarzi, Kim Siang Khaw, and Tamaki Yoshioka. Muon g-2: A review. *Nuclear Physics B*, 975:115675, feb 2022.

[14] Lorenzo Calibbi and Giovanni Signorelli. Charged lepton flavour violation: an experimental and theoretical introduction. *La Rivista del Nuovo Cimento*, 41(2):71–174, 2018.

[15] Ta-Pei Cheng and Ling-Fong Li. *Gauge theory of elementary particle physics*. Oxford university press, 1994.

[16] Roni Harnik, Joachim Kopp, and Jure Zupan. Flavor violating higgs decays. *Journal of High Energy Physics*, 2013(3), mar 2013.

[17] Georges Aad, B Abbott, Dale Charles Abbott, A Abed Abud, Kira Abeling, Deshan Kavishka Abhayasinghe, Syed Haider Abidi, H Abramowicz, H Abreu, Yiming Abulaiti, et al. Search for lepton-flavor violation in z-boson decays with τ leptons with the atlas detector. *Physical review letters*, 127(27):271801, 2021.

[18] K Uno, K Hayasaka, K Inami, I Adachi, H Aihara, DM Asner, H Atmacan, T Aushev, R Ayad, V Babu, et al. Search for lepton-flavor-violating tau-lepton decays to $\ell\gamma$ at belle. *Journal of High Energy Physics*, 2021(10):1–16, 2021.

[19] Swagato Banerjee, Vincenzo Cirigliano, Mogens Dam, Abhay Deshpande, Luca Fiorini, Kaori Fuyuto, Ciprian Gal, Tomáš Husek, Emanuele Mereghetti, Kevin Monsálvez-Pozo, Haiping Peng, Francesco Polci, Jorge Portolés, Armine Rostomyan, Michel Hernández Villanueva, Bin Yan, Jinlong Zhang, and Xiaorong Zhou. Snowmass 2021 white paper: Charged lepton flavor violation in the tau sector, 2022.

[20] Luca Nanni. Fermi theory of beta decay: A first attempt at electroweak unification. *arXiv preprint arXiv:1803.07147*, 2018.

[21] Javier Fuentes-Martín, Jorge Portolés, and Pedro Ruiz-Femenía. Integrating out heavy particles with functional methods: a simplified framework. *Journal of High Energy Physics*, 2016(9):1–26, 2016.

[22] Sacha Davidson, Paolo Gambino, Mikko Laine, Matthias Neubert, and Christophe Salomon. *Effective Field Theory in Particle Physics and Cosmology: Lecture Notes of the Les Houches Summer School: Volume 108, July 2017*, volume 108. Oxford University Press, 2020.

[23] Aneesh V. Manohar. Introduction to effective field theories, 2018.

[24] Bohdan Grzadkowski, M Iskrzyński, Mikolaj Misiak, and Janusz Rosiek. Dimension-six terms in the standard model lagrangian. *Journal of High Energy Physics*, 2010(10):1–18, 2010.

[25] MATTHIAS NEUBERT. Effective field theory and heavy quark physics. *Physics In D ≥ 4 Tasi 2004*, Jul 2006.

[26] Elizabeth E. Jenkins, Aneesh V. Manohar, and Peter Stoffer. Low-energy effective field theory below the electroweak scale: operators and matching. *Journal of High Energy Physics*, 2018(3), mar 2018.

[27] Andreas Crivellin, Saereh Najjari, and Janusz Rosiek. Lepton flavor violation in the standard model with general dimension-six operators. *Journal of High Energy Physics*, 2014(4):1–31, 2014.

[28] Vincenzo Cirigliano, Kaori Fuyuto, Christopher Lee, Emanuele Mereghetti, and Bin Yan. Charged lepton flavor violation at the EIC. *Journal of High Energy Physics*, 2021(3), mar 2021.

[29] Andrei Angelescu, Darius A. Faroughy, and Olcyr Sumensari. Lepton flavor violation and dilepton tails at the LHC. *The European Physical Journal C*, 80(7), jul 2020.

[30] Damir Bečirević, Olcyr Sumensari, and Renata Zukanovich Funchal. Lepton flavor violation in exclusive $$b\rightarrow s$$ b → s decays. *The European Physical Journal C*, 76(3), mar 2016.

[31] Tomáš Husek, Kevin Monsálvez-Pozo, and Jorge Portolés. Lepton-flavour violation in hadronic tau decays and *mu-τ* conversion in nuclei. *Journal of High Energy Physics*, 2021(1), jan 2021.

[32] A. Dedes, W. Materkowska, M. Paraskevas, J. Rosiek, and K. Suxho. Feynman rules for the standard model effective field theory in r ξ -gauges. *Journal of High Energy Physics*, 2017(6), jun 2017.

[33] Jean Pierre Delahaye, Marcella Diemoz, Ken Long, Bruno Mansoulié, Nadia Pastrone, Lenny Rivkin, Daniel Schulte, Alexander Skrinsky, and Andrea Wulzer. Muon colliders, 2019.

[34] Sergei Gninenko, Sergey Kovalenko, Serguei Kuleshov, Valery E. Lyubovitskij, and Alexey S. Zhevlakov. Deep inelastic $e - \tau$ and $\mu - \tau$ conversion in the NA64 experiment at the CERN SPS. *Physical Review D*, 98(1), jul 2018.

[35] D.B. Clark, E. Godat, and F.I. Olness. ManeParse : A mathematica reader for parton distribution functions. *Computer Physics Communications*, 216:126–137, jul 2017.

[36] Luca Fiorini. Lfv searches by atlas and cms experiments. Technical report, ATL-COM-PHYS-2021-930, 2021.

[37] K. R. Long, D. Lucchesi, M. A. Palmer, N. Pastrone, D. Schulte, and V. Shiltsev. Muon colliders to expand frontiers of particle physics. *Nature Physics*, 17(3):289–292, jan 2021.

[38] Chiara Aimè, Aram Apyan, Mohammed Attia Mahmoud, Nazar Bartosik, Alessandro Bertolin, Maurizio Bonesini, Salvatore Bottaro, Dario Buttazzo, Rodolfo Capdevilla, Massimo Casarsa, Luca Castelli, Maria Gabriella Catanesi, Francesco Giovanni Celiberto, Alessandro Cerri, Cari Cesarotti, Grigorios Chachamis, Siyu Chen, Yang-Ting Chien, Mauro Chiesa, Gianmaria Collazuol, Marco Costa, Nathaniel Craig, David Curtin, Sridhara Dasu, Jorge De Blas, Dmitri Denisov, Haluk Denizli, Radovan Dermisek, Luca Di Luzio, Biagio Di Micco, Keith Dienes, Tommaso Dorigo, Anna Ferrari, Davide Fiorina, Roberto Franceschini, Francesco Garosi, Alfredo Glioti, Mario Greco, Admir Greljo, Ramona Groeber, Christophe Grojean, Jiayin Gu, Tao Han, Brian Henning, Keith Hermanek, Tova Ray Holmes, Samuel Homiller, Sudip Jana, Sergo Jindariani, Yonatan Kahn, Ivan Karpov, Wolfgang Kilian, Kyoungchul Kong, Patrick Koppenburg, Karol Krizka, Lawrence Lee, Qiang Li, Ronald Lipton, Zhen Liu, Kenneth Long, Ian Low, Donatella Lucchesi, Yang Ma, Lianliang Ma, Fabio Maltoni, Bruno Mansoulie, Luca Mantani, David Marzocca, Navin McGinnis, Barbara Mele, Federico Meloni, Claudia Merlassino, Alessandro Montella, Marco Nardecchia, Federico Nardi, Paolo Panci, Simone Pagan Griso, Giuliano Panico, Rocco Paparella, Paride Paradisi, Nadia Pastrone, Fulvio Piccinini, Karolos Potamianos, Emilio Radicioni, Riccardo Rattazzi, Diego Redigolo, Laura Reina, Jürgen Reuter, Cristina Riccardi, Lorenzo Ricci, Ursula van Rienen, Luciano Ristori, Tania Natalie Robens, Richard Ruiz, Filippo Sala, Jakub Salko, Paola Salvini, Ennio Salvioni, Daniel Schulte, Michele Selvaggi, Abdulkadir Senol, Lorenzo Sestini, Varun Sharma, Jing Shu, Rosa Simoniello, Giordon Holtsberg Stark, Daniel Stolarski, Shufang Su, Wei Su, Olcyr Sumensari, Xiaohu Sun, Raman Sundrum, Jian Tang, Andrea Tesi, Brooks Thomas, Riccardo Torre, Sokratis Trifinopoulos, Ilaria Vai, Alessandro Valenti, Ludovico Vittorio, Liantao Wang, Yongcheng Wu, Andrea Wulzer, Xiaoran Zhao, and Jose Zurita. Muon collider physics summary, 2022.

[39] R Keith Ellis, Zoltan Kunszt, Kirill Melnikov, and Giulia Zanderighi. One-loop calculations in quantum field theory: from feynman diagrams to unitarity cuts. *Physics reports*, 518(4-5):141–250, 2012.

[40] Hiren H. Patel. Package -x 2.0: A mathematica package for the analytic calculation of one-loop integrals. *Computer Physics Communications*, 218:66–70, sep 2017.